Spring 5-20-2016

Dendrimer Modified Silica Nanoparticles as Fluorescent Chemosensors for the Detection of Copper and Cyanide Ions

Alicia Luhrs
University of San Francisco, alicia.luhrs@hotmail.com

Dendrimer Modified Silica Nanoparticles as Fluorescent Chemosensors for the Detection of Copper and Cyanide Ions

A thesis presented to the faculty

of the Department of Chemistry

at the University of San Francisco

in partial fulfillment of the requirements for the degree of

Master of Science in Chemistry

Written by

Alicia Luhrs

Bachelor of Science in Chemistry

California Polytechnic State University, San Luis Obispo

May 2016

Dendrimer Modified Silica Nanoparticles as Fluorescent Chemosensors for the Detection of Copper and Cyanide Ions

Thesis written by Alicia Luhrs

This thesis is written under the guidance of the Faculty Advisory Committee, and approved by all its members, has been accepted in partial fulfillment of the requirements for the degree of

Master of Science
in Chemistry at
the
University of San Francisco

Thesis Committee:

Lawrence D. Margerum, Ph.D.
Research Advisor

William Melaugh, Ph.D.
Professor

Ryan West, Ph.D.
Assistant Professor

Marcelo Camperi, Ph.D.
Dean, College of Arts and Sciences

Acknowledgement

I would like to thank my research advisor Dr. Margerum for all of his guidance, advice, patience, and encouragement during my time at the University of San Francisco. I would also like to thank my thesis committee members, Dr. Melaugh and Dr. West, not only for their help on this project, but for always being friendly and approachable to all of the graduate students. I would also like to sincerely thank Andy Huang and Jeff Oda for their help and patience in teaching me so much about the instruments here at USF, and for making graduate school much more entertaining. A huge thank you to Deidre Shymanski for answering my endless questions and for making the graduate students feel at home at USF. Finally, thank you to all the friends I made during my time here at USF, especially to the Margerum group members: Katie, Jon, Justin, Hank, Clara, and Brannan.

Table of Contents

List of Figure Captions

List of Table Captions

List of Recurring Structural Abbreviations

Abbreviation	Meaning	Structure
ANS	8-Anilino-1-naphthalenesulfonic acid	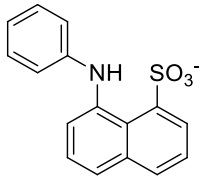
APTES	(3-Aminopropyl)triethoxysilane	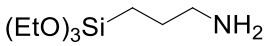
EDTA	Ethylenediaminetetraacetic acid	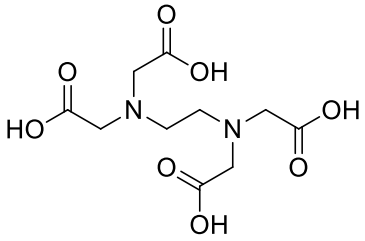
FITC	Fluorescein isothiocyanate	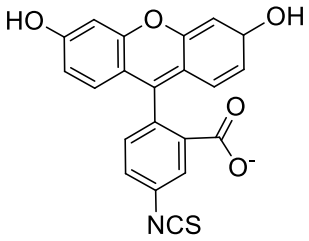
Gx	PAMAM dendrimer generation	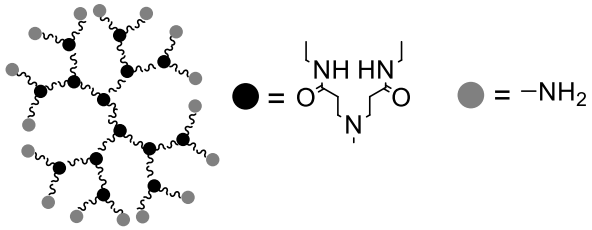
HEPES	4-(2-Hydroxyethyl)piperazine-1-ethanesulfonic acid	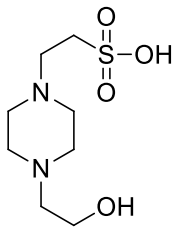

PAMAM	Polyamidoamine	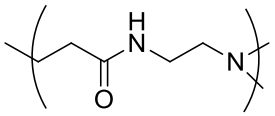
RITC	Rhodamine B isothiocyanate	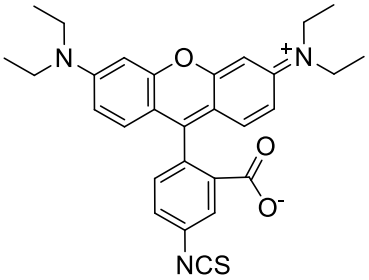
SNP	Silica Nanoparticle	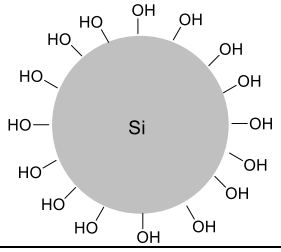
SNPGx	Dendrimer-modified SNP	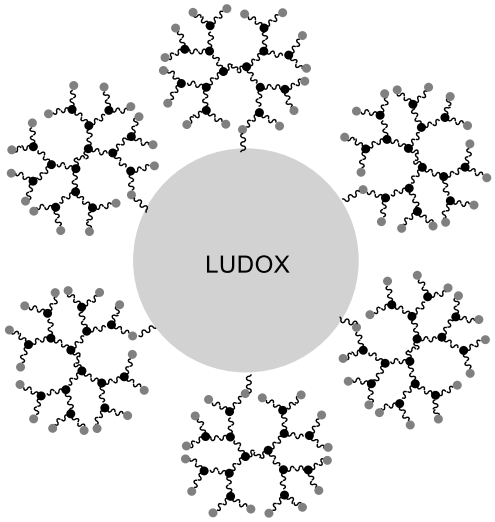

SNPGx-F	SNPGx with tethered FITC	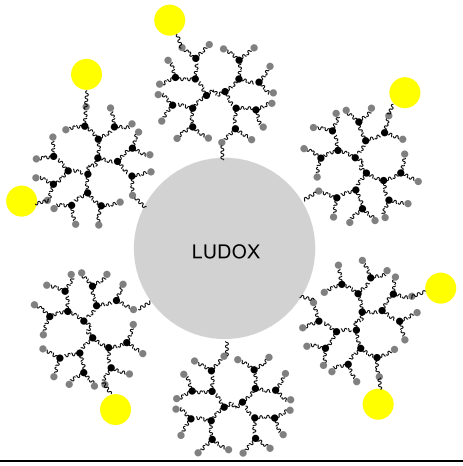
SNPGx-R	SNPGx with tethered RITC	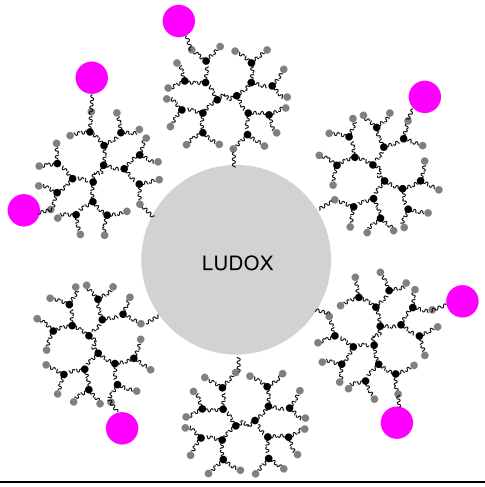
SNPG4-R-COOH	SNPG4-R with carboxylic acid surface groups	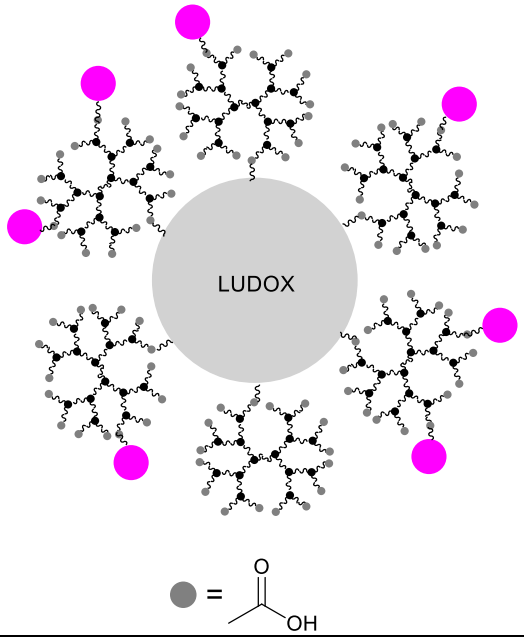

SNPG4-RF-C	SNPG4 with tethered RITC and FITC (concentrated synthesis)	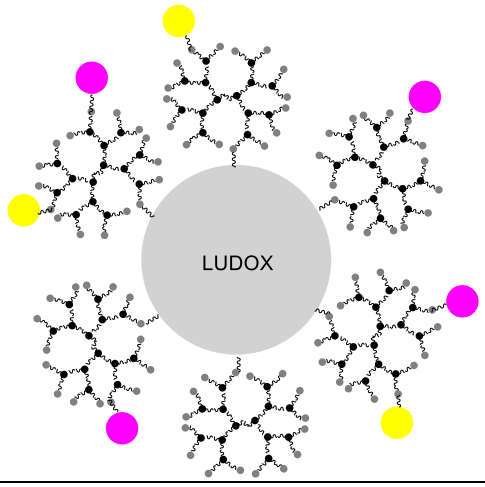
SNPG4-RF-D	SNPG4 with tethered RITC and FITC (dilute synthesis)	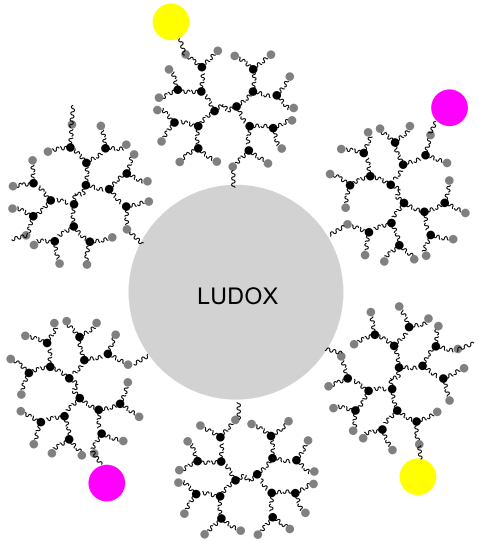

Abstract

A series of silica nanoparticle-based fluorescent chemosensors were synthesized for the sensitive and selective detection of Cu^{2+} ions in aqueous solution and subsequent CN^- ion detection. Silica nanoparticles (SNP) were modified with branching polyamidoamine (PAMAM) dendrimers, which function as selective turn-off Cu^{2+} ion chelators and platforms for the attachment of rhodamine isothiocyanate (RITC) or fluorescein isothiocyanate (FITC) fluorescent dyes. In the presence of Cu^{2+} ions, the emission of the fluorescent dye is quenched by Forster resonance energy transfer (FRET) and is dependent upon dendrimer generation, pH, fluorescent dye, and surface charge. The quenching effectiveness was analyzed by Stern-Volmer quenching analysis and increased with dendrimer generation up to G4, yielding a Stern-Volmer quenching constant of 14 (±2) x 10^5 M^{-1} and a limit of detection of 0.2 μM Cu^{2+} under optimal conditions (SNPG4-FITC). Furthermore, the fluorescence can be fully restored by the subsequent addition of CN^- ions, which is surprisingly effective compared to other strong anion chelators like EDTA and azide at low concentrations, reaching a turn-on detection limit of 1 μM CN^- (SNPG4-FITC). The turn-off, turn-on fluorescent chemosensing systems were also used as FRET sensors for 8-Anilino-1-naphthalenesulfonic acid (ANS) to prove the applicability of the systems as small organic molecule sensors. In the future, the same SNPGx-Dye sensing system can be customized to sense additional analytes like polycyclic aromatic hydrocarbons, explosives, and amino acids.

Chapter 1
Introduction

In this work, silica nanoparticles were modified with dendrimers to function as fluorescent chemosensors for the detection of copper and cyanide. This chapter focuses on the concepts that form the basis of this research, and outlines the goals of the thesis work.

1.1 Fluorescent Chemosensors

Fluorescent chemosensing is an emergent and promising approach for recognizing and quantifying both charged and neutral species. Important analytes, including metal ions, have traditionally been studied using methods like atomic absorption spectroscopy, liquid chromatography, electrochemistry and mass spectrometry.[1-2] While these methods are viable, they are often impractical due to poor sensitivity and selectivity, high cost of instrumentation, and complex detection steps.[1-2] Fluorescence has proven to be one of the simplest, fastest, and most sensitive methods of quantifying metal ions and anions.[1, 3]

The most important feature of a fluorescent chemosensor is the ability to customize the sensing system towards the analyte of interest. Traditionally, a modular approach is taken when designing a luminescent sensor, allowing each component of the sensor to be tailored to fit the system's needs. Figure 1-1 shows the ideal fluorescent chemosensor, which is made up of a platform for synthesis, a receptor for the analyte, a signaling subunit, and a linker covalently connecting the receptor and the signaling subunit.[4-5] While a number of chemosensors do not include a platform for synthesis, including one can prove advantageous, as it can be used as a solid support for the system and can control distance effects. Perhaps the most difficult component of the modular system is the receptor, as it must be specific to the analyte. The signaling subunit is most commonly a fluorescent dye, but can be any species that displays a change in output signal when the analyte is bound to the receptor.[5] The analyte of interest binds in the binding site of the receptor, and its presence is detected by a change in fluorescent emission of the signaling subunit.

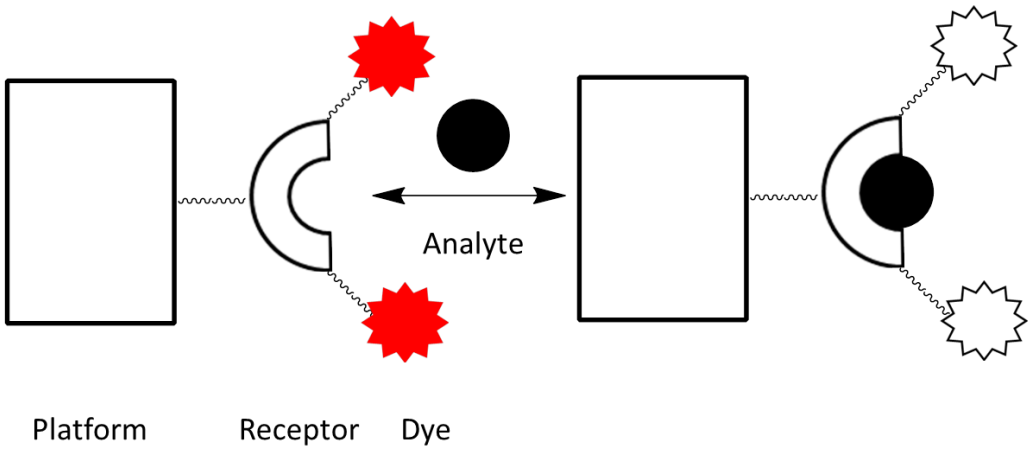

Figure 1-1. Modular approach to fluorescent "turn-off" chemosensing is shown. When the analyte is free, the system fluoresces. When the analyte is bound, it does not.

When the system is not in the presence of the analyte, the signaling dye can be excited and emission is observed. When the system encounters the analyte, a detectable change must occur. The most common form of photoluminescent sensing is "turn-off" sensing, where the fluorescence is somehow interrupted, or quenched, by the analyte, and a decrease in emission is observed.[5] The mechanism of quenching is typically one of two extensively studied pathways shown in Figure 1-2: electron transfer and energy transfer.[6] In the case of metal ion quenching, electron transfer requires that the metal must have one oxidation state that induces a transfer process with the signaling dye, and another oxidation state that does not. Energy transfer requires that the metal ion have only partially filled d-orbitals. [6] A specific type of energy transfer called Forster resonance energy transfer (FRET) is important for the work in this thesis and is discussed in section 1.4.

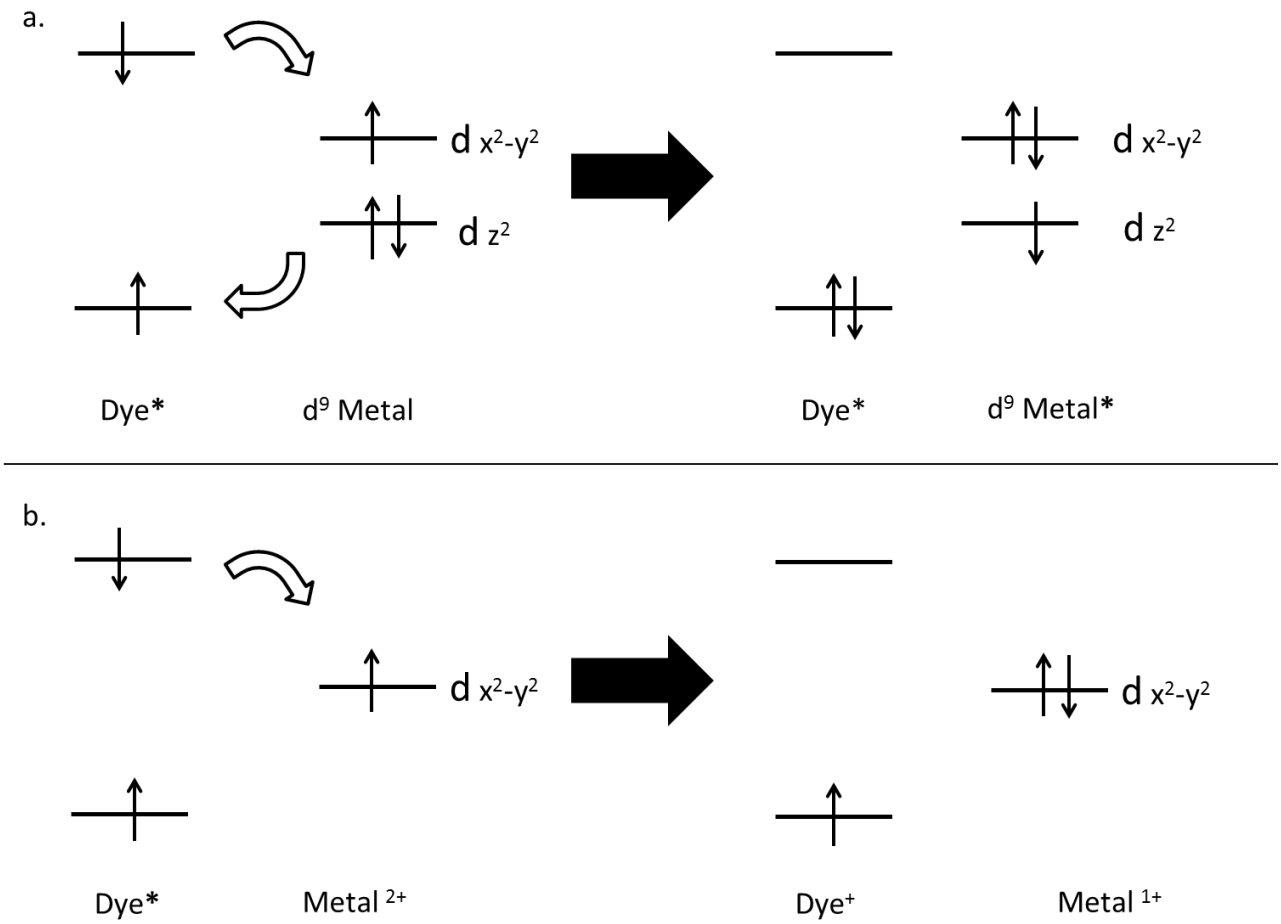

Figure 1-2. Figures adapted from Bergonzi et al.6 a). Energy transfer quenching is shown between an excited (*) dye and a metal with partially filled d-orbitals. b). Electron transfer quenching is shown between an excited (*) dye and a metal with multiple oxidation states.

If the analyte is bound to the receptor, it is possible to disrupt the quenching process by binding to or removing the analyte.[2, 7] The previously quenched fluorescence would then return, possibly back to its initial intensity. This “turn-on” sensing allows the same system to function as a dual sensor, where the initial quencher and the subsequent disruptor can both be detected and quantified with similar sensitivities. Metal ions are ideal quenchers for this type of sensing, because anions with known binding constants and solubility products can be chosen to selectively bind to them and cause an increase in the signal (Figure 1-3). Calero et al. employed this method in their quencher displacement assay work, where silica nanoparticles functionalized with fluorescent dye and metal ion binding terpyridine were quenched when cations were added, and anions were subsequently added to remove the cation and restore the fluorescent signal.[8]

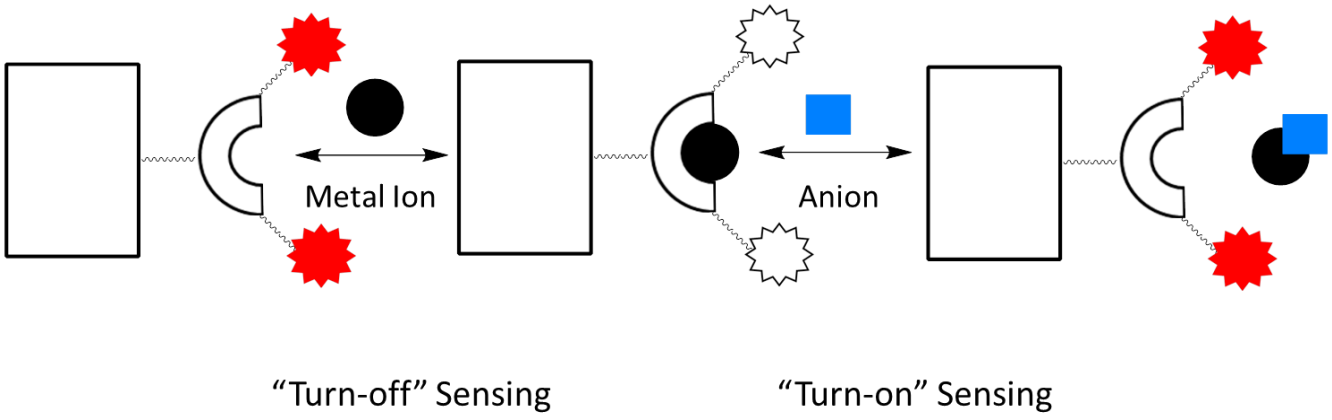

Figure 1-3. Simplified example of a “turn-off” and “turn-on” fluorescent chemosensor. When the metal ion is bound to the receptor, fluorescence is quenched. When an anion is added, the metal ion is removed from the receptor and the fluorescence returns.

Fluorescent chemosensing has quickly become one of the fastest and most sensitive methods for the detection of analytes, specifically metal ions. However, as many researchers have discovered, designing the perfect system can be difficult. It is challenging to design a system to be selective for both cations and anions, as Calero observed.[8] Moreover, assembling the largely organic and sizable modular components of the chemosensor often hinders the dispersibility of the system.[2] As most sensing is done in aqueous media, dispersibility is an incredibly important aspect to consider. If these hindrances can be overcome, fluorescent chemosensing provides the ideal customizable platform for metal ion and subsequent anion detection.

1.2 Silica Nanoparticles

Nanoparticles provide an ideal and increasingly popular platform for fluorescent chemosensing, as they are small and extremely versatile. Utilizing a platform like nanoparticles to anchor the signaling and receptor subunits can cause cooperative effects and signal amplification, since all molecules are fixed in close proximity to each other.[4, 8] Recently, systems employing quantum dots, magnetic nanoparticles, and fluorescent nanoparticles have all been utilized as platforms for chemosensing.[2, 9-10] While all of these systems have a high surface to volume ratio, they can be expensive to make and difficult to modify. Figure 1-4 shows an example of a silica nanoparticle (SNP), which can overcome these limitations, and provide distinct advantages over other nanoparticle systems. Uniform SNPs are inexpensive to purchase, and their size can be controlled if synthesized by the simple Stober method.[9, 11] The

SNP surface is made up of silanol groups, Si-OH, which are easy to modify with a wide variety of functional groups.[9]

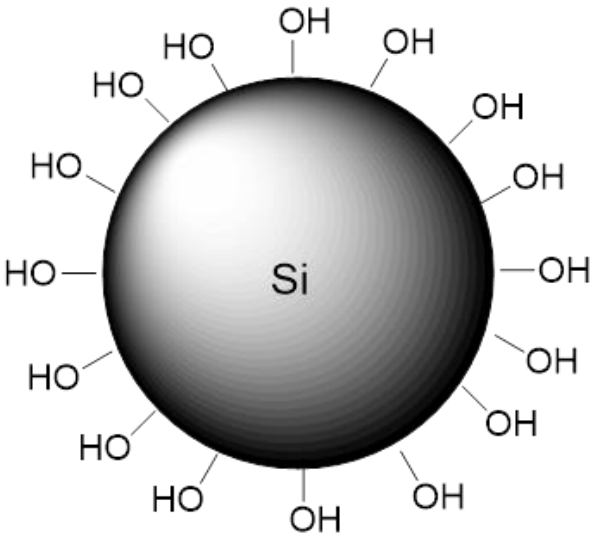

Figure 1-4. A silica nanoparticle with hydroxyl surface groups.

Arguably as important as size and surface modifications are photochemical properties. Fluorescent chemosensing relies on spectroscopic changes, so any SNP response to light would hinder the sensing. Silica nanoparticles are transparent to visible light spectroscopy and inert to energy transfer, allowing them to be used with most instrumentation.[4] For all of these reasons, SNPs have recently been one of the most popular platforms for fluorescent chemosensor design of ion sensors[4, 12], ratiometric sensors[3, 13], quencher-displacement assay sensors[8] and more.

1.2.1 Size and Dispersibility

Silica nanoparticles provide the perfect balance between size and dispersibility. Nanoparticles are inherently small, ranging anywhere from 1-100 nanometers in diameter, and tend to clump together when in aqueous solution. This aggregation would cause the nanoparticles to behave differently both in terms of their spectroscopic properties and sensing abilities. The smaller the nanoparticles are, the more likely they are to stick together. This means that larger particles are more dispersible; however, larger particles also cause scattering.[14] A solution containing large nanoparticles would appear cloudy, as light is scattering off the sizeable particles.

Choosing a size of nanoparticle to serve as a platform for fluorescent chemosensing is key, because if the solution is too aggregated or the particles are too large, the sensor will not be consistent and reliable. However, it is possible to choose a smaller particle and modify its

surface with functional groups that will contribute to its dispersibility in solution to avoid excessive light scattering.

One crucial advantage to using silica nanoparticles as a platform for chemosensing is the stability of SNP in aqueous solutions.[8] Other nanoparticles like dye-doped NPs or quantum dots can degrade over time, usually due to photobleaching.[10] Silica nanoparticles contain no fluorescent moiety, and remain unchanged if exposed to light. Additionally, SNPs that are dispersed in solution can be easily isolated by centrifugation and dried.[9] This is extremely helpful when synthesizing a modular chemosensor, as each successive synthetic step is worked up by isolating the modified particles, while the unreacted starting materials remain in solution.

As discussed previously, SNPs are inexpensive to manufacture and to purchase. For that reason, there are countless options when selecting a nanoparticle to use. Grace Chemicals is the main supplier of colloidal silica, and their "LUDOX" nanoparticles can be purchased through Sigma-Aldrich. Table 1-1 shows the vast variety of silica nanoparticles in the LUDOX product range, varying in counterion, size, surface area and sodium content.

Table 1-1. Properties of LUDOX colloidal silica nanoparticles.[15-17]

LUDOX	Counter Ion	Diameter (nm)	Silica Content (%SiO2)	Sodium Content (% Na)	Surface Area (m^2/g)	Density (g/mL) at 25°C	pH
SM-AS	NH_4^+	7	25	0.05	340	1.2	9.7-10.3
AS-30	NH_4^+	20	30	0.06	220	1.2	9.1
AS-40	NH_4^+	22	40	0.07	140	1.2	9.1
FM	Na^+	5	15	0.3	425	1.1	10
SM	Na^+	7	30	0.5	340	1.2	10
LS	Na^+	12	30	0.1	220	1.2	8.2
HS-40	Na^+	12	40	0.4	220	1.3	9.7
TM-50	Na^+	22	50	0.3	140	1.4	8.5-9.5
CL	Cl^-	12	30	0	240	1.2	4.5

The properties seen in Table 1-1 allow researchers to choose the ideal SNP based on their system. For example, if sodium content is detrimental, such as in catalysis, ammonium counter ion silica (AS) can be chosen.[17] While all colloidal silica has a negative surface charge, LUDOX-CL has a thin monolayer of alumina that creates a positively charged surface, which is useful in flocculating all other negatively charged silica.[17] In this work, LUDOX AS-30 was selected for all research due to its high surface area and well-documented surface

modifications.[4] While LUDOX AS-30 is dispersible in aqueous solution, further surface modifications that will be discussed later helped keep the SNP dispersible despite the attachment of large organic dyes.

1.2.2 Surface Chemistry Modifications

The silanol groups on the surface of the SNP react just like normal alcohols. The simplest and most common way of modifying the surface of SNPs is to use a silanated reagent. Traditionally, (3-Aminopropyl)trimethoxysilane (APTMS) or (3-Aminopropyl)triethoxysilane (APTES) have been used to convert the hydroxyl surface into an amine surface, allowing for a wider range of synthetic possibilities (Figure 1-5).[9] Each of the three methoxy or ethoxy groups replaces one of the hydroxyl groups, allowing the aminopropyl silane group to be tethered to the nanoparticle in 3 places.

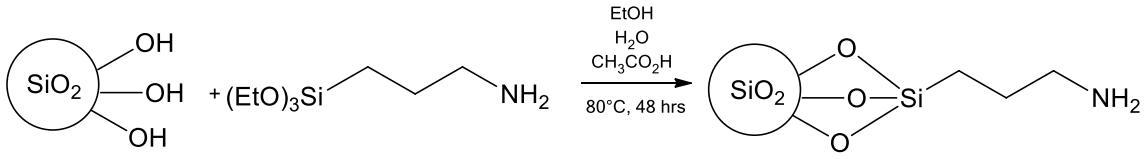

Figure 1-5. The surface modification of SNP with APTES, converting the hydroxyl surface groups to primary amines.

While converting the nanoparticle surface to amines allows for a broad range of succeeding reactions, it is also possible to silanate the modifier first, and then tether it to the nanoparticle. For example, Candel et al. synthesized a SNP with a tethered dye and chelating group by modifying the dye and chelating groups first with APTMS, and subsequently attaching them to the hydroxyl surface of the nanoparticle.[4]

The advantage of modifying the surface with an amine like APTMS or APTES first is the ability to quantify the reaction with assays. The ninhydrin assay as reported by Soto-Cantu can be used to quantify the amines on the surface of the nanoparticle.[11] Not only does this help determine reaction conditions for successive reactions, but it also provides a way of confirming that the next reaction has happened. For example, the amine density should decrease after a fluorescent dye is added to the SNP-NH_2 surface.

This quantifiable number is also a reminder that there is a limited amine density on the surface of each nanoparticle. Once all the hydroxyl groups have been converted into amines, the successive reactions are limited by that amine density. Keeping in mind that the end goal of a fluorescent chemosensor is to chelate an analyte that changes the emission of an attached

fluorescent dye, it is advantageous to have as many chelating groups as possible on the surface. In order to retain the small diameter of the SNP and overcome the small number of functional groups on the surface, branched molecules containing chelating functional groups such as dendrimers can be attached to the SNP-NH_2 surface.

1.3 Polyamidoamine (PAMAM) Dendrimers

The classic modular fluorescent chemosensor contains a receptor for the analyte, which is covalently bound to the previously discussed SNP platform. The receptor is also connected to a signaling subunit through a covalently bound linker molecule. In this work, polyamidoamine (PAMAM) dendrimers were chosen to act as both the receptor *and* the linker to the signaling subunit.

Dendrimers are a class of three-dimensional molecules having symmetric branching groups that increase with generation. They were first synthesized by Tomalia et al. in 1985, and contain three distinct architectural components: an initiator core, a repeating interior subunit, and exterior (terminal) surface groups (Figure 1-6).[18-19] As the generation (Gx) increases by one number, the interior subunit branches one more time, and the number of terminal surface groups increases by a factor of 2.

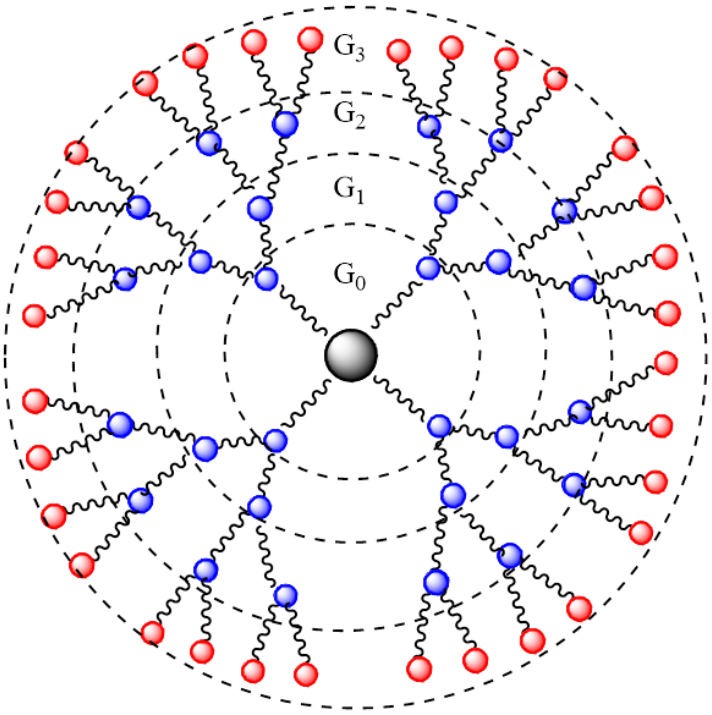

Figure 1-6. Simplified representation of a G3 dendrimer, adapted from Chang.[19] The grey dot is the initiator core, the blue dots are repeating interior subunits, and the red dots are exterior surface groups.

Previous work in this group has centered around PAMAM dendrimers, which are a specific class of dendrimers with an ethylenediamine (EDA) core, a repeating amidoamine interior branching subunit, and exterior primary amines (Figure 1-7).[18] PAMAM dendrimers have been used in this group as metal ion chelates for extraction and indicator displacement assays on controlled pore glass, and this research has led to an extensive understanding of the behavior and properties of PAMAM dendrimers.[19-22]

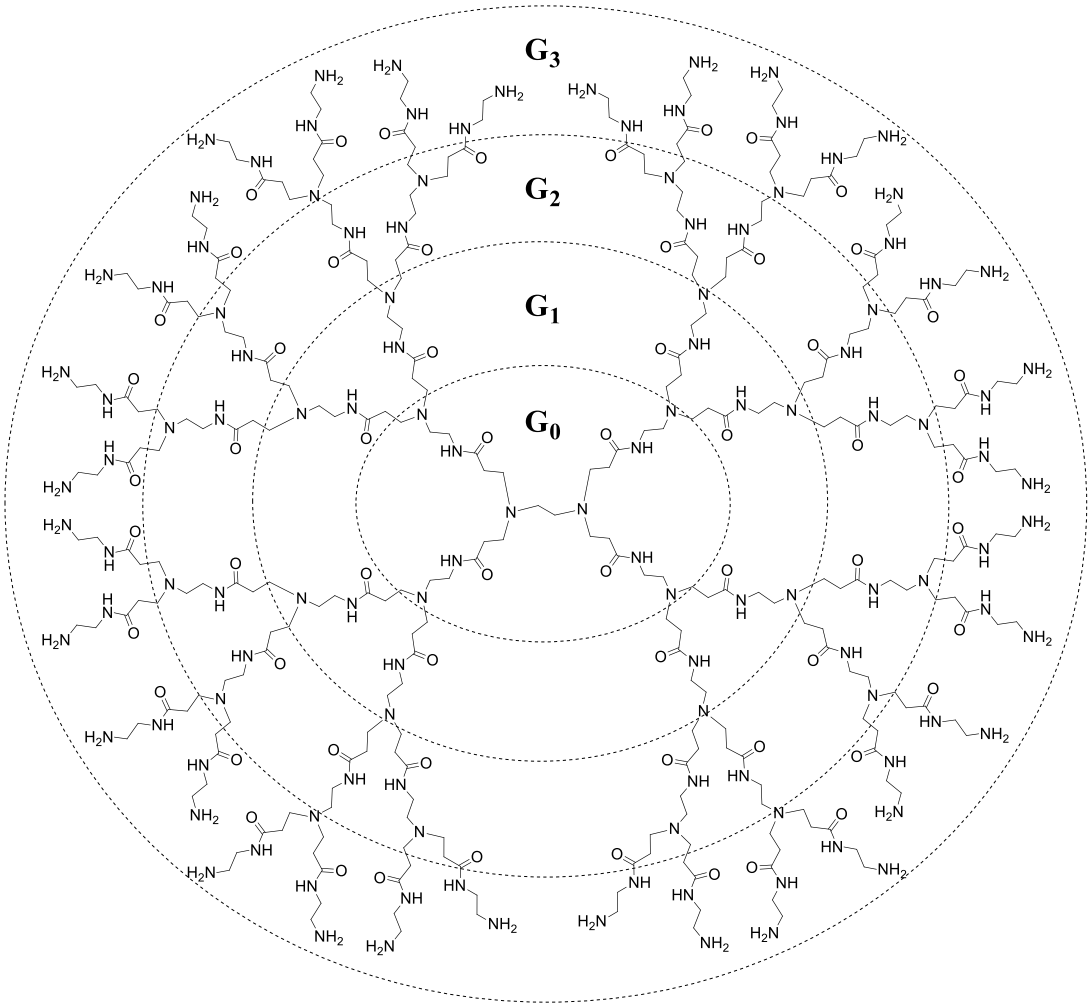

Figure 1-7. A G3 PAMAM dendrimer is shown with an EDA core, repeating amidoamine branching groups, and exterior primary amines.

1.3.1 Structure and Properties

The unique structural properties of PAMAM dendrimers are well known and can be experimentally and mathematically explained. The number of surface groups and the number of branching interior subunits are dependent on the dendrimer generation (G), initiator core

multiplicity (N_c, number of reactive sites on the core), and branch multiplicity (N_b, number of reactive sites on the branching unit). The structural properties can be calculated using the mathematical equations written by Tomalia et al.[18, 21, 23]

The number of surface groups on a PAMAM dendrimer can be calculated using Equation 1-1:

$$\text{Number of Surface Groups} = (N_c)\ ({N_b}^G) \quad \text{1-1}$$

And the number of interior branching units, or number or tertiary amines, can be calculated using Equation 1-2:

$$\text{Number of Interior Branching Units} = \left[(N_c)({N_b}^G)\right] - 2 \quad \text{1-2}$$

PAMAM dendrimers with an EDA core have an N_c value of 4, as there are 4 reactive sites on EDA, and an N_b value of 2, as each amidoamine branching group has 2 reactive sites. A G3 PAMAM dendrimer would have 4 x 2^3=32 surface amines, and [4 x 2^3]-2=30 branching groups or tertiary amines.

The molar mass of any dendrimer can be calculated using Equation 1-3, where M_c, M_b, and M_s are the molar masses of the core, branching unit, and surface group, respectively.

$$\text{Molar Mass} = M_c + N_c \left[(M_b)\left(\frac{N_b^G - 1}{N_b - 1}\right) + (M_s)(N_b^G)\right] \quad \text{1-3}$$

Table 1-2 summarizes the structural properties of G0-G5 PAMAM dendrimers, as this thesis work focuses on generations 5 and below. While the number of surface groups and branching points increase exponentially, the diameter does not.

Table 1-2. Structural properties of PAMAM dendrimers.

Generation	Molar Mass[18] (g/mol)	Number of Branching Points[18]	Number of Surface Groups[18]	Diameter (nm)[24]
0	516	2	4	1.4
1	1,428	6	8	1.9
2	3,252	14	16	2.6
3	6,900	30	32	3.6
4	14,196	62	64	4.4
5	28,788	126	128	5.7

All of these properties contribute to the overall theoretical shape and size of the dendrimer. As this thesis work focuses on attaching dendrimers to spherical nanoparticles and understanding how the dendrimer interacts with analytes, it is critical to understand how the dendrimer is structured and how it behaves. While X-ray diffraction is the most common way of

determining the structure of molecules, it cannot be used on dendrimers due to their fractal nature.[21] Computer simulations provide crucial information about how the shape of dendrimers varies with generation, and were one of the first ways that researchers were able to visualize the 3-dimensional dendrimer (Table 1-3).[25-26]

Table 1-3. Computer modeling of moments of inertia for G1-G5 PAMAM Dendrimers.[25]

Generation	% I_x	% I_z	I_z/I_x
1	11.26	50.16	4.5
2	13.85	57.54	4.2
3	18.77	51.31	2.7
4	24.59	41.54	1.7
5	29.06	36.4	1.3

Naylor et al. were the first to use computer modeling and inertia to explain the 3-dimensional shape of different generations of dendrimers. Previously, it had been assumed that dendrimers grow spherically regardless of generation. However, computer modeling proved that as generation increases, the structure of the dendrimer changes drastically due to inertial changes. Figure 1-8 shows this trend. Generations 1-3 have large inertia ratios (I_z/I_x) and are highly asymmetric, resembling disks or domes. Generation 4 begins to look more spherical, and generation 5 and above are almost perfect spheres with small inertia ratios and densely packed branches. Numerically, the closer the inertia ratio is to one, the more symmetric and spherical it will be, as the moments of inertia on all axes will be the same.

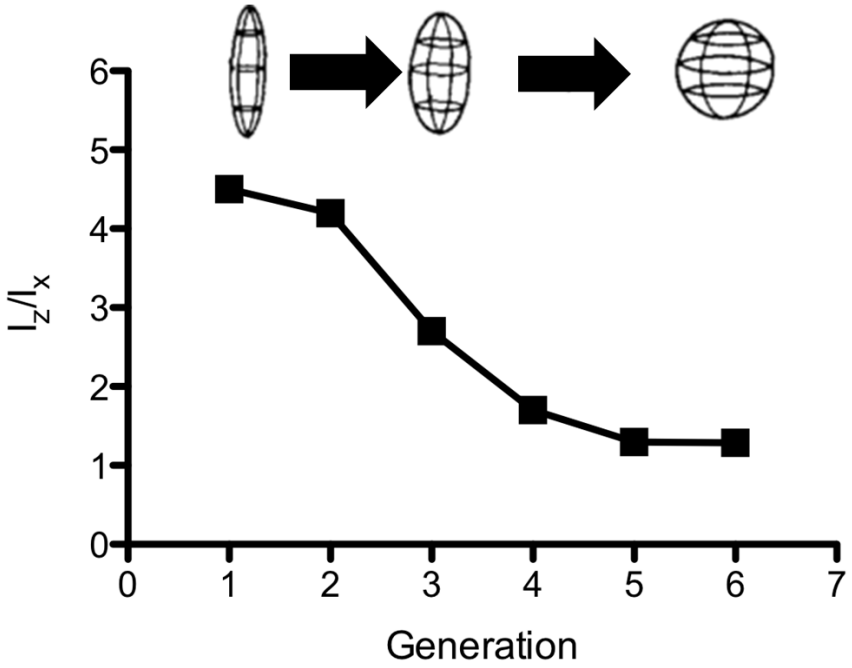

Figure 1-8. Representation of the change in 3-dimensional shape of PAMAM dendrimers with generation (Reproduced from Naylor et al.)[25]

This understanding of the shift in shape with generation is helpful in picturing what the nanoparticle will look like when surrounded by dendrimers, as well as how the dendrimer will interact with analytes.

1.3.2 pH Dependence

The protonation behavior of dendrimers in solution has been studied extensively for high generation PAMAM dendrimers, as it can determine solubility and strongly influence analyte interactions. The pK_a values of G3-G5 PAMAM dendrimers were determined by Diallo et al. through titration and are listed in Table 1-4.[27] The interior tertiary amines have lower pK_a values than their terminal primary amine counterparts, which means that the interior protonation sites have a lower proton affinity than the exterior protonation sites.

Table 1-4. The pka values of G3-G5 PAMAM dendrimers are shown.[27]

Generation	pKa	
	Interior (Tertiary) Amines	Terminal (Primary) Amines
3	6.3-6.7	9.0-9.9
4	6.3-6.9	9.0-10.3
5	6.3-7.2	9.0-10.8

Figure 1-9 shows the protonation behavior of a G3 PAMAM dendrimer in solution.[28] At low pH, the entire dendrimer is positively charged. At neutral pH values, the interior tertiary nitrogens are deprotonated, and only the surface of the dendrimer remains positively charged. At high pH values, the entire dendrimer is neutral. This observation is extremely important when discussing analyte interactions, as a charged surface can attract or repel a charged analyte. Interior charges are also significant, as analytes can reside in the interior or exterior of the dendrimer depending on the environment. Additionally, having a charged surface at neutral pH can help the largely organic molecule be dispersible in aqueous solution.[27]

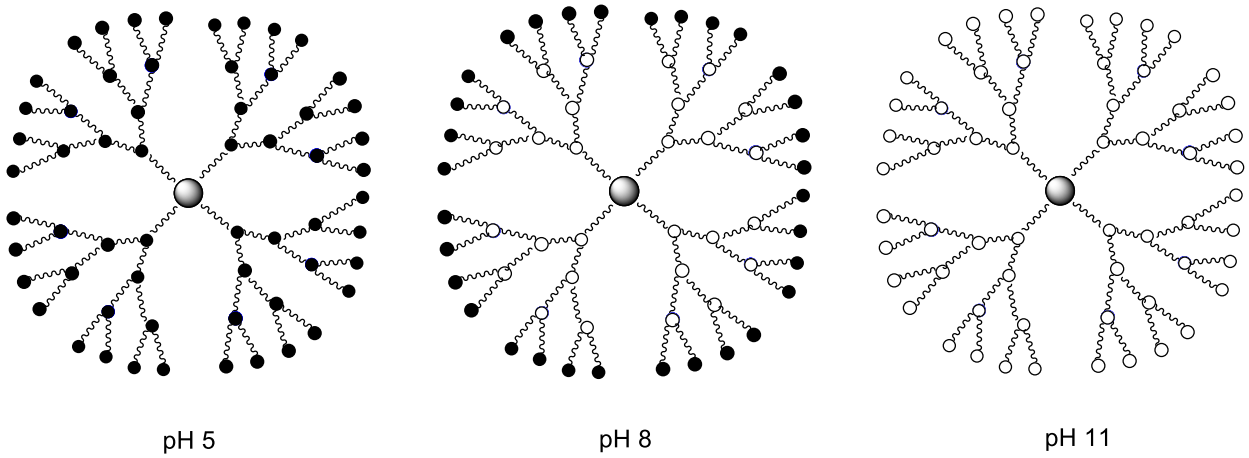

Figure 1-9. The pH dependence of a G3 PAMAM dendrimer is shown. Black shaded circles represent positive charges, and white circles represent neutral sites.[28]

As discussed above, the surface charge of the dendrimer can be controlled by changing the pH of solution. However, the exterior amine groups can only fluctuate between positive and neutral. In order to thoroughly understand the surface interactions with an analyte, positive, neutral, and negative surface charges are necessary. One key advantage of using PAMAM dendrimers in this work is that the exterior amines can be easily modified with succinic anhydride to become carboxylic acids, which are negatively charged at pH values less than 6.[29-30] The ability to create a positive, neutral, and negative surface with a neutral or positive interior just by changing pH is a key advantage to using dendrimers as analyte receptors.

1.3.3 Metal Ion Binding Sites

PAMAM dendrimers were chosen as the analyte receptor in this work because they are known to strongly chelate copper (II) ions in solution, and the binding behavior between the two

has been studied extensively by this research group and others.[19-21, 27] As discussed previously, metal ions are ideal analytes for “turn-off/on” fluorescent chemosensing because they can quench fluorescence through energy transfer by binding to the receptor, and can be subsequently removed by anions to return the signal. These metal-anion complexes have known solubility product constants and binding behaviors, which allows the anionic sensor to be customized.

Copper (II) is involved in many biological processes through both the production and regulation of enzymes such as superoxide dismutase and cytochrome C oxidase, but can lead to neurological diseases such as Alzheimer’s disease, Wilson disease, and Menkes disease when overpresent in the body.[1, 3] Because of this, the Environmental Protection Agency (EPA) has set a maximum allowable level of copper (II) in drinking water at 20 µM.[3] However, previous methods of detecting copper (II) ions in solution are time consuming and expensive, or not sensitive or selective enough. Utilizing PAMAM dendrimers as metal ion chelators enhances the sensitivity and selectivity of a copper ion sensor, while maintaining a simple synthesis and detection procedure.

The high density of nitrogen Lewis base sites in the PAMAM dendrimer provide ideal locations for copper (II) ions to chelate. There are two main electron donating groups within the dendrimer: the exterior primary amines and the interior tertiary nitrogens. If the exterior amines were protonated beyond their neutral state, copper (II) coordination would displace the protons. While a large number of coordination complex possibilities exist utilizing these Lewis base sites, studies done by Ottaviani et al. and Diallo et al. have proven through electron paramagnetic resonance (EPR) and extended X-ray absorption fine structure (EXAFS) spectroscopy that copper (II)-PAMAM complexes are usually Cu^{II}-N_4. These four coordination sites were determined by bond length to be equatorial, and the remaining axial coordination sites are solvent or counterions.[27, 31] It is also possible for Cu^{II}-N_2 complexes to form, with solvent filling the remaining coordination sites. Figure 1-10 shows these coordination models.

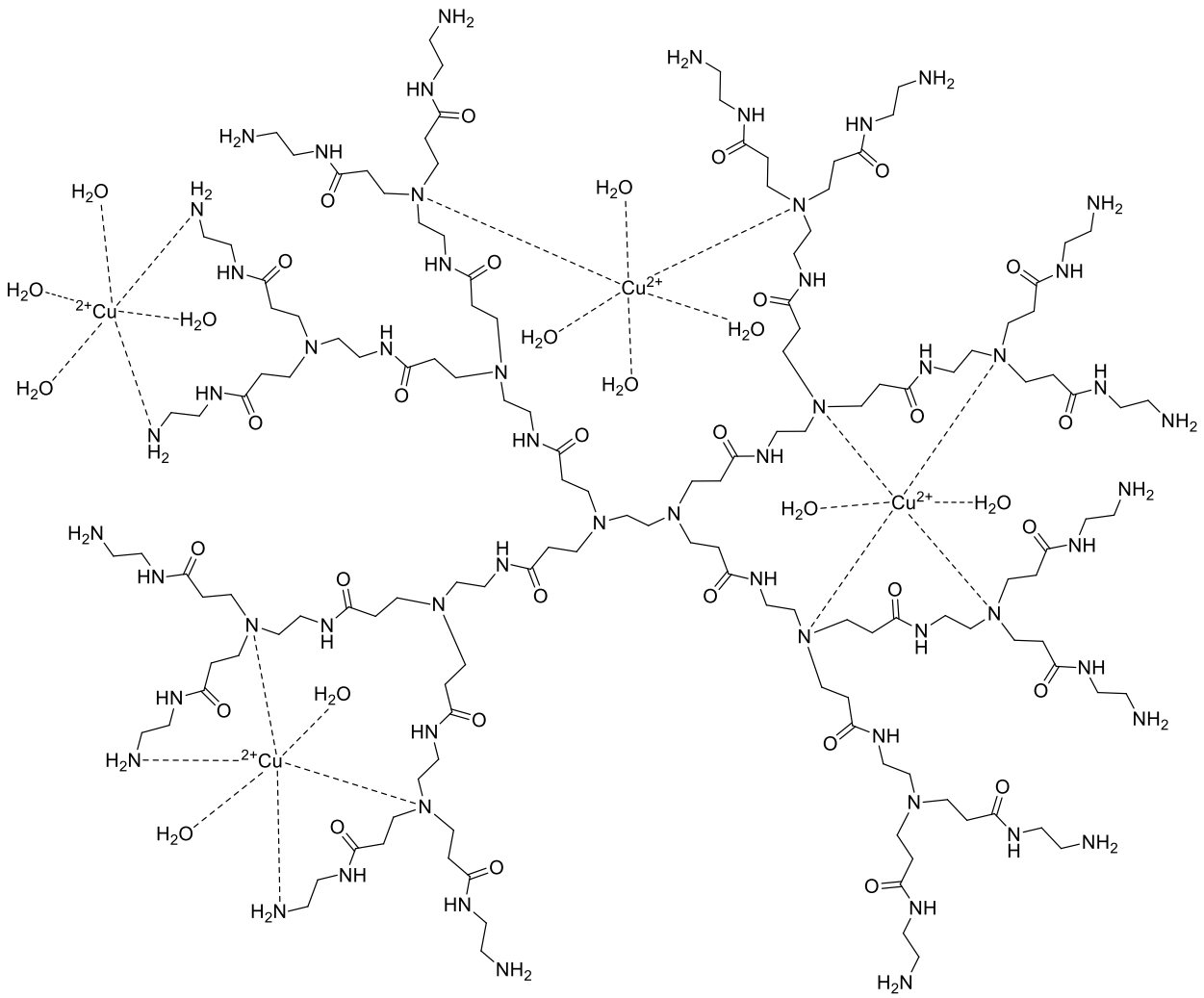

Figure 1-10. Copper(II) chelation possibilities within a G2 PAMAM dendrimer in water are shown, adapted from Ottaviani and Diallo.[27,31] All coordination complexes are Cu^{II}-N4 or Cu^{II}-N2 complexes, 2 or 4 coordinated water molecules to satisfy an octahedral geometry.

As the dendrimer behaves as both the receptor and linker to the fluorescent signaling unit, the copper (II) binding could cause a decrease in fluorescence through Forster Resonance Energy Transfer (FRET). This quenching mechanism will be explained in the next section. Once the copper (II) is coordinated with the dendrimer, anions can either bind to or remove the metal from the complex and restore the fluorescence.

1.4 Forster Resonance Energy Transfer (FRET) Quenching

As discussed in section 1.1, fluorescence quenching is due to electron transfer or energy transfer. In this work, a specific type of energy transfer called Forster Resonance Energy Transfer (FRET) is discussed. FRET is a distance dependent photophysical energy transfer

process. Non-radiative energy is transferred from a donor fluorophore to an acceptor, as long as the distance between the donor and acceptor is between 1 and 10 nm.[32] For FRET to occur, the emission spectrum of the donor must substantially overlap with the absorption spectrum of the acceptor.[33] Figure 1-11 shows this spectral overlap. The larger the overlap, the more energy transfer will occur.

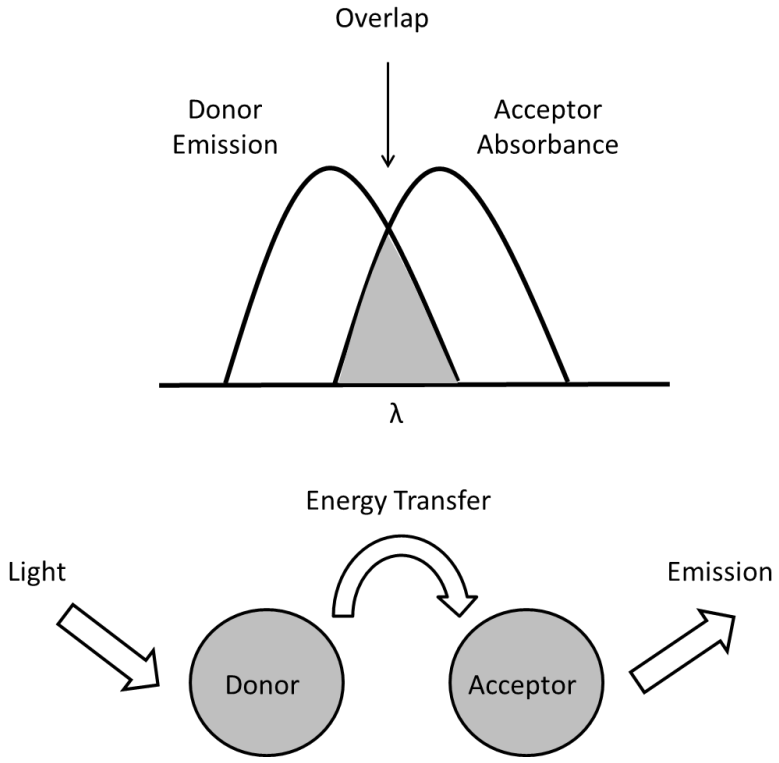

Figure 1-11. FRET energy transfer and overlap between the energy donor and the energy acceptor are shown. The donor is excited with light, some of its energy is transferred to the acceptor, and the acceptor's fluorescent emission is observed.

The most common energy donors and acceptors are fluorescent dyes. They are often described as "FRET pairs", because their spectral overlap is known and they are frequently paired together to achieve high efficiencies. Fluorescein isothiocyanate (FITC) and rhodamine B isothiocyanate (RITC), seen in Figure 1-12, are frequently used as a FRET pair, and are used throughout this work separately and together.[34-35]

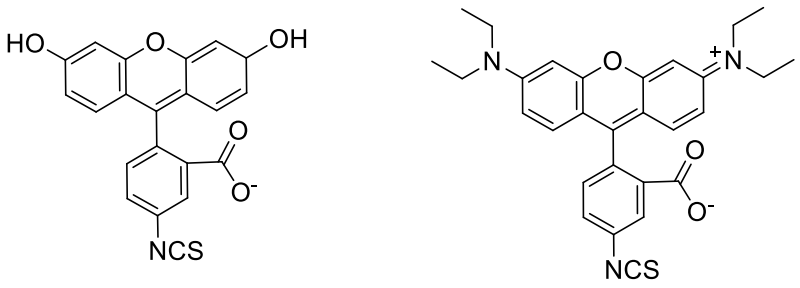

FITC

λex=495 nm
λem=525 nm

RITC

λex=520 nm
λem=576 nm

Figure 1-12. Chemical structures and excitation and emission wavelengths of Fluorescein isothiocyanate (FITC, donor) and rhodamine isothiocyanate (RITC, acceptor), a common FRET pair.[34-35]

Each dye pair has its own Forster distance (R_0), also called the critical distance, which is used along with the distance between the two dyes (r) to calculate the efficiency. When $R=R_0$, the efficiency is 50%. The sixth-power distance dependence seen in the efficiency equation 1-4 below makes FRET an extremely sensitive detection method.[32]

$$E = \frac{{R_0}^6}{{R_0}^6 + r^6} \qquad 1\text{-}4$$

Figure 1-13 shows a Jablonski diagram of the energy transfer process.[36] The donor is excited to a higher energy level by high energy light. While the donor can still fluoresce normally, if a suitable FRET acceptor is within the correct distance, some of the excited state energy is transferred non-radiatively to the acceptor, and the acceptor is excited. The acceptor emits lower energy fluorescence at its own emission wavelength. This unique FRET mechanism allows the acceptor dye to fluoresce when the system is excited at a wavelength other than the acceptor's excitation wavelength.

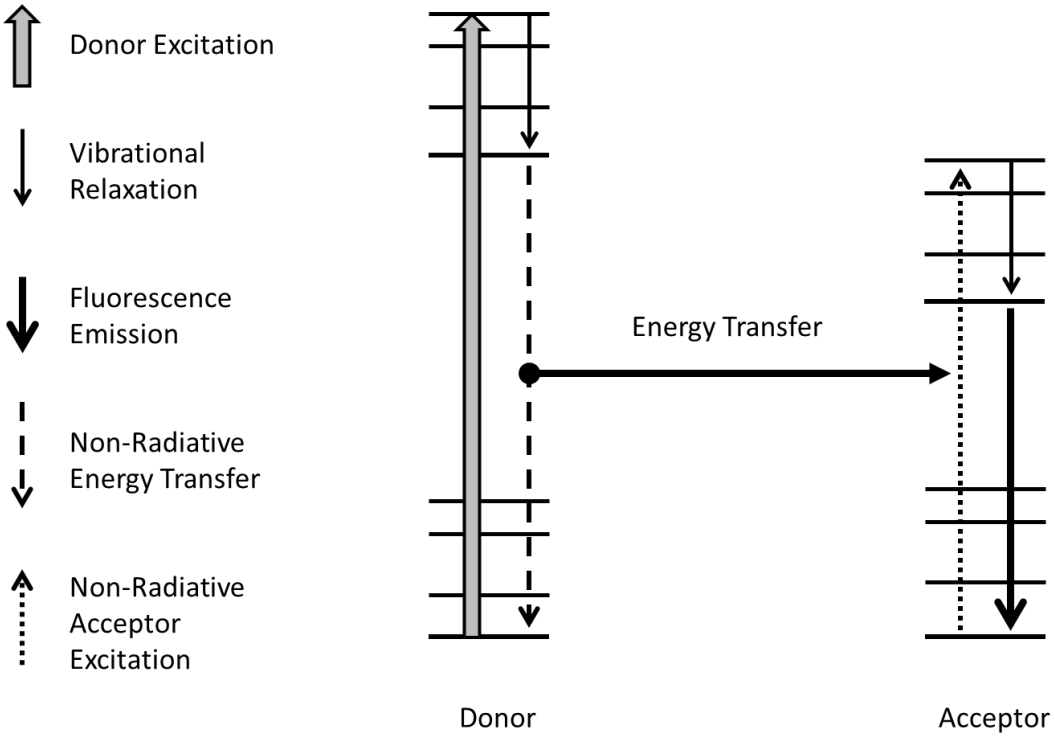

Figure 1-13. A Jablonski diagram adapted from Davidson shows the FRET process between an energy donor and acceptor.[36] A donor absorbs high energy light, transfers energy to the acceptor, and the acceptor fluoresces.

A plot of fluorescence intensity vs emission wavelength demonstrates what FRET looks like experimentally (Figure 1-14). Without FRET, the donor fluoresces normally and the acceptor does not. Under FRET conditions, the emission of the donor decreases, and the emission of the acceptor increases as energy is transferred from the donor to the acceptor.[37] This decrease in donor fluorescence is called quenching. As seen in Figure 1-13, the lower energy fluorescence of the acceptor explains why the acceptor emission wavelength is longer, or more red-shifted, than the donor emission wavelength.

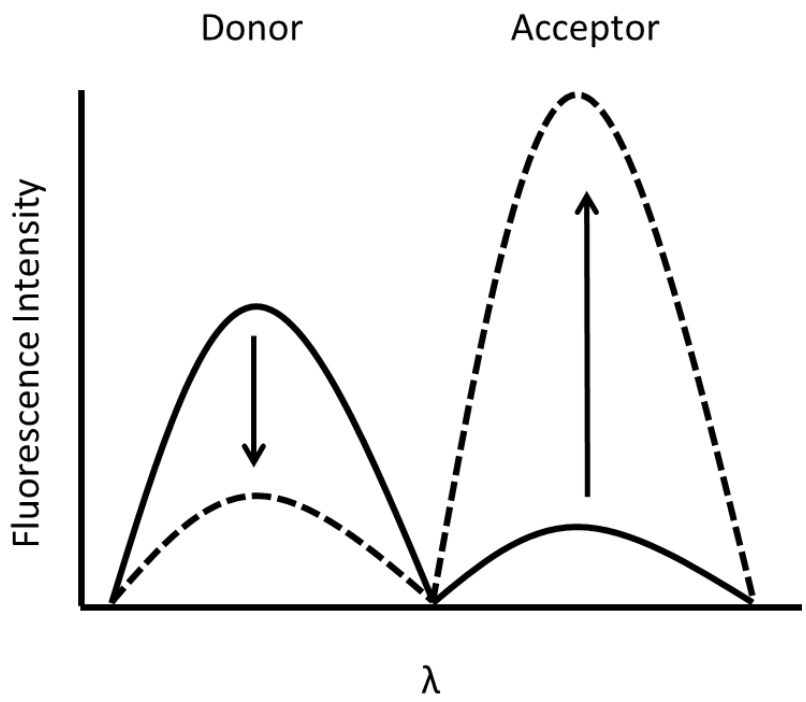

Figure 1-14. As a result of FRET, the fluorescent emission of the donor is quenched and the fluorescent emission of the acceptor is enhanced. The FRET spectra are shown by dotted lines (adapted from Kim).[37]

The FRET process can happen between two fluorescent dyes, but it can also occur between a fluorescent dye and an absorbing metal coordination complex, like in a fluorescent chemosensor. If the emission of the donor, the fluorescent dye, overlaps with the absorbance of the acceptor, the metal coordination complex, FRET will occur if the spacing is correct. Cu^{II}-Gx complexes absorb light around 605 nm, so both FITC and RITC have emission spectra that overlap with its absorption spectrum.[38] Figure 1-15 shows the FRET spectra of RITC and Cu^{II}-Gx.

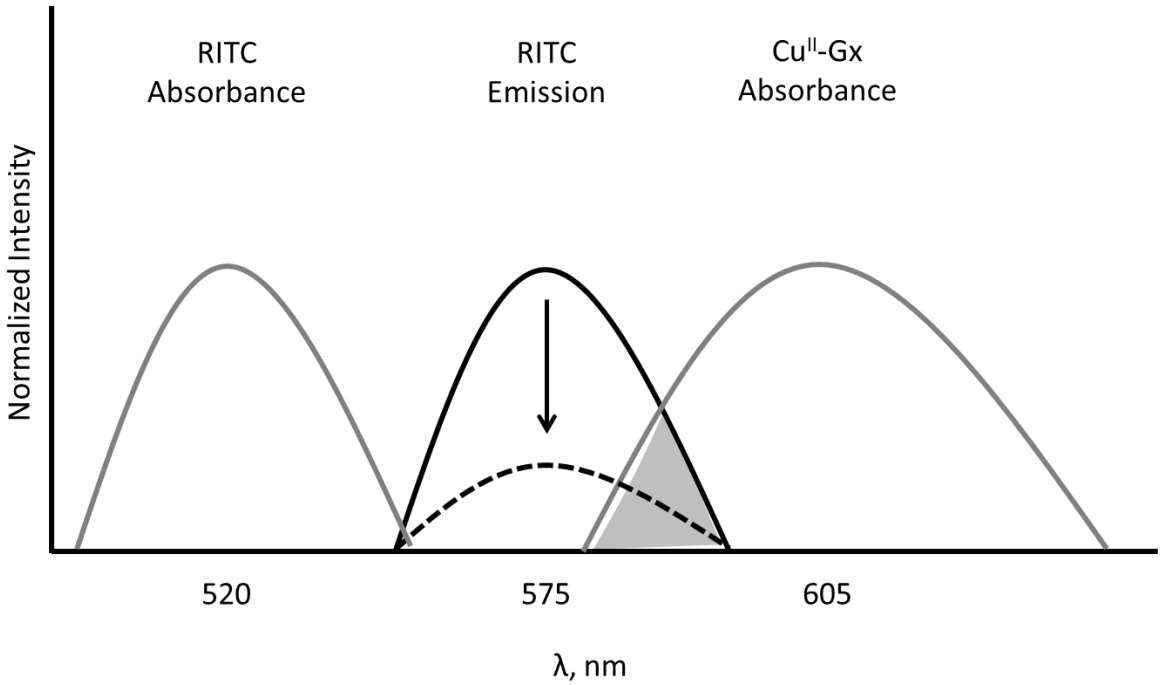

Figure 1-15. The normalized fluorescence (black) and absorption (grey) spectra of RITC and Gx in the absence (solid lines) and presence (dotted lines) of copper (II). FRET occurs under the assumption that the dye (RITC) and the dendrimer (Gx) are within the accepted FRET distance.

When the dye is excited, some of its energy is transferred to the Cu^{II}-Gx complex. This effectively quenches the emission of the fluorescent dye. This is called "turn-off" sensing. The acceptor complex does not fluoresce in the visible spectrum, so it is not seen in the fluorescence emission spectrum. If copper is removed from the system, "turn-on" sensing occurs as the fluorescence returns because the dye is no longer transferring energy to the Cu^{II}-Gx complex.

1.5 Research Goals

This thesis work focuses on synthesizing a nanoparticle-based fluorescent chemosensor for copper (II) ions, with the hypothesis that using PAMAM dendrimers as multi-functional surface modifiers will optimize the sensitivity and selectivity of the sensor. Frist, a series of nanoparticle-based sensors that differ in dendrimer generation and fluorescent dye were synthesized. These sensors were used to determine the optimum "turn-off" sensing characteristics for copper (II) ion sensing by varying dye, generation, pH, and surface charge. To study the "turn-on" sensing applications of the chemosensor, cyanide ion (CN^-) was

subsequently added to the system to bind to or remove copper (II) from the dendrimer and restore the fluorescence. Figure 1-16 summarizes the research goals.

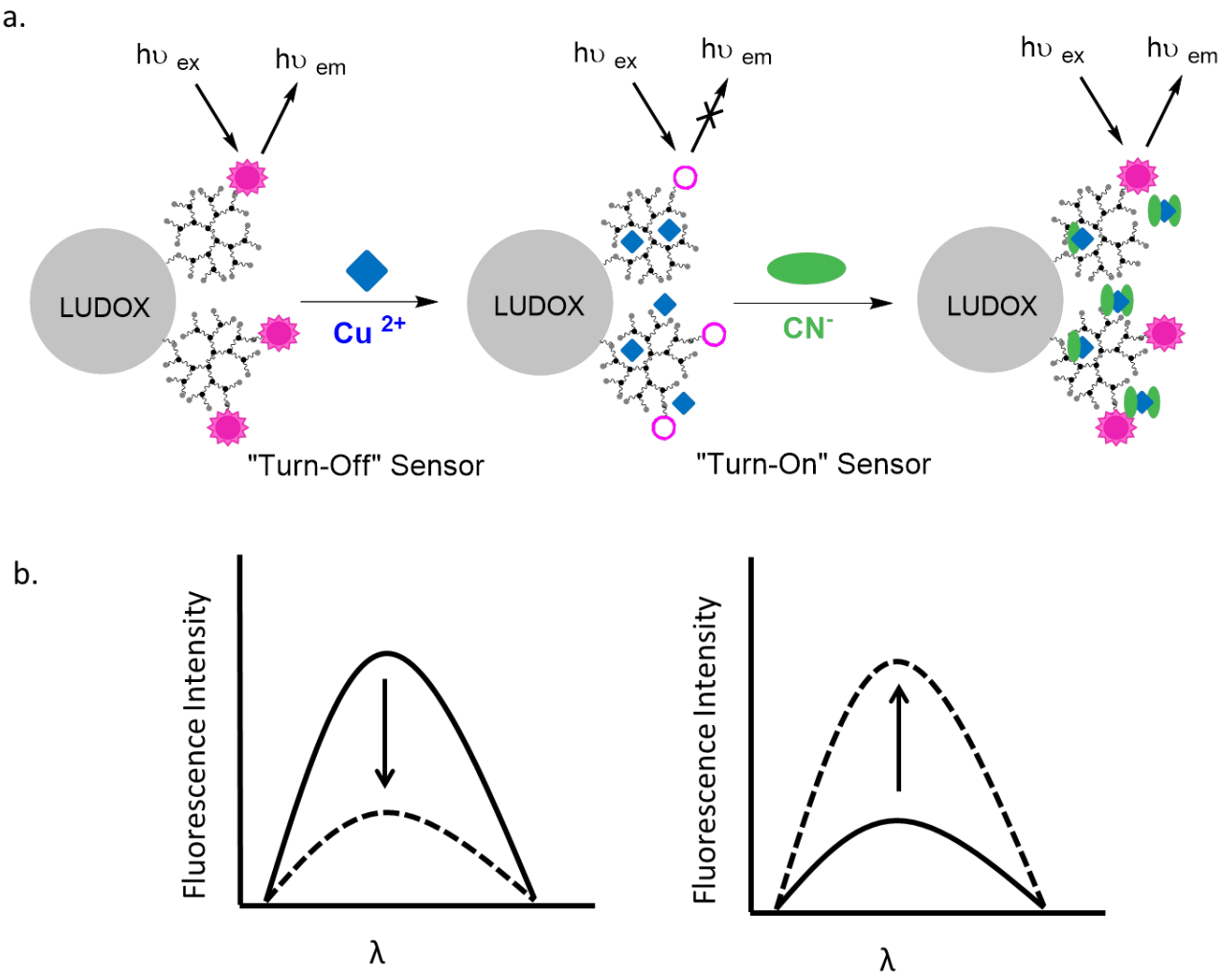

Figure 1-16. a) The overall fluorescent chemosensor is shown. The LUDOX SNP platform is tethered to Gx PAMAM dendrimers, which behave as both the receptor for copper (II) ions and the covalent linker to the signaling subunit, RITC or FITC fluorescent dye. When copper (II) is present, the fluorescence is quenched by energy transfer. When cyanide ion is present, it interrupts quenching and the fluorescence is restored. b) The corresponding emission spectra are shown, where the dotted line represents fluorescence after the respective substrate has been added.

1.6 References

1. Jeong, Y.; Yoon, J., Recent progress on fluorescent chemosensors for metal ions. *Inorg. Chim. Acta* **2012,** *381*, 2-14.
2. Shang, L.; Zhang, L.; Dong, S., Turn-on fluorescent cyanide sensor based on copper ion-modified CdTe quantum dots. *Analyst (Cambridge, U. K.)* **2009,** *134* (1), 107-113.
3. Zong, C.; Ai, K.; Zhang, G.; Li, H.; Lu, L., Dual-Emission Fluorescent Silica Nanoparticle-Based Probe for Ultrasensitive Detection of Cu2+. *Anal. Chem. (Washington, DC, U. S.)* **2011,** *83* (8), 3126-3132.
4. Candel, I.; Calero, P.; Martinez-Manez, R.; Sancenon, F.; Dolores Marcos, M.; Pardo, T.; Soto, J., Sensing properties of silica nanoparticles functionalized with anion binding sites and sulforhodamine B as fluorogenic signalling unit. *Inorg. Chim. Acta* **2012,** *381*, 188-194.
5. Fabbrizzi, L.; Licchelli, M.; Rabaioli, G.; Taglietti, A., The design of luminescent sensors for anions and ionisable analytes. *Coord. Chem. Rev.* **2000,** *205*, 85-108.
6. Bergonzi, R.; Fabbrizzi, L.; Licchelli, M.; Mangano, C., Molecular switches of fluorescence operating through metal centered redox couples. *Coord. Chem. Rev.* **1998,** *170*, 31-46.
7. Zeng, Q.; Cai, P.; Li, Z.; Qin, J.; Tang, B. Z., An imidazole-functionalized polyacetylene: convenient synthesis and selective chemosensor for metal ions and cyanide. *Chem. Commun. (Cambridge, U. K.)* **2008,** (9), 1094-1096.
8. Calero, P.; Hecht, M.; Martinez-Manez, R.; Sancenon, F.; Soto, J.; Vivancos, J. L.; Rurack, K., Silica nanoparticles functionalised with cation coordination sites and fluorophores for the differential sensing of anions in a quencher displacement assay (QDA). *Chem. Commun. (Cambridge, U. K.)* **2011,** *47* (38), 10599-10601.
9. Jung, H.-S.; Moon, D.-S.; Lee, J.-K., Quantitative analysis and efficient surface modification of silica nanoparticles. *J. Nanomater.* **2012**, 593471, 8 pp.
10. Bau, L.; Tecilla, P.; Mancin, F., Sensing with fluorescent nanoparticles. *Nanoscale* **2011,** *3* (1), 121-133.
11. Soto-Cantu, E.; Cueto, R.; Koch, J.; Russo, P. S., Synthesis and Rapid Characterization of Amine-Functionalized Silica. *Langmuir* **2012,** *28* (13), 5562-5569.
12. Cui, J.; Wang, S.; Huang, K.; Li, Y.; Zhao, W.; Shi, J.; Gu, J., Conjugation-induced fluorescence labelling of mesoporous silica nanoparticles for the sensitive and selective detection of copper ions in aqueous solution. *New J. Chem.* **2014,** *38* (12), 6017-6024.
13. Wang, L.; Tan, W., Multicolor FRET Silica Nanoparticles by Single Wavelength Excitation. *Nano Lett.* **2006,** *6* (1), 84-88.
14. Hotze, E. M.; Phenrat, T.; Lowry, G. V., Nanoparticle aggregation: challenges to understanding transport and reactivity in the environment. *J. Environ. Qual.* **2010,** *39* (6), 1909-1924.
15. LUDOX Colloidal Silica. Grace, Ed. 2012.
16. Tikhonov, A. M.; Asadchikov, V. E.; Volkov, Y. O., On the formation of a macroscopically flat phospholipid membrane on a hydrosol substrate. *JETP Letters* **2015,** *102* (7), 478-482.
17. LUDOX Colloidal Silica in Catalyst Applications. Grace, Ed. 2015.
18. Tomalia, D. A.; Baker, H.; Dewald, J.; Hall, M.; Kallos, G.; Martin, S.; Roeck, J.; Ryder, J.; Smith, P., A new class of polymers: starburst-dendritic macromolecules. *Polym. J. (Tokyo)* **1985,** *17* (1), 117-32.
19. Chang, C.-C. End-group Modifications to PAMAM Dendrimers Tethered on Glass Supports: Development of Indicator Displacement Assays (IDA) Based on Tethered Copper Chelates. M.S., University of San Franciso 2009.

20. Liu, C. Surface Tethered PAMAM Dendrimers On Controlled Pore Glass As Color Release Sensors For Phosphates. University of San Francisco, 2013.
21. Good, A. Metal Binding Behavior of Unmodified and Modified Surface Tethered PAMAM Dendrimers. University of San Francisco, 2008.
22. Chao, W. W.-S. Part 1: Solid Supports Modified with Dendrimers for Metal Ion Extraction. University of San Francisco, 2007.
23. Tomalia, D. A.; Naylor, A. M.; Goddard, W. A., III, Starburst dendrimers: control of size, shape, surface chemistry, topology and flexibility in the conversion of atoms to macroscopic materials. *Angew. Chem.* **1990,** *102* (2), 119-57.
24. Sigma-Aldrich Properties of PAMAM-NH2 Dendrimers. http://www.sigmaaldrich.com/materials-science/nanomaterials/dendrimers/properties.html.
25. Naylor, A. M.; Goddard, W. A., III; Kiefer, G. E.; Tomalia, D. A., Starburst dendrimers. 5. Molecular shape control. *J. Am. Chem. Soc.* **1989,** *111* (6), 2339-41.
26. Maiti, P. K.; Cagin, T.; Wang, G.; Goddard, W. A., III, Structure of PAMAM Dendrimers: Generations 1 through 11. *Macromolecules* **2004,** *37* (16), 6236-6254.
27. Diallo, M. S.; Christie, S.; Swaminathan, P.; Balogh, L.; Shi, X.; Um, W.; Papelis, C.; Goddard, W. A., III; Johnson, J. H., Jr., Dendritic Chelating Agents. 1. Cu(II) Binding to Ethylene Diamine Core Poly(amidoamine) Dendrimers in Aqueous Solutions. *Langmuir* **2004,** *20* (7), 2640-2651.
28. Cakara, D.; Kleimann, J.; Borkovec, M., Microscopic Protonation Equilibria of Poly(amidoamine) Dendrimers from Macroscopic Titrations. *Macromolecules* **2003,** *36* (11), 4201-4207.
29. Shi, X.; Thomas, T. P.; Myc, L. A.; Kotlyar, A.; Baker, J. J. R., Synthesis, characterization, and intracellular uptake of carboxyl-terminated poly(amidoamine) dendrimer-stabilized iron oxide nanoparticles. *Physical Chemistry Chemical Physics* **2007,** *9* (42), 5712-5720.
30. Majoros, I. J.; Keszler, B.; Woehler, S.; Bull, T.; Baker, J. R., Jr., Acetylation of Poly(amidoamine) Dendrimers. *Macromolecules* **2003,** *36* (15), 5526-5529.
31. Ottaviani, M. F.; Montalti, F.; Turro, N. J.; Tomalia, D. A., Characterization of Starburst Dendrimers by the EPR Technique. Copper(II) Ions Binding Full-Generation Dendrimers. *The Journal of Physical Chemistry B* **1997,** *101* (2), 158-166.
32. Hillisch, A.; Lorenz, M.; Diekmann, S., Recent advances in FRET: distance determination in protein-DNA complexes. *Curr. Opin. Struct. Biol.* **2001,** *11* (2), 201-207.
33. Hink, M. A.; Visser, N. V.; Borst, J. W.; Van Hoek, A.; Visser, A. J. W. G., Practical Use of Corrected Fluorescence Excitation and Emission Spectra of Fluorescent Proteins in Förster Resonance Energy Transfer (FRET) Studies. *Journal of Fluorescence* **2003,** *13* (2), 185-188.
34. Rhodamine B Isothiocyanate http://www.sigmaaldrich.com/catalog/product/aldrich/283924?lang=en&region=US.
35. Fluorescein Isothiocyanate. http://www.sigmaaldrich.com/catalog/substance/fluoresceinisothiocyanateisomeri38938332632711?lang=en&region=US.
36. Davidson, M. W.; Fellers, T. J.; Herman, B.; Frohlich, V. E. C.; Lakowicz, J. R. Molecular Expressions. Optical Microscopy Primer: Specialized Techniques. https://micro.magnet.fsu.edu/primer/techniques/index.html.
37. Kim, Y.; Shin, S. A.; Lee, J.; Yang, K. D.; Nam, K. T., Hybrid system of semiconductor and photosynthetic protein. *Nanotechnology* **2014,** *25* (34), 342001/1-342001/20.
38. Zhou, L.; Russell, D. H.; Zhao, M.; Crooks, R. M., Characterization of Poly(amidoamine) Dendrimers and Their Complexes with Cu2+ by Matrix-Assisted Laser Desorption Ionization Mass Spectrometry. *Macromolecules* **2001,** *34* (11), 3567-3573.

Chapter 2
Synthesis and Characterization of Fluorescent Dendrimer Modified Silica Nanoparticles

This chapter outlines the synthesis of silica nanoparticles modified with PAMAM dendrimers and fluorescent dyes (SNPGx-Dye), and summarizes the methods and results of their characterization.

2.1 Introduction

As discussed in Chapter 1, a fluorescent chemosensor is made up of a platform for synthesis, a receptor for the analyte, a signaling subunit, and a linker covalently connecting the receptor and the signaling subunit.[1-2] In this work, 20 nm commercial LUDOX silica nanoparticles (SNP) are the platform, PAMAM dendrimers are the receptor and covalent linker, and fluorescein isothiocyanate (FITC) and rhodamine B isothiocyanate (RITC) are the signaling subunits. Utilizing SNP as the platform simplifies the work up of every synthetic step, as the modified nanoparticles can be isolated by centrifugation. Covalently tethered PAMAM dendrimers function as both copper (II) ion chelators and as covalent linkers to the fluorescent dyes on the surface. Only the synthesis and characterization of these chemosensors are discussed in this chapter; their ion sensing results are introduced in Chapter 3.

2.2 Materials and Instrumentation

All reagents were used directly without further purification. Anhydrous solvents were dried over 3 Å molecular sieves in a 160°C oven for 24 hours. All relevant information for chemicals used in this chapter, including the acronyms used in this thesis, is listed after each chemical.

2.2.1 Chemicals

The following chemicals were obtained: LUDOX AS-30 colloidal silica (Sigma-Aldrich, 30% wt. in H_2O, CAS 7631-86-9, FW 60.08); (3-Aminopropyl)triethoxysilane (APTES, Sigma-Aldrich, 99%, CAS 919-30-2, FW 221.37); Ethanol (Sigma-Aldrich, 200 proof, 99.5%, CAS 64-17-5, FW 46.07); Acetic acid (Pharmco-Aaper, glacial, 99.7%, CAS 64-19-7, FW 60.05); 1,1'-Carbonyldiimidazole (CDI, Sigma-Aldrich, 99%, CAS 530-62-1, FW 162.15); Sodium phosphate dibasic (Sigma-Aldrich, 99.0%, CAS 7558-79-4, FW 141.96); 1,4-Dioxane (EMD Millipore, anhydrous, 99.9%, CAS 123-91-1, FW 88.11); PAMAM dendrimer generation 1, ethylene diamine core (G1, Sigma-Aldrich, 20% wt. in MeOH, CAS 142986-44-5, FW 1429.88); PAMAM

dendrimer generation 3, ethylene diamine core (G3, Sigma-Aldrich, 20% wt. in MeOH, CAS 153891-46-4, FW 6908.84); PAMAM dendrimer generation 4, ethylene diamine core (G4, Sigma-Aldrich, 10% wt. in MeOH, CAS 163442-67-9, FW 14214.17); PAMAM dendrimer generation 5, ethylene diamine core (G5, Sigma-Aldrich, 5% wt. in MeOH, CAS 163442-68-0, FW 28824.81); Dimethyl sulfoxide (DMSO, Sigma-Aldrich, 99.5%, CAS 67-68-5, FW 78.13); Rhodamine B isothiocyanate (RITC, Santa Cruz Biotechnology, 95%, CAS 36877-69-7, FW 536.08); Fluorescein isothiocyanate (FITC, Sigma-Aldrich, 90%, CAS 3326-32-7, FW 389.38); Succinic anhydride (Sigma-Aldrich, 99%, CAS 108-30-5, FW100.07); 1,2,3-Indantrione (ninhydrin, Baker, 99%, CAS 485-47-2, FW 178.15); 5-amino-1-pentanol (Alfa Aesar, 97%, CAS 2508-29-4, FW 103.17); Imidazole (Sigma-Aldrich, 99%, CAS 288-32-4, FW 68.1).

2.2.2 Instrumentation

UV-Visible measurements were conducted on a Varian Cary 5000 spectrophotometer using Cary WinUV Software. Sonication was carried out in a Branson 2210 temperature controlled sonicator. Centrifugation was performed using both Beckman J2-21 and Beckman J2-MC centrifuges, both with the Beckman JA-20 rotor. Attenuated Total Reflectance Fourier Transform Infrared spectrometry (ATR-FTIR) measurements were done on a Perkin-Elmer Spectrum 100 ATR-FTIR with Spectrum software. Zeta potential measurements were done on a Malvern ZS90 Zetasizer with Malvern software, located at St. Could State University in St. Cloud, Minnesota.

2.3 Preparation of Fluorescent G1-G5 Silica Nanoparticles

A sequence of four reactions was carried out to synthesize a series of SNP-Gx-Dye chemosensors that varied in dendrimer generation and fluorescent dye. First, LUDOX SNPs were modified with (3-aminopropyl)triethoxysilane (APTES) to convert the surface hydroxyl groups into amines. Next, 1,1'-carbonyldiimidazole (CDI) was added to activate the surface for dendrimer attachment. G1-G5 PAMAM dendrimers were subsequently tethered to the nanoparticle through CDI. Finally, fluorescein isothiocyanate (FITC) or Rhodamine isothiocyanate (RITC) were bound to the dendrimer through their isothiocyanate functional groups. The synthetic scheme is shown in Figure 2-1. Some of these SNP systems were further modified with succinic anhydride to convert the surface amines to carboxylic acids.

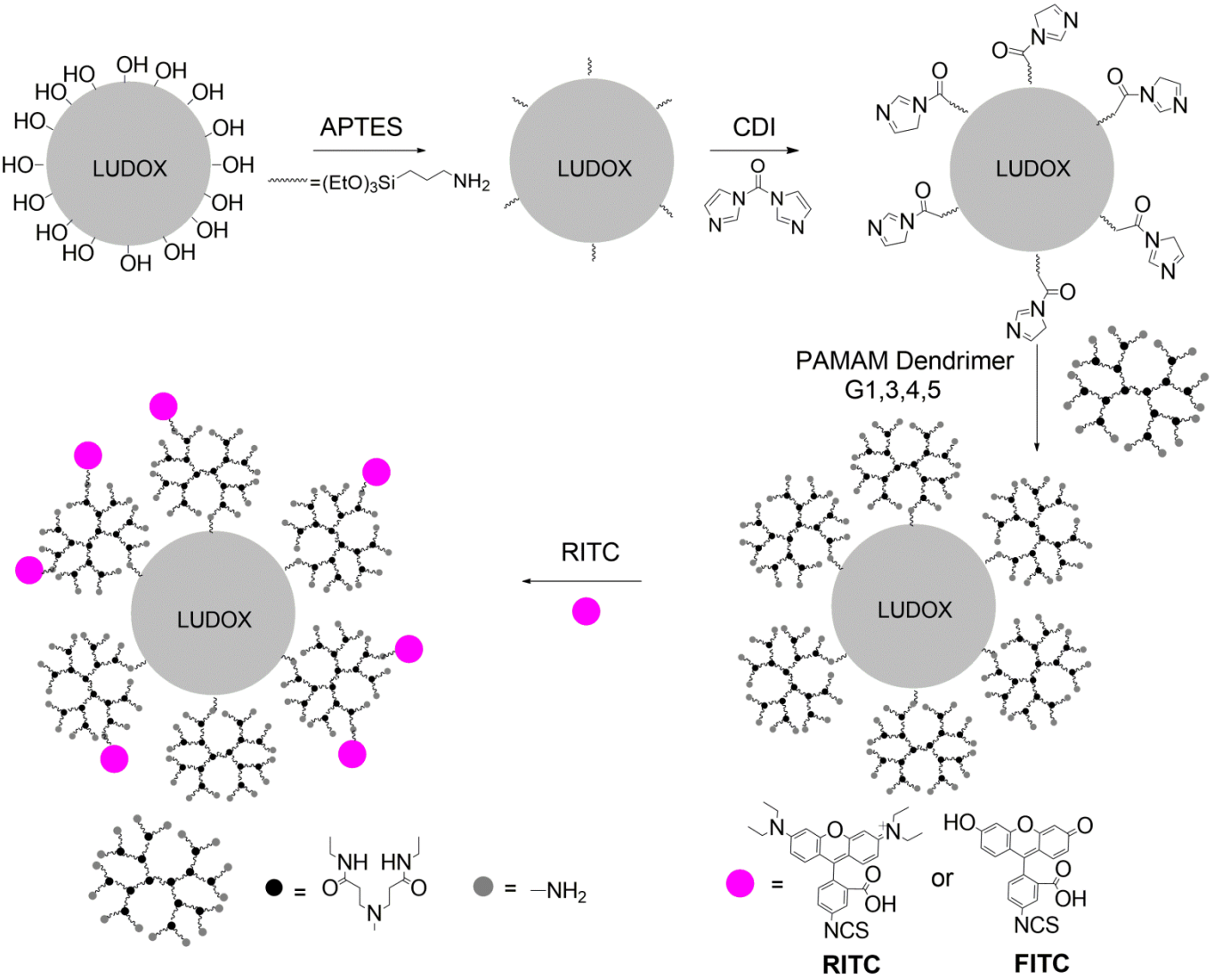

Figure 2-1. The overall 4 step synthesis of SNPGx-Dye chemosensors.

2.3.1 Synthetic Procedures

Synthetic steps 2 and 3 (CDI activation and dendrimer attachment) were adapted for silica nanoparticles based on previous work done in this research group on controlled pore glass (CPG) modified with APTES.[3-4] Steps 1 and 4 were adapted from previous work done by Candel *et al*. on SNP based anion sensors and Kwon *et al*. on lead chemosensors.[1, 5]

2.3.1.1 LUDOX Surface Modification with Amines

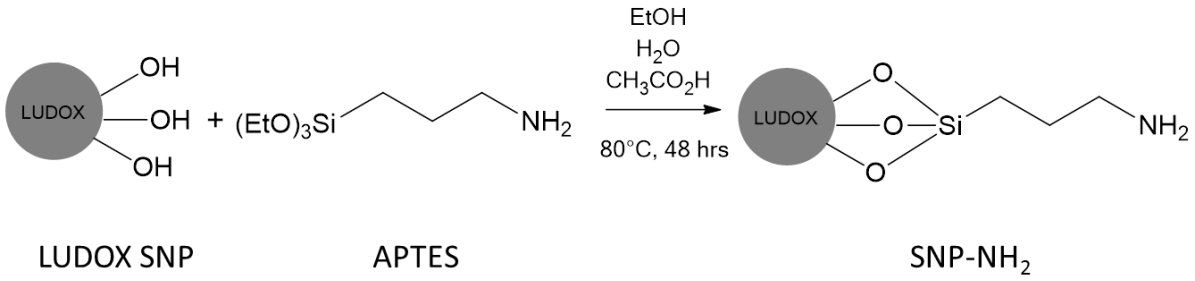

Figure 2-2. LUDOX SNP surface modification with APTES. This surface modification allows an activating group to be added in the next step, followed by dendrimer addition.

LUDOX particles (20 mL) as a 30% wt solution in water were taken up in 220 mL of a degassed solvent system of 1:1:1.6 H_20:CH_3CO_2H:EtOH. Liquid APTES (1.2 mL, 5.2 mmol) was added and the solution was stirred at 80°C under a nitrogen atmosphere for 48 h.[1] The ethanol was evaporated under reduced pressure and the pH of the remaining reaction mixture was raised to 5 with sodium bicarbonate. The material was centrifuged at 15,000 RPM for 55 min. The supernatant was decanted, and the resulting solid was washed with ethanol and centrifuged at 15,000 RPM for 35 min. The supernatant was decanted, and the washing was repeated twice. The remaining material was vacuum dried and stored in a desiccator overnight, yielding 1.49 g of a white solid.

2.3.1.2 CDI Activation of SNP-NH2 for Dendrimer Attachment

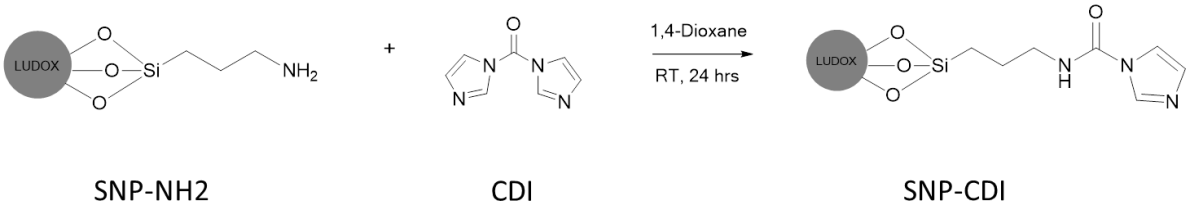

Figure 2-3. CDI activation of SNP-NH2 to prepare for dendrimer addition.

SNP-NH_2 (1.30 g) and CDI (0.30 g, 1.9 mmol, 40x excess) were taken up in 15 mL of dry 1,4-dioxane. The reaction was stirred at room temperature under a nitrogen atmosphere for 24 h. The resulting mixture was centrifuged at 15,000 RPM for 60 min. The supernatant was decanted, and the resulting solid was washed with dioxanes and centrifuged at 15,000 RPM for 30 min. The supernatant was decanted, and the washing was repeated twice. The remaining

material was vacuum dried and stored in a desiccator overnight, yielding 1.14 g of an off-white solid.

2.3.1.3 Gx PAMAM Dendrimer Attachment to SNP-CDI

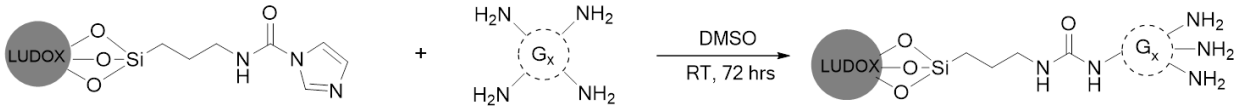

SNP-CDI | Gx PAMAM Dendrimer | SNPGx

Figure 2-4. G1, G3, G4, and G5 PAMAM dendrimer addition to CDI activated SNP.

PAMAM dendrimer solutions (G1, G3, G4, and G5; 10% v/v in methanol) were pipetted into scintillation vials, and the solvent was evaporated by nitrogen flow. The amount of dendrimer solution used was determined using a table of dendrimer properties previously determined by this research group (Table 2-1).[3] The remaining thin film was taken up in 20 mL of dimethyl sulfoxide (DMSO) and transferred to a round bottom flask. SNP-CDI (570 mg for the G4 reaction) was added to the flask, and the reaction was stirred at room temperature under a nitrogen atmosphere for 72 h.[3] The resulting mixture was centrifuged at 15,000 RPM for 60 min. The supernatant was decanted, and the resulting solid was washed with ethanol and centrifuged at 15,000 RPM for 30 min. The supernatant was decanted, and the washing was repeated twice. The remaining material was vacuum dried and stored in a desiccator overnight, yielding a 474 mg of a yellow solid for the G4 reaction(**SNPGx**).

Table 2-1. Volumes of dendrimer used per one gram of CDI-activated SNP.[3]

Generation	Volume (mL)
1	0.139
2	0.182
3	0.250
4	0.659
5	1.86

2.3.1.4 Dye Attachment to SNPGx

RITC Attachment:[5]

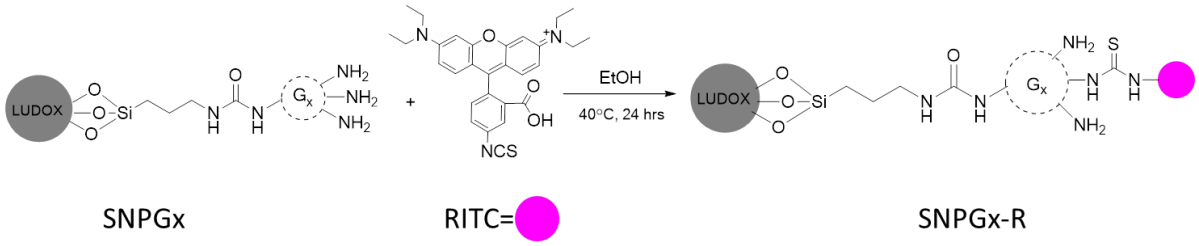

Figure 2-5. SNPGx modification with RITC fluorescent dye.

SNPGx (380 mg for SNPG4) was taken up in 70 mL dry ethanol, and 5-10 mg RITC was added. The reaction was stirred at 40°C under a nitrogen atmosphere for 24 h away from light. The resulting mixture was centrifuged at 15,000 RPM for 60 min. The fluorescent supernatant was decanted, and the resulting solid was washed with ethanol and centrifuged at 15,000 RPM for 30 min. The supernatant was decanted, and the washing was repeated until no fluorescence remained in the wash. The remaining material was vacuum dried and stored in a desiccator overnight, yielding 242 mg of a pink solid for the G4 reaction (**SNP-Gx-R**).

FITC Attachment:[5]

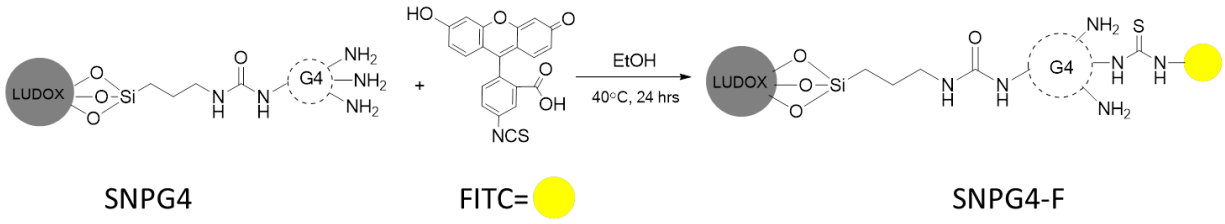

Figure 2-6. SNPG4 modification with FITC fluorescent dye.

SNPG4 (380 mg) were taken up in 70 mL dry ethanol, and 5-10 mg FITC was added. The reaction was stirred at 40°C under a nitrogen atmosphere for 24 h away from light. The resulting mixture was centrifuged at 15,000 RPM for 60 min. The fluorescent supernatant was decanted, and the resulting solid was washed with ethanol and centrifuged at 15,000 RPM for 30 min. The supernatant was decanted, and the washing was repeated until no fluorescence remained in the wash. The remaining material was vacuum dried and stored in a desiccator overnight, yielding 220 mg of a yellow solid (**SNP-G4-F**).

2.3.1.5 Carboxylation of Dendrimer Surface Amines

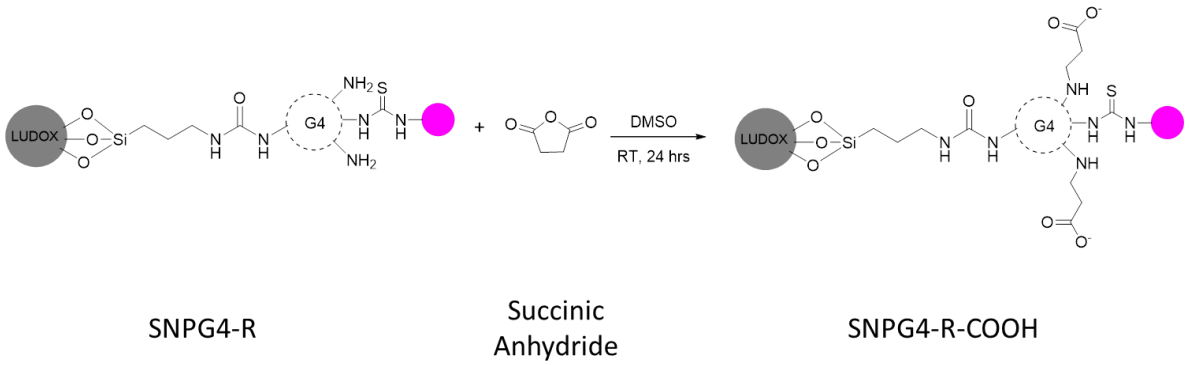

Figure 2-7. Conversion of dendrimer surface amines to carboxylic acid with succinic anhydride.

SNPG4-R (150 mg) were taken up in 10 mL of DMSO. A solution of succinic anhydride (150 mg, 1.5 mmol) in 5 mL DMSO was added to the nanoparticle solution and stirred for 24 h at room temperature.[6] The resulting mixture was centrifuged at 15,000 RPM for 60 min. The supernatant was decanted, and the resulting solid was washed with ethanol and centrifuged at 15,000 RPM for 30 min. The supernatant was decanted, and the washing was repeated twice. The remaining material was vacuum dried and stored in a desiccator overnight, yielding 130 mg of a pink solid (**SNP-G4-R-COOH**).

2.3.2 Characterization

The series of SNP-Gx-Dye systems were characterized after each synthetic step by the methods introduced below. The results of these characterizations can be found in section 2.4.

2.3.2.1 Amine Quantification by Ninhydrin Assay

A series of 4 mL standard solutions of 5-amino-1-pentanol were prepared in ethanol, and 1 mL of a prepared 1,2,3-Indantrione monohydrate (ninhydrin) solution (0.35% w/v in ethanol) was added to each standard. The standards were heated at 65°C for 35 min, and turned varying shades of blue. The absorbance was measured by visible spectroscopy at 588 nm after the standards cooled to room temperature. A calibration curve was created from the standards. SNPGx (0.10 g) were sonicated in ethanol for 30 min, and 1 mL of the ninhydrin solution was added. The solution was sonicated again for 10 min, centrifuged, and the amines in the supernatant were quantified.[7] This procedure was repeated following dendrimer attachment, and again after carboxylation of the surface amines. During the assay following carboxylation, the absorbance from the attached RITC dyes increased the absorbance of the sample.

Therefore, following dye loading results, a constant amount of RITC was added to each 5-amino-1-pentanol standard to account for the dye interference.

2.3.2.2 Imidazole Quantifiaction

A series of standard solutions of imidazole were prepared in water from a 10 mM stock solution, and 2 mL of a prepared sodium dibasic phosphate solution (5.0 mM) was added to each standard. A calibration curve was created from the UV absorbance measurements of the standards at 208 nm. A sample of SNP-CDI (10 mg) was taken up in 15 mL of the phosphate solution. The sample was sonicated for 2 h at 50°C, and imidazole groups on the surface were quantified using the calibration curve.[8]

2.3.2.3 SNPGx-R and SNPGx-F Dye Loading

A series of standard solutions of RITC or FITC were created in ethanol, and visible absorbance measurements were taken at the peak wavelength (RITC=520 nm, FITC=495 nm) to create a calibration curve. A sample of SNP-Gx-Dye (~7 mg) was sonicated in 4 mL of ethanol for 30 minutes. The measurements at the corresponding wavelength and the calibration curve were used to quantify the dye loading of the nanoparticles.

2.3.2.4 FTIR

Dry samples of LUDOX, SNPG4, SNPG4-R, and SNPG4-R-COOH were analyzed by attenuated total reflectance Fourier transform infrared spectroscopy (ATR-FTIR) at room temperature using a Perkin Elmer 100.

2.3.2.5 Zeta Potential

Solutions of SNPG4-R and SNPG4-R-COOH were made in 2:1 EtOH:H_2O with a concentration of 0.06 mg/mL and a salt concentration of 10 mM NaCl and the pH was adjusted to 2, 4, 5, 6, 7, 8, and 10. Less than 1 mL of the sample was put in a DTS1070 disposable folded capillary cell and the zeta potential was measured with a 633 nm laser Malvern zetasizer (St. Could State University). The Smoluchowski approximation was used in the settings of the software.

2.4 Results and Discussion

The synthetic and characterization results of the procedures described in section 2.3.2 are discussed below.

2.4.1 Amine Density

The ninhydrin assay described in section 2.3.2.1 was done on the particles listed in Table 2-2 below. Ninhydrin reacts only with primary amine groups to form a blue-purple complex known as “Ruhemann’s purple”, or RP, as seen in Figure 2-8. [9-10]

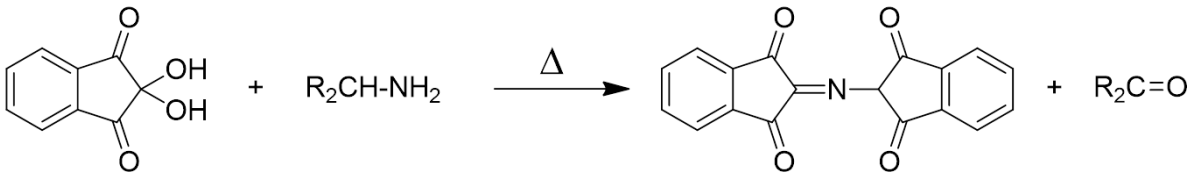

Ninhydrin (colorless) | Primary Amine | Ruhemann’s Purple λ_{max}=588 nm

Figure 2-8. The reaction between ninhydrin and a primary amine is shown, forming Ruhemann’s purple complex that is the basis of the amine density assay. Adapted from Bottom.[10]

As the amines on the SNP are surface bound, not all will react as in Figure 2-8. Therefore, the results of the ninhydrin assay shown in Table 2-2 in μmol/g and atoms NH_2/nm^2 only represent the available amines. Equation 2-2 was adapted from the standard Equation 2-1 below to simplify the conversion to atoms NH_2/g; Avagadro’s number, g is the grams of dry nanoparticles used, and A is the surface area of where V is the volume of the solution in liters, N_A is one nanoparticle in nm^2/g.[3, 11-12] In Equation 2-1, the [NH_2] must be in mol/L; in Equation 2-2, the [NH_2] is in mol/g.

$$\text{Amine Density}\left(\frac{atoms\ NH_2}{g\ NP}\right) = \frac{[NH_2](V)(N_A)}{(A)(g)} \qquad 2\text{-}1$$

$$\text{Amine Density}\left(\frac{atoms\ NH_2}{g\ NP}\right) = \frac{[NH_2](N_A)}{(A)} \qquad 2\text{-}2$$

As the dendrimer generation increases, the amine density values also increase. As the number of theoretical primary amines on the surface of the dendrimer doubles with each increasing generation, it was expected that the amine density of the dendrimers on SNP would also double. The experimental data in Table 2 falls below that trend, especially between G4 and G5. As discussed in Chapter 1, the shape PAMAM dendrimers change from flat disks to large spheres at generation 3. The large and spherical nature of higher generations may cause the dendrimer loading on the nanoparticle to plateau, as there is a limited amount of SNP surface area to bind to. The ninhydrin can only react with available primary amines, and the larger

dendrimers may have more closely packed and inaccessible amines. In addition, the open structured smaller dendrimers may be binding to the SNP with a more of their terminal amines than the larger spherical dendrimers. The results of the amine density quantification prove that the dendrimer addition reaction was successful for each generation.

Table 2-2. Amine densities for SNPGx-Dye determined by the ninhydrin assay in two common units.

System	Amine Density (μmol/g)	Amine Density (atoms NH_2/nm^2)
$SNPNH_2$-R	16	0.04
SNPG1-R	39	0.10
SNPG3-R	59	0.15
SNPG4-R	113	0.30
SNPG5-R	136	0.36
SNPG4-F	113	0.30
SNPG4-R-COOH	24	0.06

The ninhydrin assay was performed on SNPG4-R-COOH after the primary surface amines were converted into carboxylic acids to determine if the reaction was successful. The reaction decreased the surface amines by about 80%, which shows that the majority of the primary amines on the surface were converted successfully. This was consistent with the FTIR analysis in section 2.4.3.

2.4.2 Dye Loading

The amount of dye on the surface of the nanoparticle systems was quantified using the dye loading procedure described in section 2.3.2.3. Table 2-3 summarizes the results of the quantification.

Table 2-3. Dye loading for RITC and FITC on SNPGx-Dye.

System	Dye loading (μmol/g)
Amine NP-R	8.6
SNPG1-R	8.9
SNPG3-R	9.3
SNPG4-R	38
SNPG5-R	26
SNPG4-F	62
SNPG4-R-COOH	38

The dye loading for the lower generation dendrimers are similar, with a large jump between G3 and G4. This is most likely due to the shift in shape from disked to spherical; G1 and G3 are spread out flatly around the SNP and have similar spacing between available primary amines, while G4 and G5 are more densely packed around the SNP. The highest dye loading is on G4 particles, which suggests that it has the most accessible primary amines for dye attachment. The decrease in dye loading from G4 to G5 indicates that the limit of the close packing of spheres on the surface of the SNP may be reached at G4. While the results of the ninhydrin assay show that G5 has more available primary amines than G4, the dye loadings suggest that the large RITC cannot necessarily access all of those primary amines. The increase in dye loading between SNPG4-R and SNPG4-F also suggests that the primary amines are more easily accessed by FITC than RITC. However, FITC was only used in one synthesis and therefore this hypothesis cannot be confirmed.

The emission intensities of SNPGx-R and SNPGx-F were virtually unchanged from simple RITC and FITC solutions in the same solvent system (λ_{em} SNPGx-R=576 nm, λ_{em} SNPGx-F=525 nm). This behavior suggests that the dyes tethered to the dendrimer on the SNP experience similar environments to their free counterparts in solution. This may mean that the dyes are solvated near the outside of the dendrimer and not buried within it, although no additional work was done to confirm this. The excitation and emission maximums for RITC and FITC depend largely on the solvent system; to eliminate this variable, 2:1 EtOH:H_2O was used throughout this thesis work.

2.4.3 FTIR

Attenuated total reflectance Fourier transform infrared spectroscopy (ATR-FTIR) was performed on the particles in section 2.3.2.4 to confirm the success of various synthetic steps. The resulting spectra are seen in Figure 2-9 below.

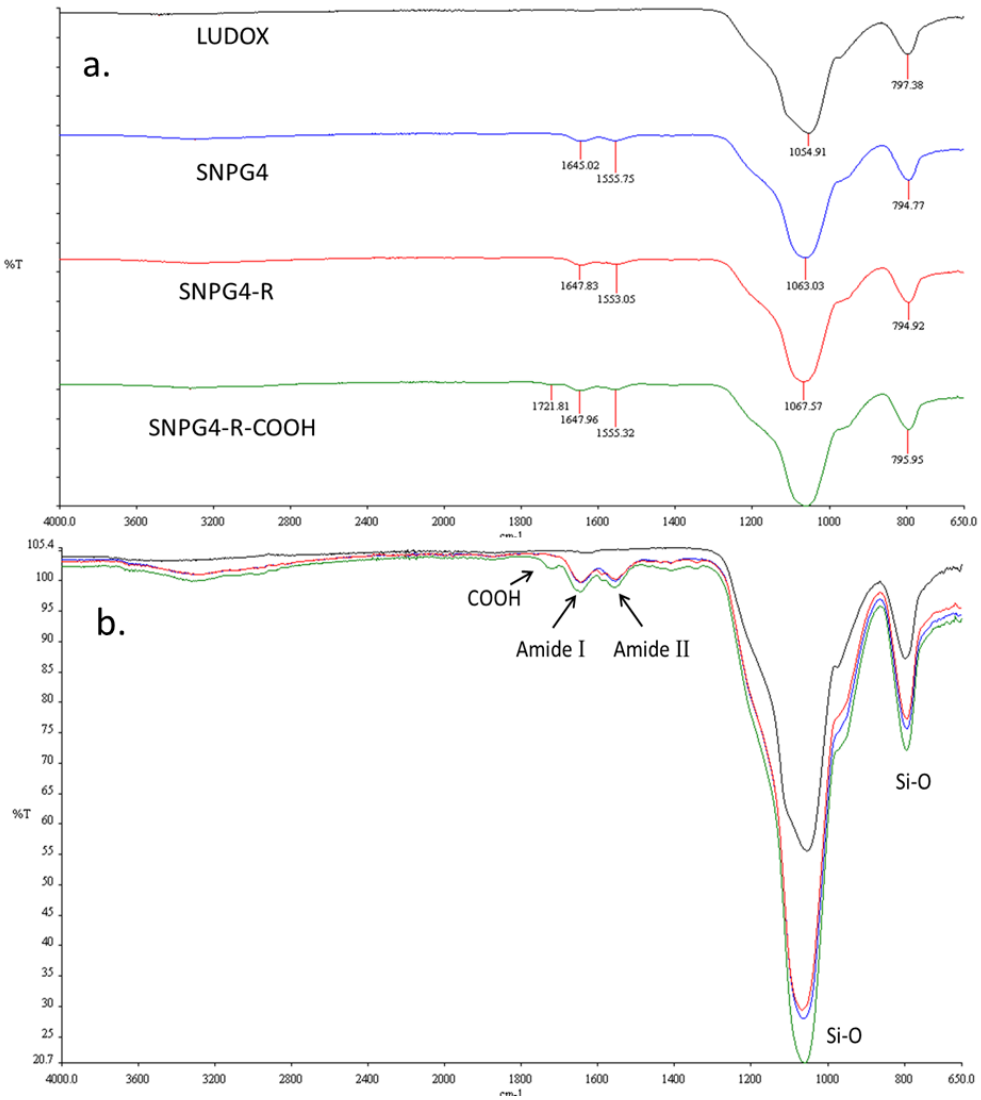

Figure 2-9. a) ATR-FTIR spectra of LUDOX SNP (black), SNPG4 (blue), SNPG4-R (red), and SNPG4-R-COOH (green). b) The spectra in (a) are overlaid to easily determine the differences in their peaks.

All four samples exhibit the typical Si-O stretching from the LUDOX SNP around 793 cm^{-1} and 1100 cm^{-1}.[13] The amide groups in PAMAM dendrimers have two characteristic IR stretching frequencies: 1660 cm^{-1} (Amide I) and 1560 cm^{-1} (Amide II).[14] The appearance of the Amide I and Amide II peaks in Figure 2-9b supports the results of the amine density quantification and confirms the success of the dendrimer addition reaction. The spectrum for SNPG4-R-COOH exhibits a small peak at 1722 cm^{-1} that the previous spectra do not. This falls within the 1690-1760 cm^{-1} range of stretching frequencies that are typical of C=O carboxylic acid bonds.[15] The appearance of the 1722 cm^{-1} peak in the SNPG4-R-COOH spectrum confirms that the conversion of surface amines to carboxylic acids was successful, which is corroborated by the decrease in amine density. Table 2-4 summarizes these FTIR results.

Table 2-4. Theoretical and experimental FTIR stretching frequencies for LUDOX, SNPG4, SNPG4-R, and SNPG4-R-COOH.

Bond	FTIR Frequency (cm^{-1})				
	Theoretical	LUDOX	SNPG4	SNPG4-R	SNPG4-R-COOH
Si-O	793.4	797.38	794.77	794.92	795.95
	1100	1054.91	1063.03	1067.57	1069.45
Amide II	1560	-	1555.75	1553.05	1555.32
Amide I	1660	-	1645.02	1647.83	1647.96
Carboxylic Acid C=O	1690-1760	-	-	-	1721.81

The FTIR spectra are all overpowered by the large concentration of silica in each sample; the amide and carbonyl peaks are dwarfed in comparison to the silica peaks. While this does not inhibit the visualization of the amides or carbonyls, it does affect the ability to observe a change in frequency upon the addition of RITC dye. The overlaid spectra for SNPG4 and SNPG4-R in Figure 2-9b are essentially identical. The concentration of silica, amides, and carboxylic acids dominates the much smaller concentration of dyes, causing any RITC stretches to be hidden. However, the dye addition is confirmed both by a visual color change of the particles, as well as the dye loading quantification.

2.4.4. Dispersibility

The ability to fully disperse modified nanoparticles in solution is an important factor in the success of nanoparticle based sensors.[16] The dispersibility of nanoparticles is largely solvent dependent, and nanoparticles modified with organic components are often difficult to disperse in

aqueous solution.[17] This is problematic because many potential analytes are in drinking water or aqueous biological media. Often, this problem is solved by mixing the aqueous media with an organic solvent that aids in dispersibility of SNP.[18] However, using PAMAM dendrimers as surface modifiers and building blocks in the synthesis of the sensor aids in the dispersibility of the SNP without the addition of an organic solvent. At neutral pH, the hydrophilic dendrimers have a positive surface charge and a neutral interior, which helps the SNPGx-Dye system be dispersible in aqueous solution.[19]

This research group has not had access to any instrumentation to quantitatively determine the dispersibility of the SNP in the chosen 2:1 EtOH:H_2O solvent system. However, the sonicated SNP used in the fluorimetry experiments in Chapter 3 have not produced any noise due to scattering from large aggregations. There is no flocculation visible to the naked eye. Zeta potential was used to begin to understand the aggregation behavior of the SNP systems in solution, and is discussed in section 2.4.5. While future work in the group will further address quantitative dispersibility measurements by dynamic light scattering and zeta potential, large aggregations of SNP have not proven problematic for any of the current aqueous sensing.

2.4.5 Zeta Potential

Zeta potential is a relatively new instrumental technique of determining the stability of particles in solution due to surface charge. Since zeta potential has never been used in this research group, some theory will be discussed alongside the experimental results.

2.4.5.1. Theory

Zeta Potential (ζ) is a measure of the electrostatic charge that a particle has in suspension, and is known to be a main factor in the stability of particles in solution.[20] Any charged particle in solution has two liquid layers of ions surrounding its surface: an inner layer of tightly bound ions on the surface called the Stern layer, and an outer diffuse layer with loosely bound ions (Figure 2-10).[20-21] A negatively charged particle has a positively charged Stern layer of counter-ions bound tightly to its surface. The diffuse layer would be positively charged closer to the particle, but would eventually balance out at large distances from the particle. Within the diffuse layer, there is a natural boundary, or “slipping plane”, where the particle and its surrounding ions form a stable entity.[20]

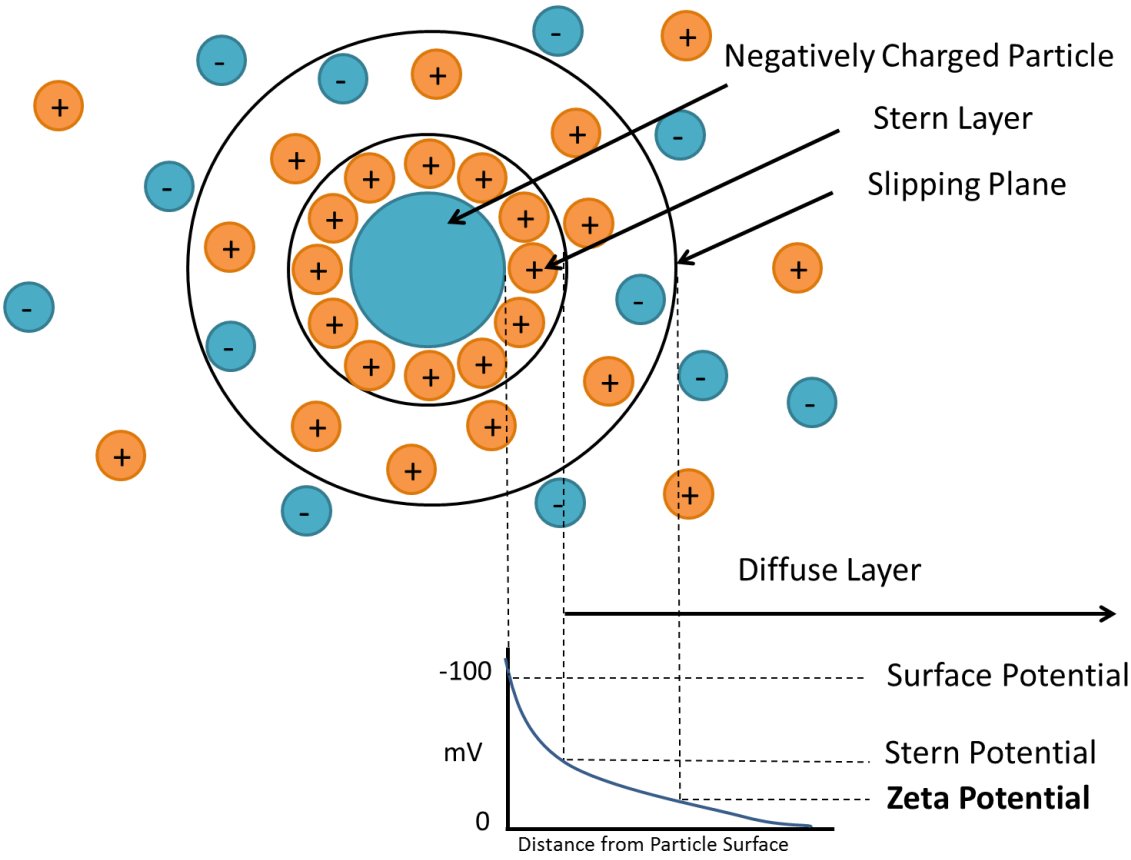

Figure 2-10. The zeta potential of a negatively charged particle is shown. The tightly bound stern layer surrounds the particle, and zeta potential is measured at the slipping plane in the diffuse layer. Adapted from Malvern.[20]

As a particle moves through solution, the ions within the slipping plane boundary move with it. The ions outside the slipping plane stay with the solution and do not move with the particle. The potential at the slipping plane as the particle moves through solution is called the zeta potential.[20, 22] The magnitude of zeta potential determines the stability of the particles in solution, or the ability of the particles to resist aggregation. Particles with large positive or negative zeta potentials (±30 mV or larger) will repel each other easily, and will not aggregate.[20] Particles with low zeta potentials will not repel each other enough to resist aggregation.

The sign of zeta potential does not necessarily correlate with the sign of the surface charge of the particle. While positively or negatively charged surfaces will always have respective positive or negative zeta potentials, neutral particles can have zeta potentials of either sign. A graph of zeta potential vs pH as seen in Figure 2-11 helps to visualize this.[23]

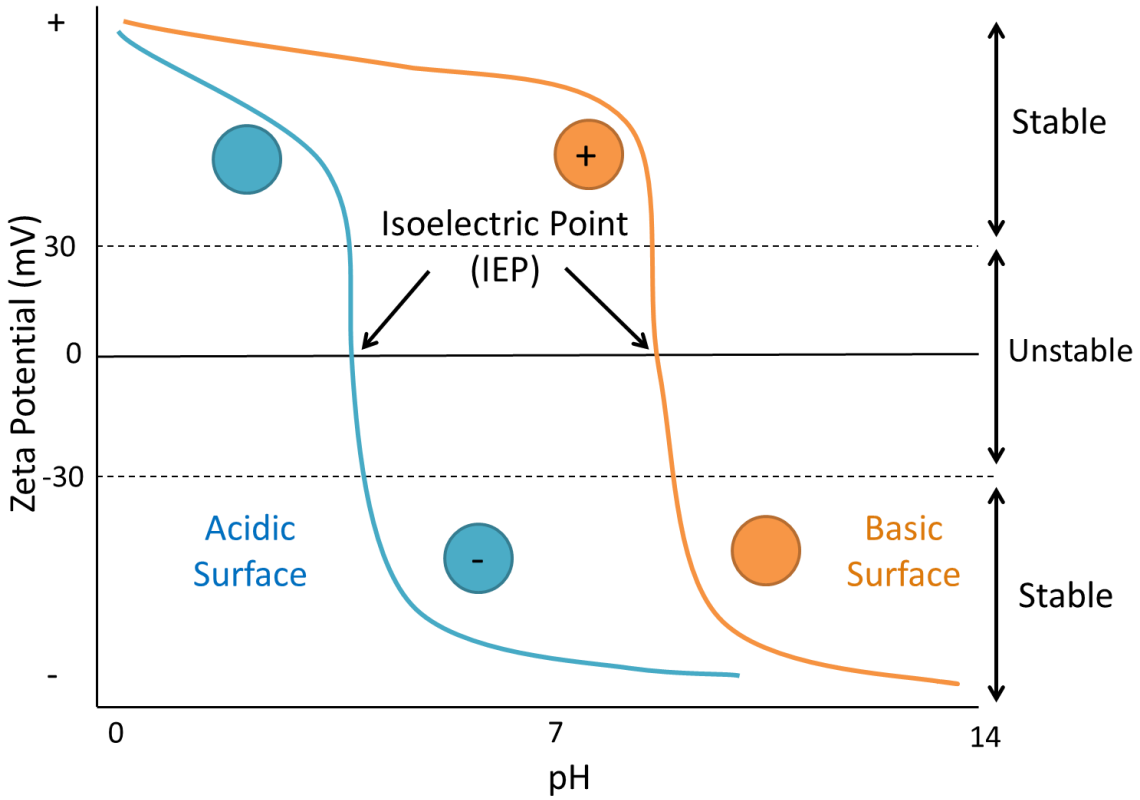

Figure 2-11. A graph of zeta potential vs pH adapted from Fairhurst demonstrates the difference between acidic (blue) and basic (orange) particles. Circles with no charge represent neutral particles.[23]

Acidic surfaces such as carboxylic acids are neutral at low pH, and are deprotonated giving a negative charge at high pH. However, in their neutral state they have a positive zeta potential. This happens because the neutral carboxylic acids do not attract ions, so the addition of excess acid to lower the pH causes a buildup of positively charged ions, resembling a positively charged surface. Basic surfaces such as amines experience similar behavior: at low pH they are protonated and are positively charged with a positive zeta potential, at high pH they are neutral but have a negative zeta potential due to the buildup of excess base.

A graph of zeta potential vs pH also determines the stable pH range for the particles. Outside of ±30 mV, the particles are very stable to aggregation. Another important aspect of the graph is the isoelectric point (IEP) of the particle. The IEP is the point where the sign of the zeta potential is zero, and the particles have no resistance to aggregation.[24] As seen in Figure 2-11, an acidic surface will have an IEP less than 7, and a basic surface shifted right with an IEP greater than 7.[23]

2.4.5.2 Results

Zeta potential was used to analyze the differences between SNPG4-R and SNPG4-R-COOH, and to determine their stable pH ranges in 2:1 EtOH:H_2O. A graph of zeta potential vs pH in Figure 2-12 summarizes the zeta potential results.

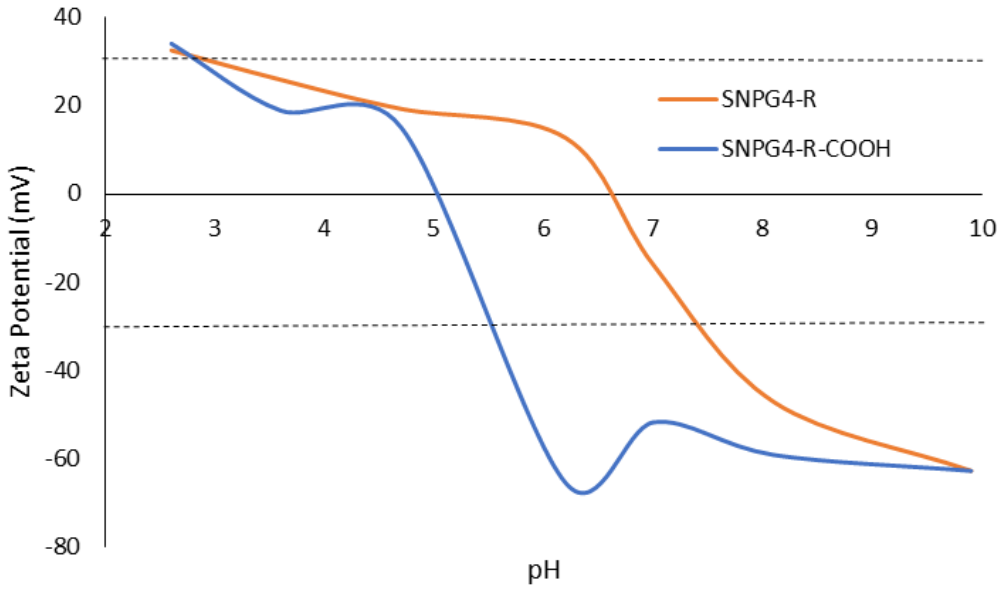

Figure 2-12. Zeta potential vs pH for SNPG4-R and SNPG4-R-COOH in 2:1 EtOH:H_2O with [NaCl] =10mM. The dotted potential lines between ±30 mV represent the instability region.

The most obvious difference between the two sets of particles in Figure 2-12 is their IEPs. While the shapes of the two curves are similar, the IEP of SNPG4-R-COOH (~5.2) is shifted left compared to the IEP of SNPG4-R (~6.8). This confirms that the carboxylic acid reaction was successful in converting the surface amines into carboxylic acids. The right shifted IEP of SNPG4-R, expected to be basic, is essentially neutral. Zeta potential depends on anything on the surface of the nanoparticle; this includes not only the surface amines or carboxylic acids, but also the dyes on the surface. Therefore it is important to realize that these IEPs do not represent exact pK_a values of the surface functional groups; rather, they represent the pH of least stability towards aggregation.

As particles are most stable at pH values with zeta potentials outside of ±30 mV, both sets of particles should resist aggregation at or above ~pH 7. This is extremely helpful in validating the metal ion and anion sensing experiments that will be discussed in Chapter 3, most of which are done at pH 7.

2.5 Conclusion

The series of SNPGx-Dye was successfully synthesized through a four step process and characterized. Amine density quantification and FTIR proved that the addition of PAMAM dendrimers was successful, and dye loading standard curves confirmed that dye was tethered to the dendrimer. The optimum combination for dendrimer generation and dye loading was SNPG4-F, due to the size and shape of both components. The conversion of surface amines to carboxylic acids was confirmed by the amine density assay and FTIR, as well as zeta potential analysis. Zeta potential also determined that the SNP systems are most stable at pH > 7. If possible, the dispersibility of the SNP in aqueous media should be further quantified in the future. The nanoparticle systems synthesized in this chapter will be used in Chapters 3 for metal and anion sensing, and in Chapter 4 for FRET sensing.

2.6 References

1. Candel, I.; Calero, P.; Martinez-Manez, R.; Sancenon, F.; Dolores Marcos, M.; Pardo, T.; Soto, J., Sensing properties of silica nanoparticles functionalized with anion binding sites and sulforhodamine B as fluorogenic signalling unit. *Inorg. Chim. Acta* **2012,** *381*, 188-194.
2. Fabbrizzi, L.; Licchelli, M.; Rabaioli, G.; Taglietti, A., The design of luminescent sensors for anions and ionisable analytes. *Coord. Chem. Rev.* **2000,** *205*, 85-108.
3. Liu, C. Surface Tethered PAMAM Dendrimers On Controlled Pore Glass As Color Release Sensors For Phosphates. University of San Francisco, 2013.
4. Chang, C.-C. End-group Modifications to PAMAM Dendrimers Tethered on Glass Supports: Development of Indicator Displacement Assays (IDA) Based on Tethered Copper Chelates. M.S., University of San Franciso 2009.
5. Kwon, J. Y.; Jang, Y. J.; Lee, Y. J.; Kim, K. M.; Seo, M. S.; Nam, W.; Yoon, J., A Highly Selective Fluorescent Chemosensor for Pb2+. *J. Am. Chem. Soc.* **2005,** *127* (28), 10107-10111.
6. Shi, X.; Thomas, T. P.; Myc, L. A.; Kotlyar, A.; Baker, J. J. R., Synthesis, characterization, and intracellular uptake of carboxyl-terminated poly(amidoamine) dendrimer-stabilized iron oxide nanoparticles. *Physical Chemistry Chemical Physics* **2007,** *9* (42), 5712-5720.
7. Soto-Cantu, E.; Cueto, R.; Koch, J.; Russo, P. S., Synthesis and Rapid Characterization of Amine-Functionalized Silica. *Langmuir* **2012,** *28* (13), 5562-5569.
8. Stoellner, D.; Scheller, F. W.; Warsinke, A., Activation of cellulose membranes with 1,1'-carbonyldiimidazole or 1-cyano-4-dimethylaminopyridinium tetrafluoroborate as a basis for the development of immunosensors. *Anal. Biochem.* **2002,** *304* (2), 157-165.
9. Friedman, M., Applications of the Ninhydrin Reaction for Analysis of Amino Acids, Peptides, and Proteins to Agricultural and Biomedical Sciences. *Journal of Agricultural and Food Chemistry* **2004,** *52* (3), 385-406.
10. Bottom, C. B.; Hanna, S. S.; Siehr, D. J., Mechanism of the ninhydrin reaction. *Biochemical Education* **1978,** *6* (1), 4-5.
11. Jung, H.-S.; Moon, D.-S.; Lee, J.-K., Quantitative analysis and efficient surface modification of silica nanoparticles. *J. Nanomater.* **2012**, 593471, 8 pp.
12. Moon, J. H.; Kim, J. H.; Kim, K.-j.; Kang, T.-H.; Kim, B.; Kim, C.-H.; Hahn, J. H.; Park, J. W., Absolute Surface Density of the Amine Group of the Aminosilylated Thin Layers: Ultraviolet−Visible Spectroscopy, Second Harmonic Generation, and Synchrotron-Radiation Photoelectron Spectroscopy Study. *Langmuir* **1997,** *13* (16), 4305-4310.
13. Metin, C. O.; Lake, L. W.; Miranda, C. R.; Nguyen, Q. P., Stability of aqueous silica nanoparticle dispersions. *Journal of Nanoparticle Research* **2010,** *13* (2), 839-850.
14. Hong, M.-Y.; Lee, D.; Kim, H.-S., Kinetic and Equilibrium Binding Analysis of Protein-Ligand Interactions at Poly(amidoamine) Dendrimer Monolayers. *Anal. Chem.* **2005,** *77* (22), 7326-7334.
15. Pavia, D. L.; Lampman, F. M.; Kriz, G. S.; Vyvyan, J. R., *Introduction to Spectroscopy, Fourth Edition*. Cengage Learning: 2009.
16. Mackay, M. E.; Tuteja, A.; Duxbury, P. M.; Hawker, C. J.; Van Horn, B.; Guan, Z.; Chen, G.; Krishnan, R. S., General Strategies for Nanoparticle Dispersion. *Science (Washington, DC, U. S.)* **2006,** *311* (5768), 1740-1743.
17. Iijima, M.; Kamiya, H., Layer-by-Layer Surface Modification of Functional Nanoparticles for Dispersion in Organic Solvents. *Langmuir* **2010,** *26* (23), 17943-17948.
18. Tadano, T.; Zhu, R.; Muroga, Y.; Hoshi, T.; Sasaki, D.; Yano, S.; Sawaguchi, T., A new mechanism for the silica nanoparticle dispersion-agglomeration transition in a poly(methyl methacrylate)/silica hybrid suspension. *Polym J* **2014,** *46* (6), 342-348.

19. Cakara, D.; Kleimann, J.; Borkovec, M., Microscopic Protonation Equilibria of Poly(amidoamine) Dendrimers from Macroscopic Titrations. *Macromolecules* **2003,** *36* (11), 4201-4207.
20. Malvern, Zeta Potential: An Introduction in 30 Minutes. Malvern Instruments: 2013.
21. The Zeta Potential. www.colloidal-dynamics.com/docs/CDEITut1.pdf.
22. Revil, A.; Pezard, P. A.; Glover, P. W. J., Streaming potential in porous media: 1. Theory of the zeta potential. *Journal of Geophysical Research: Solid Earth* **1999,** *104* (B9), 20021-20031.
23. Fairhurst, D., An Overview of the Zeta Potential Part 3: Uses and Applications. *American Pharmaceutical Review* **2013**.
24. Bergman, L.; Rosenholm, J.; Duchanoy, A.; Kankaanpaa, P.; Heino, J.; Linden, M.; Ost, B., Electrokinetic Characterization of Functionalized Silica Nanoparticles. *Malvern Instruments Application Note* **2014**, 1-6.

Chapter 3

Metal Ion and Anion Sensing Using Fluorescent Dendrimer Modified SNP

As outlined in Chapter 1, the goals of this research are to synthesize a series of sensitive and selective copper (II) ion fluorescent chemosensing systems, and to further use those systems as subsequent anion detectors. This chapter summarizes the metal ion and anion sensing results of the SNPGx-Dye systems synthesized in Chapter 2.

3.1 Introduction

Sensitivity and selectivity are two particularly important components of a successful sensor. The SNPGx-Dye systems are designed to function as sensitive and selective copper (II) ion sensors, under the hypothesis that PAMAM dendrimers selectively form an absorption band with coordinated copper (II) that quench nearby fluorescence and provide a large and generation-dependent number of coordination sites.[1] This turn-off sensing should be reversible if the copper is removed from the coordination complex or if the quenching is interrupted. Theoretically, any small chelating anion with an affinity for copper would be a suitable substrate for turn-on sensing. While many copper (II) sensors exist, this dendrimer modified SNP-based system provides a simple customizable chemosensor that can be optimized by changing the dendrimer generation, pH, surface functional group, and fluorescent dye, all while in aqueous solution using simple instrumentation. Figure 3-1 shows the turn-off and turn-on sensing schematic.

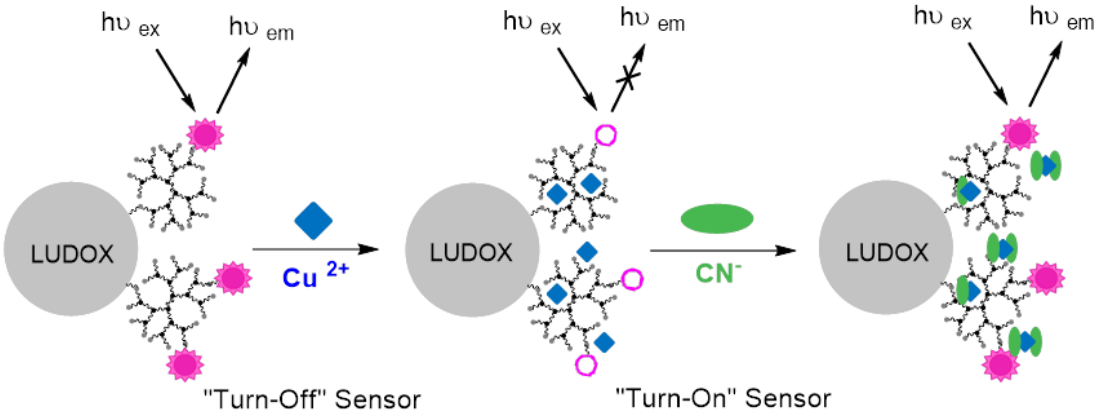

Figure 3-1. The turn-off and turn-on sensing on SNPGx-Dye systems, where copper ion quenches the fluorescence and cyanide ion restores it.

3.2 Experimental

The following sections summarize the materials, instrumentation, and procedures used to test the SNPGx-Dye systems as metal ion and anion sensors. Only materials and instrumentation not described in Chapter 2 are listed below, including the acronyms used in this thesis. All reagents were used directly without further purification.

3.2.1 Materials

The following chemicals were obtained: 4-(2-Hydroxyethyl)piperazine-1-ethanesulfonic acid (HEPES, Sigma-Aldrich, 99.5%, CAS 7365-45-9, FW 238.30); Copper (II) chloride dihydrate (Baker, 99.9%, CAS 10125-13-0, FW 170.48); Nickel (II) chloride hexahydrate (Acros, 97%, CAS 7791-20-0, FW 237.71); Zinc (II) chloride (Baker, 97.9%, CAS 7646-85-7, FW 136.28); Lead (II) chloride (Merck, 97%, CAS 7758-95-4, FW 278.18); Cadmium (II) chloride (Sigma-Aldrich, 99%, CAS 10108-64-2, FW 183.32); Silver (I) chloride (Sigma-Aldrich, 99%, CAS 7783-90-6, FW 143.32); Cobalt (II) chloride (Sigma-Aldrich, 97%, CAS 7646-79-9, FW 129.84); Iron (III) chloride hexahydrate (EM Science, 97%, CAS 10025-77-1, FW 270.32); Sodium cyanide (Sigma-Aldrich, 97%, CAS 143-33-9, FW 49.01); Ethylenediaminetetraacetic acid disodium salt dehydrate (EDTA, Baker, 99.7%, CAS 6381-92-6, FW 372.24); Sodium azide (EM Science, 98%, CAS 26628-22-8, FW 65.01); Sodium phosphate tribasic (Baker, 98%, CAS 10101-89-0, FW 380.16); 8-Anilino-1-naphthalenesulfonic acid (ANS, Sigma-Aldrich, 97%, CAS 82-76-8, FW 299.34).

3.2.2 Instrumentation

Fluorescence spectroscopy was performed on a Horiba Jobin Yvon FluoroMax-4 spectrofluorometer using Jobin Yvon FluorEssence Software. Emission spectra were collected with excitation and emission slit widths of 5 nm, and the emission spectra collection started $\geq$10 nm to the red of the excitation wavelength. SNPGx-R samples were excited at 520 nm and the emission was collected from 540-640 nm (λ_{max}=576 nm). SNPGx-F samples were excited at 495 nm and the emission was collected from 510-630 nm (λ_{max}=525 nm). All metal ion and anion titration volumes were delivered using P2, P5, P10, P20, P200, and P1000 calibrated micropipettes.

3.2.3 Procedures

Calibrations and blanks:

The fluorometer was calibrated with deionized water before each titration. No turn-off calibrations were required. For turn-on calibrations, anion interference with the fluorescent dye was corrected by repeating the turn-on titration without copper to account for each anion's effect on the fluorescence intensity. These "blanked" intensities were subtracted from the actual intensities from the turn-on titrations with copper present.

Turn-off metal ion titrations:

A sample of $SNPG_x$-Dye nanoparticles (0.06-0.07 mg/mL) was taken up in a 2:1 solution of ethanol:HEPES buffer (10mM, pH 7) and sonicated for 30 min at room temperature. The fluorescence intensity of 3.00 mL of the solution was measured on the fluorometer. Acidified metal ion chloride salt solutions of interest (Cu^{2+}, Zn^{+}, Ni^{2+}, Ag^{+}, $Cd^{2+,}$ Pb^{2+}, Co^{2+}, Fe^{3+}, all at pH 2) were titrated into the solution, and the effect on fluorescence intensity was observed with an equilibrium time of 5 min.

Turn-on anion titrations:

Anionic sodium salt solutions of interest ($EDTA^{2-}$, CN^{-}, N_3^{-}, PO_4^{3-}) were titrated into the previous solution following the completion of the metal ion titration (20 μM Cu^{2+}). The effect on fluorescence intensity was observed with an equilibration time of 7 min.

Limits of Detection and Quantitation:

A solution of 0.066 mg/mL SNPG4-R in 2:1 EtOH: HEPES buffer (10mM, pH 7) was sonicated for 30 minutes. Copper (II) was titrated into the solution in small increments, and the fluorescence was recorded after a five minute equilibrium time period. The raw fluorescence intensities (CPS) were plotted against the concentration of copper (II), and the slope of the line of best fit was determined. Seven replicate samples were created containing 0.066 mg/mL SNPG4-Dye in 2:1 EtOH: HEPES buffer (10mM, pH 7) and a copper concentration three times larger than the most concentrated sample used previously. The mathematic determination of the limits is described in section 3.5.

3.3 Metal Ion Detection Results (Turn-off Sensing)

The results of a series of metal ion "turn-off" sensing experiments are discussed below by observing the effect of dendrimer generation, pH, surface functional group, and organic dye on metal ion quenching.

3.3.1 Selectivity for Copper (II)

As discussed in Chapter 1, PAMAM dendrimers provide a large number of metal ion chelating locations that increase with generation. The SNPGx-Dye systems were designed to have fluorescent dyes tethered to the dendrimers so that PAMAM-metal ion complexes would be in close proximity to the dyes. This encourages distant dependent quenching and results in the detection of any chelated metal ions. Specifically, the sensor was designed to test for copper (II) ions, as PAMAM-Cu^{II} complexes are known to form a blue absorption band at 605 nm when copper (II) is coordinated.[1-2]

Figure 3-2 shows the fluorescence emission decrease during a titration of SNPG4-R with copper (II). A small blue-shift in maximum emission wavelength was observed upon the addition of copper. A similar shift was seen by Chen *et al*. upon addition of copper (II) to fluorescent polyethyleneimine (PEI) nanoparticles.[3] While this wavelength shift was not investigated in this thesis work, a shift in wavelength is representative of a change in electronic environment, which confirms an interaction between dendrimer bound copper and the dye.

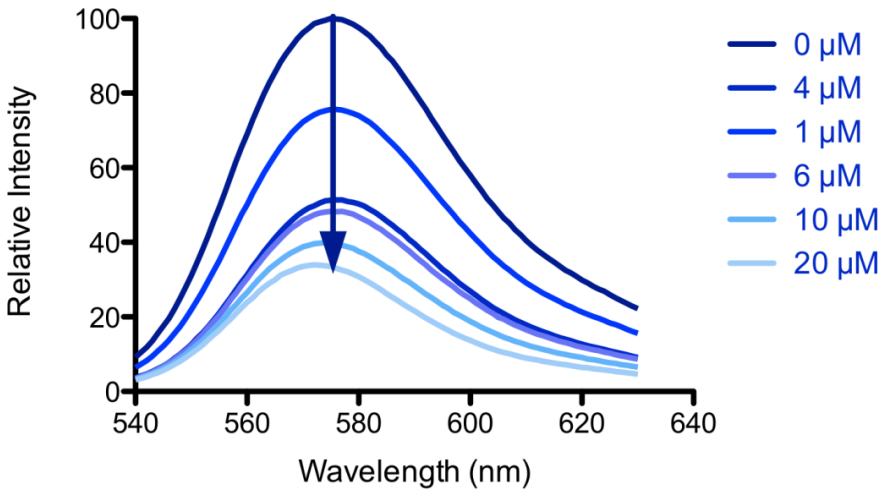

Figure 3-2. Relative fluorescence emission for 0.066 mg/mL SNPG4-R with increasing amounts of copper (II) ions in 2:1 EtOH:HEPES buffer (10 mM, pH 7)

Figure 3-3 shows the quenching results of metal ion titrations for SNPG4-R following the procedure described in section 3.2.3 with copper (II), zinc (II), nickel (II), silver (I), cadmium (II), lead (II), cobalt (II), and iron (III).

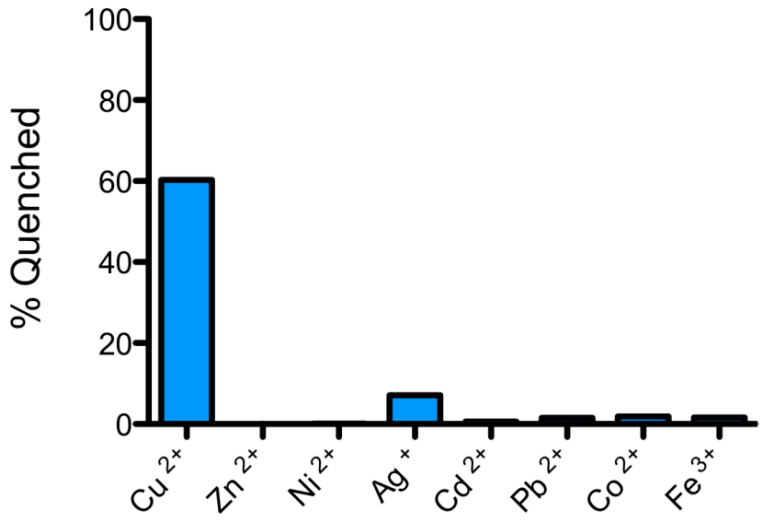

Figure 3-3. Percent signal quenching [$(1-I/I_o)*100$) with λ_{em}=576 nm] results for 0.066 mg/mL SNPG4-R in 2:1 EtOH:HEPES buffer (10 mM, pH 7) with 20 μM metal ions.

The quenching results in Figure 3-3 prove that the sensor is selective for copper (II) over the other common metal ions. This supports the hypothesis that the quenching is likely a Forster Resonance Energy Transfer (FRET) quenching mechanism discussed in section 1.4, where the RITC or FITC dye is the energy donor and PAMAM-Cu^{II} complex is the energy acceptor. It may be helpful to think of FRET as an enhanced version of the basic energy transfer mechanism described in section 1.1. Energy transfer quenching between a metal ion and a fluorescent dye requires only that the metal ion have partially filled d-orbitals.[4] This basic energy transfer may be the source of the 5% quenching that is observed for silver (I). Similarly, FRET quenching relies on energy transfer, but its effects are intensified by the spectral overlap between the emission spectrum of an energy donor and the absorption spectrum of the energy acceptor.

In their paper on dendrimer-encapsulated metal nanoparticles, Crooks and coworkers wrote that copper (II) has a unique relationship with PAMAM dendrimers because it forms a complex.[5] Other metal ions, including nickel (II), iron (III), and lead (II) can be absorbed into the interior of dendrimers, but they do not form coordination complexes.[5-6] The results in Figure 3-3 suggest that the mere presence of a metal ion within the dendrimer interior is not enough to induce dynamic FRET quenching, as only copper (II) causes significant quenching.

Zhau *et al*. studied the interaction between PAMAM dendrimers and lead (II) in detail, and determined that an absorption band formed at 250 nm as the system underwent a slow ligand-exchange reaction involving interior amines and solvent.[6] This further supports the FRET quenching mechanism, as a 250 nm absorption band would not be suitable for FRET quenching with either RITC or FITC due to its blue shifted wavelength.

These results on SNPG4-R demonstrate a selectivity for copper (II) due to FRET quenching by the coordination complex absorption band. As a control, the quenching response due to copper (II) remained unchanged in the presence or absence of 2 equivalents of nickel (II), zinc (II), and cadmium (II). This result confirms that the sensor would be able to sense copper (II) regardless of other metal ions in solution.

3.3.2 Effect of Dendrimer Generation on Copper (II) Quenching

The hypothesis that copper (II) quenching is proportional to dendrimer generation was tested to determine the most effective SNPGx-Dye system. As discussed in section 2.4.1, the number of available amines on SNPGx increased with generation, but did not double as predicted by dendrimer structure. The lower progression of available amines was attributed to the shape and size of the dendrimers; the larger, more spherical generations reached a limit of close packing on the surface of the SNP at generation 4. The quenching (I/I_o) for each SNPGx-Dye system is plotted in Figure 3-4.

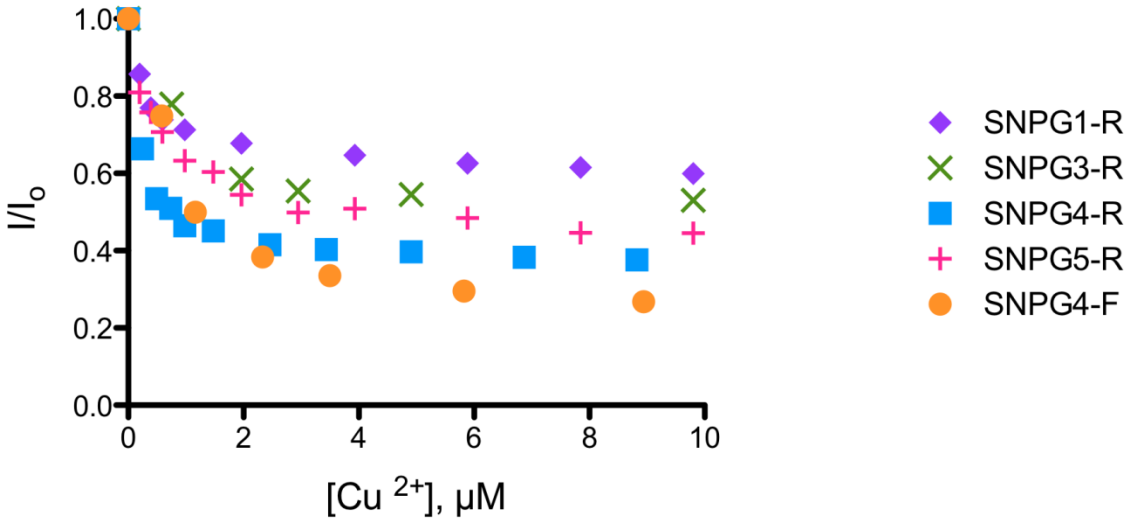

Figure 3-4. Normalized fluorescence intensity (I/I_o) quenching results for 0.066 mg/mL SNPGx-Dye in 2:1 EtOH:HEPES buffer (10 mM, pH 7) with added copper, where I and I_o are the fluorescent emission in the presence and absence of the copper, respectively.

The general hypothesis is confirmed, as larger generations experience more quenching by copper (II). The two most efficient quenching systems were SNPG4-R and SNPG4-F, additionally confirming the hypothesis that the size and shape of the dendrimer is an important factor in copper coordination and quenching effectiveness. While G4 and G5 were found to have similar numbers of available surface amines by the ninhydrin assay (113 vs 136 μmol/g), the G4 quenching results are significantly and consistently better. One possible explanation is that the G4 dendrimer molecules on the surface are not as tightly packed as the G5 dendrimers, leaving them more open to interior copper coordination. The G5 dendrimers may be so tightly packed that some of their coordination sites are inaccessible, or the interior amine binding sites may be blocked by tightly packed copper (II) coordinated surface amines. This results in less copper binding and therefore less quenching. Following G4 as the most effective quencher, G5 is the next most efficient followed by G3 and G1.

3.3.2.1 Stern-Volmer Analysis of Copper (II) Quenching

The results discussed in section 3.3.2 depict the generational dependence of *saturation* quenching by copper (II) ions. Fitting the *initial* linear region of the quenching data to the Stern-Volmer (SV) equation helps to quantify the quenching and compare it to other systems. The Stern-Volmer equation is shown as equation 3-1, where I_o and I are the fluorescence intensity in the absence and presence of the quencher, respectively, K_{SV} is the Stern-Volmer quenching constant, and $[Q]$ is the concentration of the quencher.[7]

$$\frac{I_o}{I} = 1 + K_{SV}\,[Q] \qquad 3\text{-}1$$

The SV equation is widely used to model collisional quenching, also called dynamic quenching.[8] While the mechanism of quenching for the research in this thesis has not been confirmed, strong evidence suggests FRET quenching, as discussed previously. Although the Stern-Volmer equation was originally intended to interpret collisional quenching, it can also be applied to other types of quenching. Chen *et al*. used the SV equation to describe quenching due to copper ion binding, followed by a redox reaction on the surface of cadmium sulfide quantum dots.[9] The Stern-Volmer equation has also been applied to a number of quenching systems that claim FRET as their mechanism.[8, 10-11] For example, Buboltz *et al*. investigated the limits of the previously reported claim that dilute acceptor concentrations allowed the SV equation to apply under FRET conditions.[8, 10] They found that at remarkably high, even excess concentrations of acceptor, the Stern-Volmer predictions were applicable to FRET quenching. Considering the maximum acceptor:donor (copper:dye) ratio for the *initial* linear region of the

quenching data used in this thesis work was less than 1, it seems appropriate to use the Stern-Volmer equation to model this quenching.

A best fit plot to the Stern-Volmer equation for SNPG4-R is shown in Figure 3-5. Theoretically, a plot of I_o/I vs. $[Cu^{2+}]$ gives a y-intercept of 1 and a slope that is equal to K_{SV}, the Stern-Volmer quenching constant. It is important to notice that the copper ion concentration in Figure 3-5 is restricted to the initial, linear quenching region, and does not extend to the 20 μM saturation quenching.

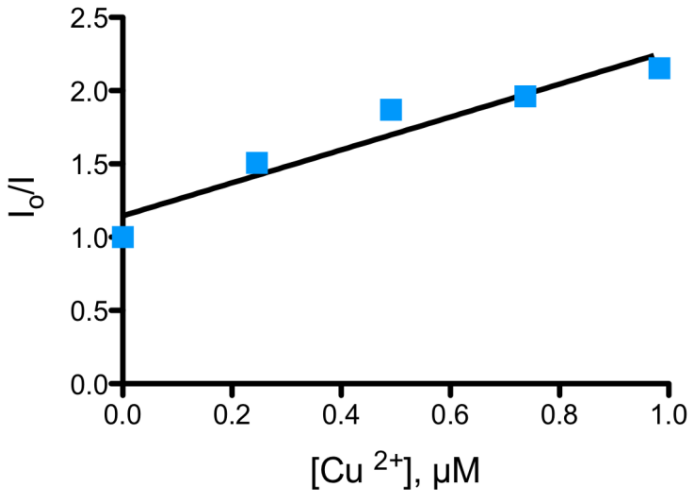

Figure 3-5. Quenching data for 0.066 mg/mL SNPG4-R in 2:1 EtOH:HEPES (10 mM, pH 7) with added copper is best fit to the Stern-Volmer equation, giving a Stern-Volmer constant of $11x10^5$ M^{-1}.

Table 3-1 summarizes the results for the Stern-Volmer quenching constants with copper (II) for all synthesized systems for the initial linear region of the quenching data. A larger K_{SV} value represents a more efficient quenching system. As discussed in section 3.3.2, generation 4 is the most efficient quenching system, followed by G1, G5, and G3. The large SV quenching constant confirms the effectiveness of G4 over the other generations, even though the saturation quenching of G4 and G5 appeared similar. The remaining generations (SNPGx-R, where x=1,3, and 5) are almost indistinguishable from each other considering their standard deviations. This implies that G4 is the most effective generation both at initial and saturation concentrations of copper (II).

Table 3-1. Stern-Volmer quenching constants for added Cu^{2+} to SNPGx tethered dyes.

System	Ksv (*10^5 M^{-1})
SNPG1-R	6.1 ± 0.9
SNPG3-R	3.6 ± 0.1
SNPG4-R	11 ± 2
SNPG5-R	5.5 ± 0.8
SNPG4-F	14 ± 2

The Stern-Volmer quenching constants for analogous systems were compared to those in Table 3-1 to determine the effectiveness of the SNPGx-Dye systems. Work done by Cui *et al*. on mesoporous SNP modified with 2-aminomaleimide functioned as a turn-off sensor for copper (II), and they reported a K_{SV} value of 2.6 x 10^4 M^{-1}.[12] They cited a decrease in electron donating ability of their chelator by copper (II) chelation as a mechanism. This suggests that the incorporation of a dendrimer and FRET may result in a much larger K_{SV} and therefore more sensitive detection. Shang and coworkers employed CdTe quantum dots in turn off sensing for copper (II) with a K_{SV} value of 2.9 x 10^7 M^{-1} by collisional quenching.[13] The higher K_{SV} for collisional quenching suggests that the SV approximation works best for collisional quenching, or that quantum dots provide a platform for more efficient quenching.

In their work on a FRET based dual-emissive fluorescent silica nanoparticles modified with polyethyleneimine (PEI), Zong *et al*. reported a K_{SV} value of 1.3 x 10^6 M^{-1}, which falls just between the K_{SV} values obtained for SNPG4-R and SNPG4-F.[11] While Zong's research relies on energy transfer between an exterior RITC dye and a copper-PEI complex, they also incorporate a reference FITC dye in the interior of the nanoparticle as a control measurement as seen in Figure 3-6.

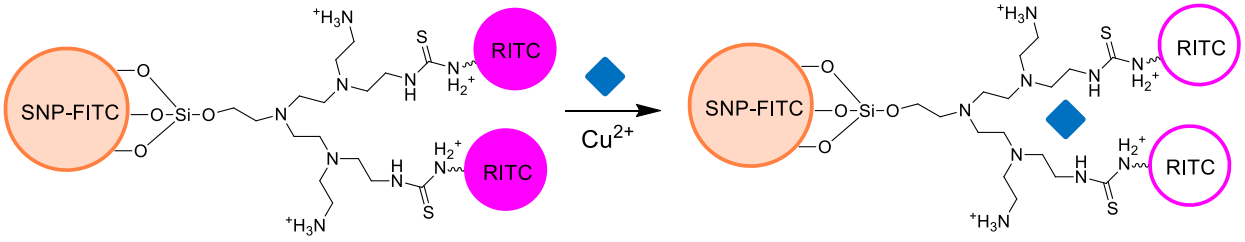

Figure 3-6. The PEI-modified dual-emission SNP sensor for copper studied by Zong *et al*., where energy is transferred from PEI-bound copper to tethered RITC dyes, yielding a Stern-Volmer constant of 1.3 x 10^6 M^{-1}. A reference FITC dye is incorporated into the nanoparticle as a control.

The similarities between the systems investigated in this thesis work and the work by Zong *et al*. are numerable, as PEI has similar functional group structure as PAMAM dendrimers. Achieving a similar Stern-Volmer constant for copper (II) quenching supports the FRET mechanism hypothesized in this work. However, the similarity in copper (II) quenching effectiveness suggests that the incorporation of a reference dye in the core of their synthesized nanoparticles may be unnecessary; similar effectiveness can be achieved following the less expensive, simpler synthesis presented in this thesis. This work also presents an advantage over the work done by Zhou in that it can also function as a selective anion sensor, which is not discussed by Zhou. One difference between the two systems is that the PEI-modified nanoparticles have a more extended linear range than was observed in this work. This suggests that an acceptor:donor ratio closer to one may bring the FRET and Stern-Volmer models closer, as Zhou depicted each PEI molecule having one tethered dye, whereas dyes may not be tethered to each dendrimer arm in this work.

3.3.3 Effect of pH on Copper (II) Quenching

As discussed in Chapter 1, pH plays an important role in the charge distribution on PAMAM dendrimers. The role of pH on copper (II) quenching was investigated using only SNPG4-R, as it was the most successful and abundant of the originally synthesized SNPGx-R systems. The G4 pKa of the interior tertiary amines is 6.3-6.9, and the pKa of the exterior primary amines is 9.0-10.3.[2] The copper (II) titration experiments described in section 3.2.3 were repeated at pH 5, 7, and 9 to determine the effect of pH on copper quenching. The results are summarized in Figure 3-7.

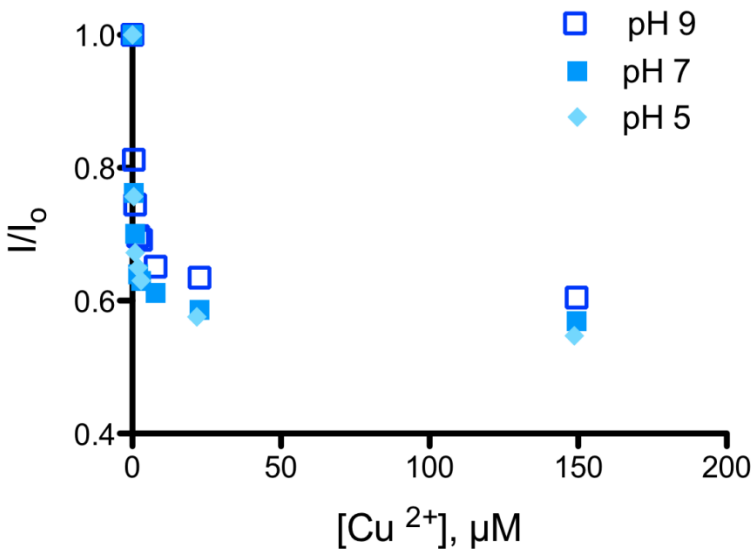

Figure 3-7. Normalized fluorescence intensity (I/I_o) quenching results for 0.066 mg/mL SNPG4-R in 2:1 EtOH:HEPES buffer (10 mM) with added copper at pH 5, 7, and 9.

At pH 5, both interior and exterior amines are fully protonated and positively charged. At pH 7, the exterior amines are positively charged and the interior amines are deprotonated and neutral. At pH 9, the interior amines are still neutral, and most of the exterior amines are deprotonated and neutral (see Figure 1-9). It was hypothesized that the positively charged copper (II) would be less repelled by the neutral charges at pH 7 and 9, and would give more efficient quenching. However, as seen in Figure 3-7, pH has no effect on the quenching ability of the system; the data points for each pH are within 5% of each other. This same phenomenon was not observed by Diallo *et al*. in their studies of copper (II) binding to free dendrimer in solution.[2] These results suggests that it is possible that the SNP-tethered dendrimer-dye system either shields the dendrimer from its changing environment, or that the copper will coordinate with the *tethered* dendrimer regardless of its positive or neutral charges. It could be that the pH values used in the experiment were not significant enough to induce a substantial change in charge, especially at high pH. In section 3.3.4, the surface amines are modified to achieve a negative charge with drastic changes in quenching.

3.3.4 Effect of Surface Charge on Copper (II) Quenching

The results in section 3.3.3 demonstrate that positive and neutral charges within the dendrimer or on the surface have little effect on copper (II) quenching. Therefore, the surface amines were modified with succinic anhydride as described in section 2.3.1.5 to convert the

terminal amines into carboxylic acids. The carboxyl-terminated exterior of a G3 PAMAM dendrimer has a reported pKa of 6.6, and a similar pKa is assumed for the SNPG4-COOH surface synthesized in Chapter 2.[14] The interior of the dendrimer still only fluctuates between positive and neutral depending on pH. The systems compared were SNPG4-R at pH 7 (positive exterior, neutral interior) and SNPG4-R-COOH at pH 7 (negative exterior, neutral interior) and pH 5 (neutral exterior, positive interior). Figure 3-8 summarizes these charged systems.[15]

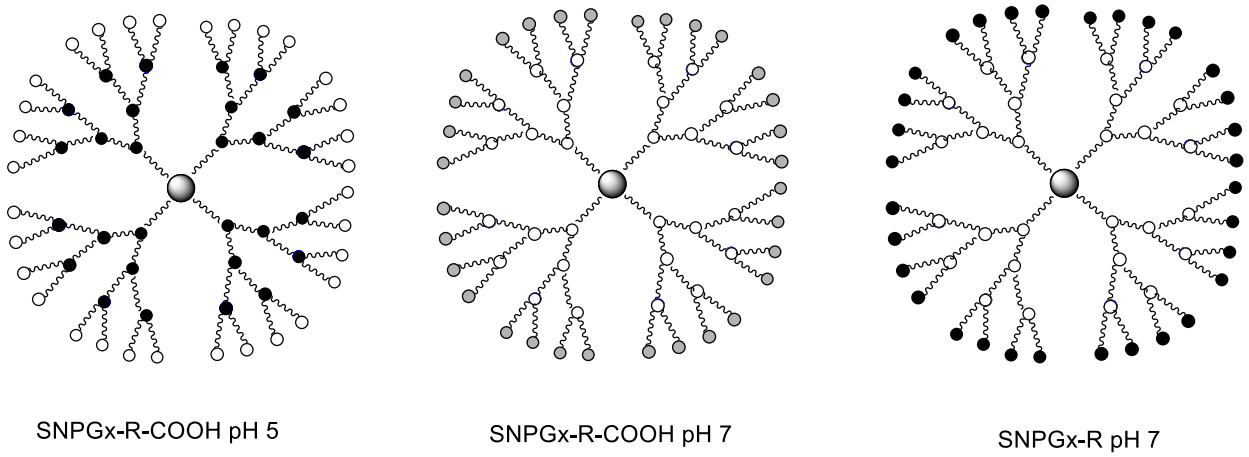

Figure 3-8. Approximate pH dependence of a PAMAM dendrimer is shown based on published pKa values of Cakara and Montealegre. Black shaded circles represent positive charges, white circles represent neutral sites, grey circles represent negative charges, and the central faded sphere represents the EDA dendrimer core.[14-15]

Figure 3-9 summarizes the results of the copper (II) ion quenching titrations. The system with the greatest saturation quenching is SNPG4-R-COOH at pH 7, where the surface charge is negative and the interior is neutral. This result suggests that the positively charged copper is electrostatically attracted to the negatively charged surface in addition to the other amine chelating sites, which leads to more effective quenching. The least effective quenching system SNPG4-R-COOH at pH 5. Compared to SNPG4-R at pH 7, this implies the copper is not chelated as strongly by the terminal carboxylic acids as by terminal amine groups.

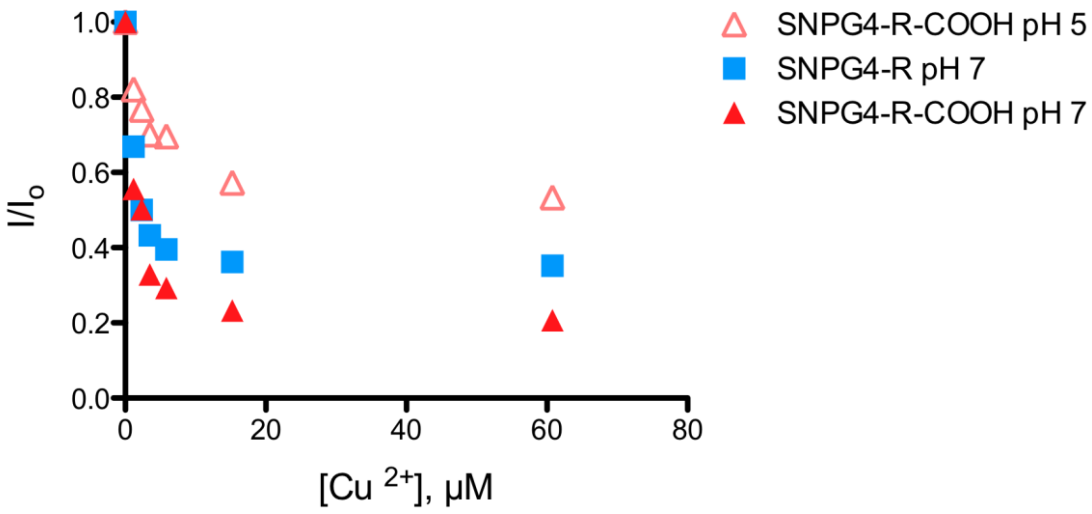

Figure 3-9. Normalized fluorescence intensity (I/I_o) quenching results for 0.066 mg/mL SNPG4-R and SNPG4-R-COOH in 2:1 EtOH:HEPES buffer (10 mM) with added copper at pH 5 and 7.

The trend seen in Figure 3-9 shows that the systems with neutral interiors experience more efficient quenching than their positive counterpart. The positively charged copper (II) is more likely to chelate the neutral species than a positive species due to electrostatic repulsion. The neutral amines on the dendrimer also have stronger Lewis base character, allowing for better covalent bonding. The data suggests that most of the copper is complexed in the interior of the dendrimer, as a neutral interior provides a better environment for quenching and chelation. This hypothesis that the copper is mostly interior-bound will be revisited in section 3.4 when they system is used to test for anions.

3.3.5 Effect of Organic Dye on Copper (II) Quenching

The effect of dendrimer tethered organic dye on copper (II) quenching was compared using rhodamine isothiocyanate (RITC) and fluorescein isothiocyanate (FITC), whose structures are shown in Chapter 1. The excitation and emission spectra of FITC are blue shifted compared to RITC. Figure 3-10 shows the spectral FRET overlap between the dyes and the 605 nm Cu^{II}-Gx complex presumed to form when copper is added to the dendrimer.

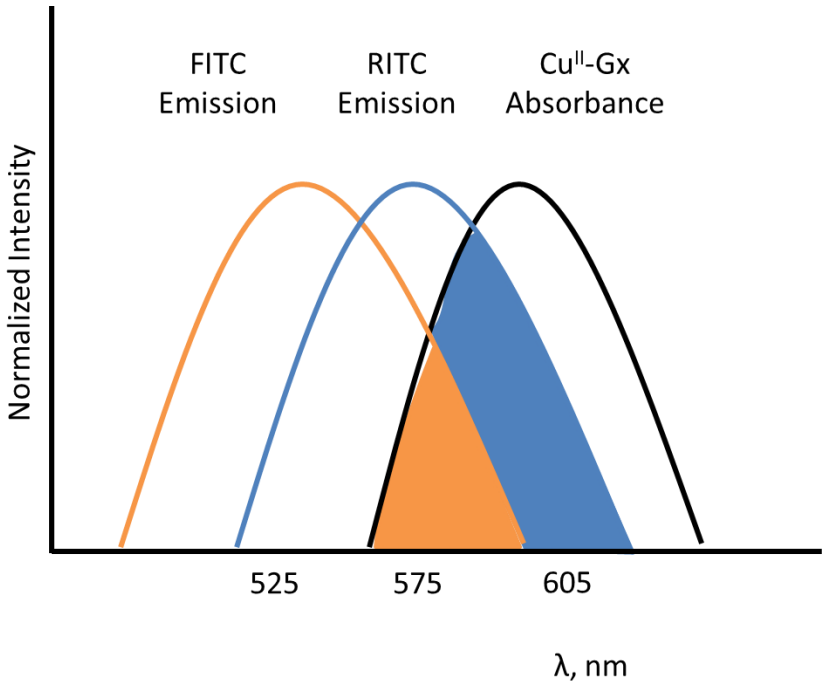

Figure 3-10. The stylized FRET overlap between the Cu^{II}-Gx acceptor absorbance band and RITC and FITC donor emission. The FITC overlap is represented by the orange area, and the RITC overlap is the sum of the orange *and* blue areas.

The spectral overlap of RITC with Cu^{II}-Gx is larger than FITC, so the quenching observed with RITC should be more efficient. However, the experimental results do not support this hypothesis. Copper quenching with FITC gives almost 80% saturation quenching, whereas with RITC only 65% is quenched. Figure 3-11 depicts these results.

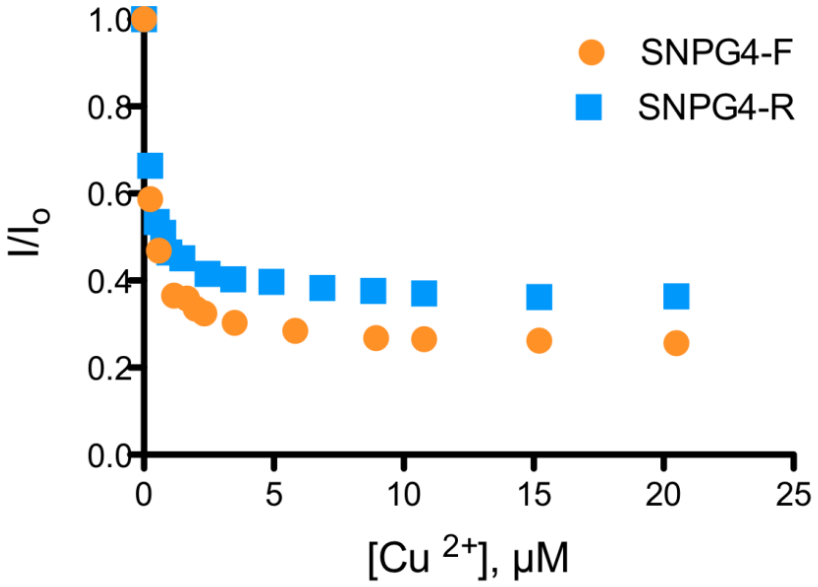

Figure 3-11. Normalized fluorescence intensity (I/I_o) quenching results for 0.066 mg/mL SNPG4-R and SNPG4-F in 2:1 EtOH:HEPES buffer (10 mM, pH 7) with added copper.

FITC and RITC have very similar quantum yields, around 95-100 depending on solvent, which does not explain the discrepancy between their effectiveness.[16-17] The dye loading results discussed in section 2.4.2 provide the most likely basis for the unexpected FITC advantage. Following the same synthetic procedure, almost 50% more FITC dyes were loaded onto the exterior of the dendrimers than RITC (62 μmol/g compared to 38). This unanticipated result may be due to the structure of the dyes, shown in Figure 3-12.[18-19]

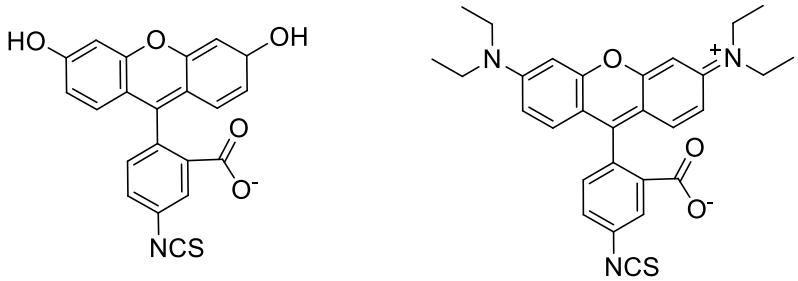

FITC

λex=495 nm
λem=525 nm

RITC

λex=520 nm
λem=576 nm

Figure 3-12. Chemical structures and excitation and emission wavelengths of Fluorescein isothiocyanate (FITC) and rhodamine isothiocyanate (RITC).[18-19]

RITC carries a positive charge on one of its tertiary nitrogen groups branching off the aromatic ring system, but exists as a zwitterion at neutral pH due to its carboxylic acid functional group.[20] This overall neutral molecule may experience repulsion between its partially positive aromatic ring system and the positive surface of the dendrimer, making it more difficult for the RITC dyes to get close enough to react with the dendrimer. The partial positive aromatic charges on RITC may also repel each other, forcing the dyes to be spread out and be highly loaded. The FITC has neutral branching arms, which leave FITC with a negative overall charge due to its carboxylic acid.[21] This would attract the FITC to the dendrimer's positive surface, enabling it to react more efficiently than RITC. The oxygen containing arms on FITC are much less bulky than the nitro-alkyl arms of RITC, which could allow the dyes to be more closely packed on the dendrimers surface.

3.3.5.1 Effect of Organic Dye on the Stern-Volmer Constant

The Stern-Volmer equation introduced in section 3.3.2.1 quantifies the quenching efficiencies at low copper (II) concentrations. Figure 3-13 shows the Stern-Volmer fits to SNPG4-F and SNPG4-R quenching data with copper (II). As discussed previously, Stern-Volmer analysis only focuses on the initial, linear region of the quenching curve.

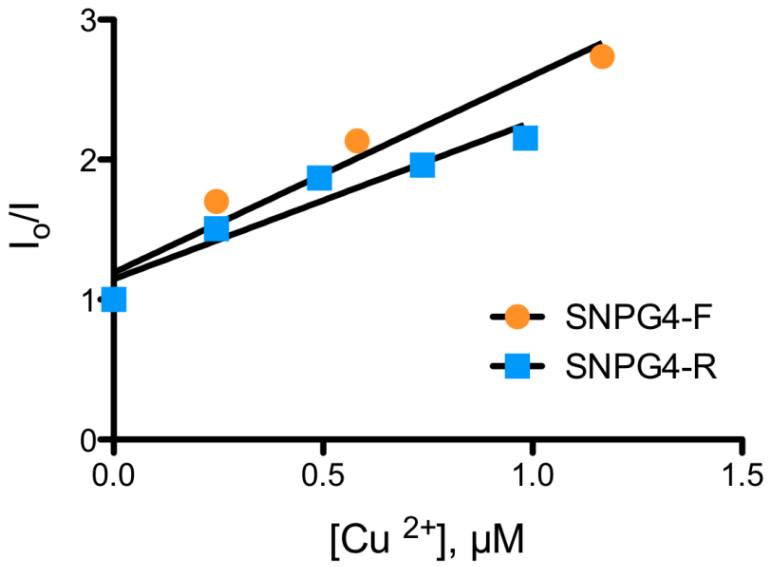

Figure 3-13. Quenching data for 0.066 mg/mL SNPG4-R and SNPG4-F in 2:1 EtOH:HEPES (10 mM, pH 7) with added copper is fit to the Stern-Volmer equation.

The K_{SV} values for SNPG4-F and SNPG4-R are 14 ± 2 and 11 ± 2 M^{-1}, respectively (shown in Table 3-1). These values are not significantly different by *t*-test at the 95% confidence interval, which uses the standard deviations, means, and number of repetitions to determine if two means are significantly different from each other.[22] This suggests that while FITC clearly outperforms RITC with saturation quenching by copper (II), in the initial linear region they are very similar.

3.3.5.2 Effect of Organic Dye on a Modified Stern-Volmer Analysis

As the initial linear region of copper (II) quenching does not provide much insight into any differences between FITC and RITC, a modified version of the Stern-Volmer equation is applied to the entirety of the quenching data. The modified Stern-Volmer equation was previously applied by Cui *et al*., whose work focused on copper sensing with mesoporous SNP modified with 2-aminomaleimide.[12] The modified Stern-Volmer equation accounts for fluorescent species that may be inaccessible to the quencher.[12, 16] In Equation 3-2 shown below, I_o, I, and $[Q]$ have the same meaning they do in the original SV equation, f_a is the fraction of initial fluorescence that is accessible to the quencher, and K_a is the Stern-Volmer constant of the accessible fraction.

$$\frac{I_0}{I_o - I} = \frac{1}{f_a K_a [Q]} + \frac{1}{f_a} \qquad 3\text{-}2$$

While fluorescent dyes have been depicted throughout this work as being tethered to the exterior of the dendrimer extending into free space, the location of the dyes on the surface of the dendrimer is not known. It is possible that some of the fluorescent dyes may be tethered in a way that causes them to be buried within the dendrimer. The tethered dendrimers are not perfectly spaced or symmetric on the SNP surface; therefore the spacing between dye molecules and copper coordination sites is variable. The less bulky, neutrally charged FITC has proven to react more easily with the dendrimer than RITC, which could cause different loading positions and new hydrophobic areas on the surface. Figure 3-14 shows the same data fit to the modified Stern-Volmer plot following equation 3-2.

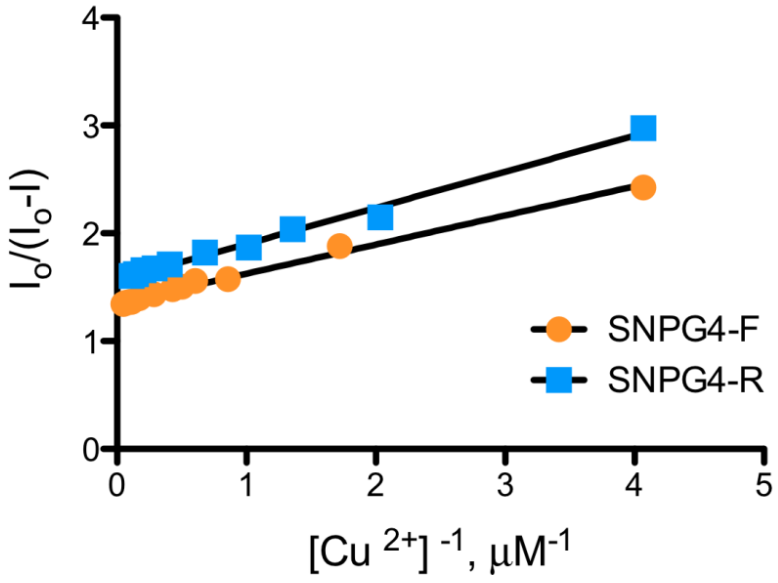

Figure 3-14. Quenching data for 0.066 mg/mL SNPG4-R and SNPG4-F in 2:1 EtOH:HEPES (10 mM, pH 7) with added copper is fit to the modified Stern-Volmer equation.

The fraction of accessible fluorescence (f_a) was determined from the y-intercept, and the SV quenching constant for the accessible fraction (K_a) was calculated from the slope. Table 3-2 summarizes the results of the modified SV experiments.

Table 3-2. Modified Stern-Volmer parameters for SNPG4-R and SNPG4-F for Cu^{2+} quenching.

	SNPG4-R	SNPG4-F
f_a	0.64	0.74
K_a ($*10^6\ M^{-1}$)	4.6	5.0

The modified SV analysis suggests that SNPG4-F has 10% more accessible dyes than SNPG4-R. The original quenching data shown in section 3.3.5 supports this, as the two systems differed in quenching by ~ 15%. This suggests that the higher loading of FITC leads to more accessible dyes. The SV quenching constants of the accessible fraction are very comparable for the two systems, which mirrors the original similarities between the K_{SV} values obtained in section 3.3.5.1.

Together, all the results do not support the hypothesis that RITC should be a more effective quencher because of better spectral overlap, as FITC outperforms RITC. This seems to be due to the higher loading, size, and overall negative charge of the FITC dye. SV and

modified SV analysis suggest that RITC has less accessible dyes, but that the quenching constants of RITC and FITC are similar despite the location or concentration of the dyes on the dendrimer.

3.4 Anion Detection Results (Turn-on Sensing)

The SNPGx-Dye + copper (II) systems were tested as subsequent turn-on sensors for small copper binding anions that could disrupt the quenching mechanism. The turn-on sensing was investigated by studying the effect of dendrimer generation, pH, surface charge, organic dye, and anion on the fluorescent return.

3.4.1 Selectivity for Cyanide

A distinct advantage of using dendrimers as copper chelators is that the copper binding should be reversible; that is, a stronger chelating molecule could bind to the copper and remove it from the dendrimer, restoring the original fluorescence of the tethered dye. Figure 3-15 shows the fluorescence emission spectra of copper quenched SNPG4-R with increasing amounts of cyanide. The blue shift that was observed upon copper quenching is reversed when cyanide is added, red-shifting back to the original emission maximum. This shift was also observed by other turn-off, turn-on systems involving copper and cyanide.[23-24]

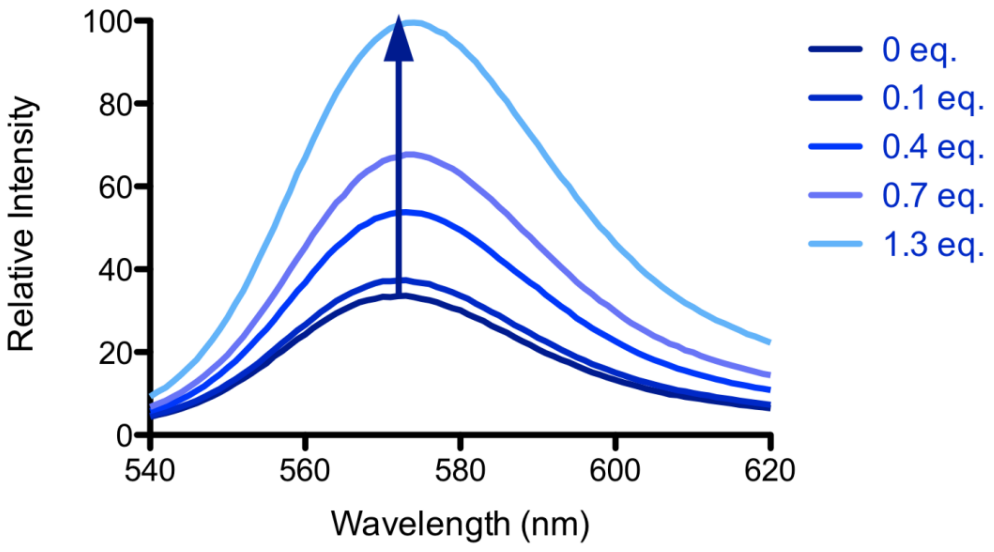

Figure 3-15. Relative fluorescence emission for 0.066 mg/mL SNPG4-R after 20 μM copper quenching with increasing amounts of cyanide in 2:1 EtOH:HEPES buffer (10 mM, pH 7).

The turn-on application of the SNPGx-Dye + copper (II) systems was not designed with selectivity as its main goal. Theoretically, any small anion with an affinity for copper would be able to penetrate the dendrimer and bind to or remove the copper. However, the results of anion titrations into quenched Cu^{II}-Gx systems did not support this hypothesis. Figure 3-16 shows the Lewis structures of the four copper binding anions tested in this work.

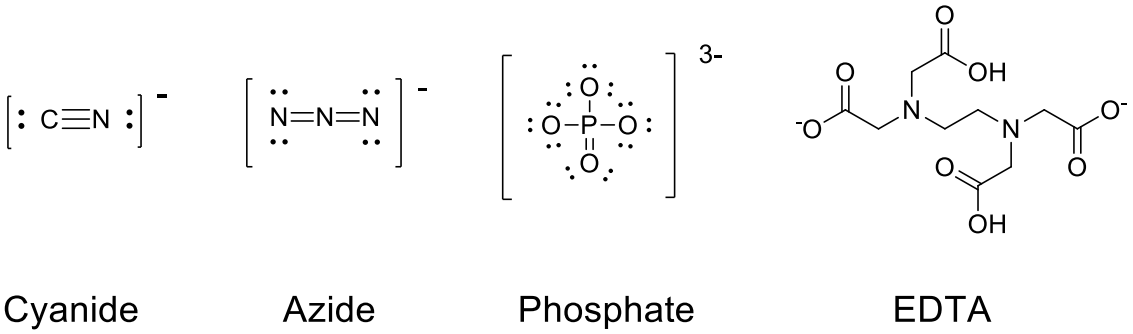

Figure 3-16. Lewis structures of four copper binding anions: cyanide, azide, phosphate, and ethylenediaminetetraacetic acid (EDTA).

Figure 3-17 demonstrates the unexpected results of adding two equivalents of the four common binding anions from Figure 3-16 to copper quenched SNPG4-R. The percent fluorescence return is not shown from zero, as copper (II) quenches the fluorescence to 40%.

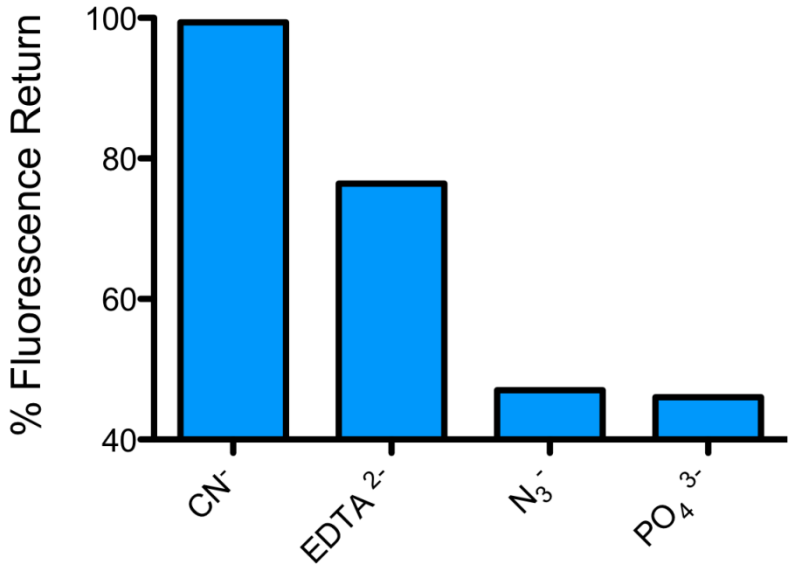

Figure 3-17. Percent fluorescence return after the addition of 2 equivalents of anions for 0.066 mg/mL SNPG4-R in 2:1 EtOH:HEPES buffer (10 mM, pH 7) after 60% quenching by 20 μM Cu2+.

It is clear that there is a preference for cyanide over ethylenediaminetetraacetic acid ($EDTA^{2-}$), azide (N_3^-), and phosphate (PO_4^{3-}) at these mole ratios. This apparent selectivity for cyanide is extremely surprising, since azide is known to bind to copper and induce a new absorbance band in many nitrogen containing coordination complexes.[25-26] The dendrimer bound copper should bind with incoming azide, disrupting the quenching process; however, this result is not observed even after adding 10 equivalents of azide. Casella *et al*. demonstrated that the binding behavior of azide to copper is exceptionally sensitive to the identity and charge of other ligands in the coordination sphere.[27] In their study of azide binding to nitrogen and oxygen containing copper coordination complexes, they observed two trends relevant to this work. Firstly, the more positive the charge of the complex, the higher the binding constant between azide and copper will be. Secondly, the more oxygen rich the coordination complex is, the lower the binding constant. This implies that positive, nitrogen based ligands are optimal for azide binding. At pH 7, the interior of a G4 PAMAM dendrimer is neutral and the exterior is positively charged; this suggests that the azide molecules would prefer to bind at the copper coordinated exterior of the dendrimer. However, as discussed in section 3.3.4, most of the copper is thought to be in the interior of the dendrimer. This may explain, along with the oxygen-containing amides within the dendrimer, why azide was not a suitable anion for turn-on sensing.

EDTA was also outperformed by cyanide at two equivalents. EDTA is a strong chelator for copper (II), and is used to easily remove copper from other nanoparticle based sensors.[11, 28-29] Figure 3-18 shows the results of the full anion titrations of copper quenched SNPG4-R systems.

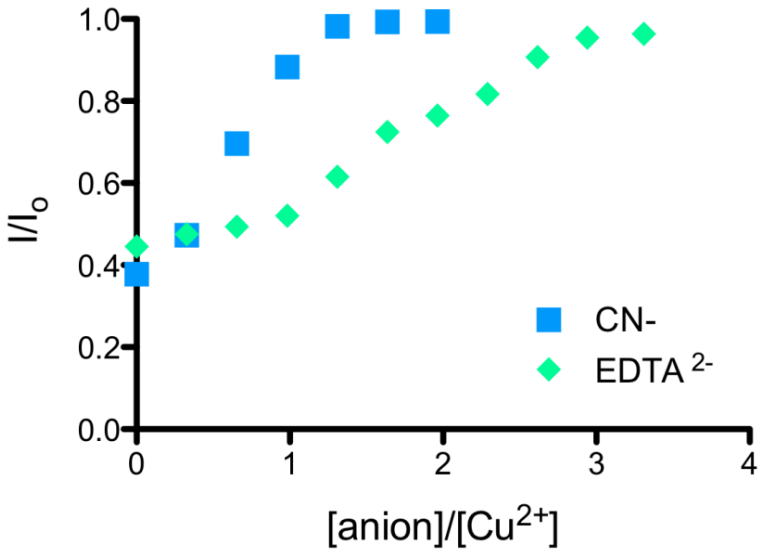

Figure 3-18. Normalized fluorescence return (I/I_o) after the addition of 2 equivalents of anions for 0.066 mg/mL SNPG4-R in 2:1 EtOH:HEPES buffer (10 mM, pH 7) after 60% quenching by 20 μM Cu^{2+}.

The results of EDTA and cyanide titrations show that although both anions are eventually able to fully restore the fluorescence, cyanide is more efficient (1.3 equivalents compared to 3). The main difference between the two anions, other than the magnitude of their charge, is their size. EDTA is a bulky, branched polydentate ligand, whereas cyanide is small and monodentate. These results confirm the prior hypothesis that the majority of the copper is chelated in the interior of the dendrimer, since the much smaller cyanide is able to bind to the copper much more easily than bulky EDTA. A larger concentration of EDTA is needed to force the equilibrium to chelate all the bound copper.

3.4.1.1 Mechanism of Turn-on Sensing with Cyanide

The mechanism of turn-on sensing of copper quenched SNPGx-Dye with cyanide has proven difficult to comprehend. Figure 3-19 summarizes the three main possibilities that have evolved from the cyanide experiments performed for this thesis: 1) One cyanide ion binds to, but does not remove the copper within its dendrimer coordination complex and interrupts copper quenching; 2) One cyanide ion binds to each copper ion and removes it from the dendrimer as $CuCN_{(s)}$, restoring the fluorescence; and 3) Two cyanide ions bind to each copper ion and remove it from the dendrimer as $Cu(CN)_{2(s)}$, restoring the fluorescence. Each mechanism has both literature support and experimental support.

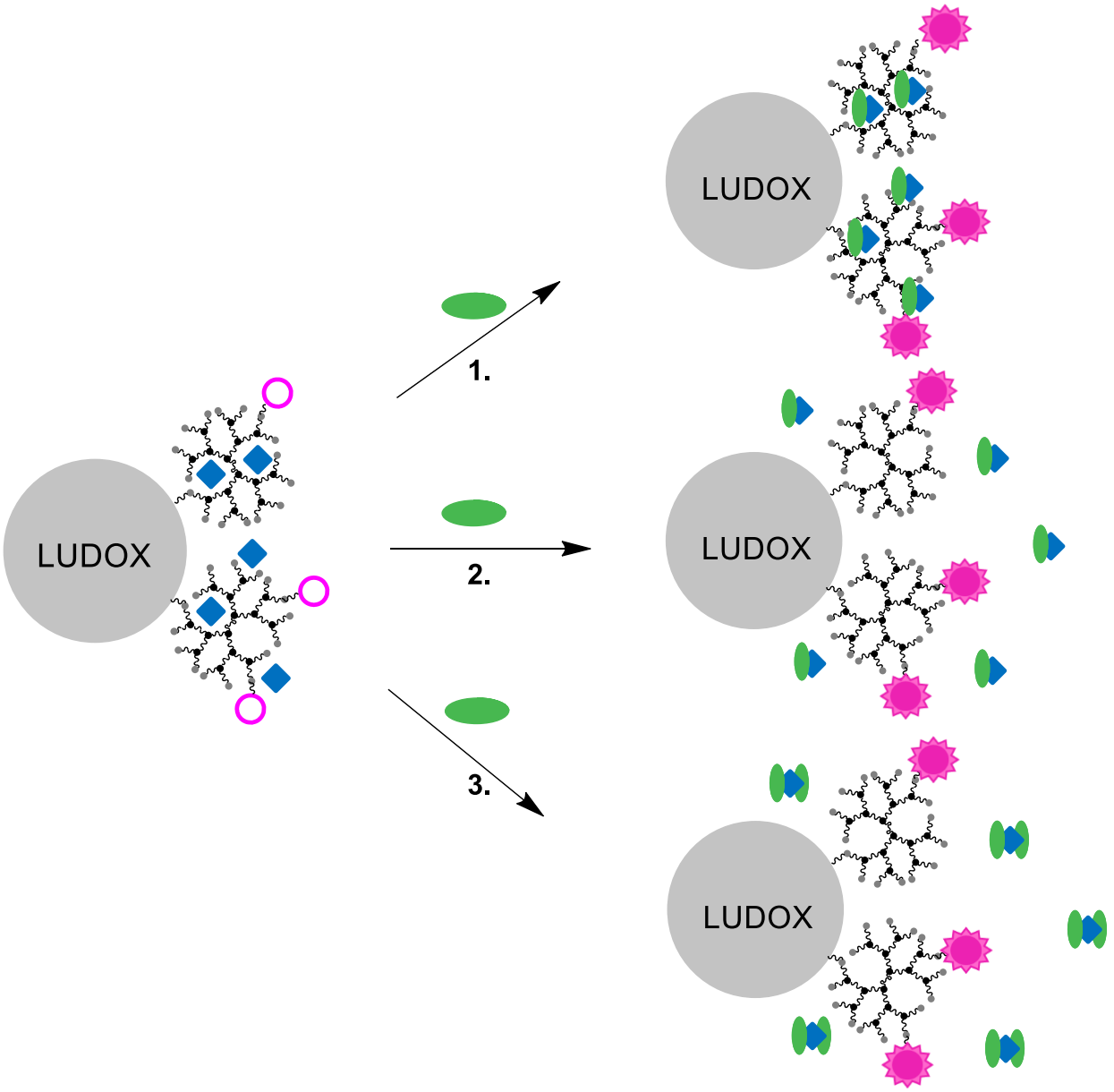

Figure 3-19. The three possible mechanisms of fluorescence restoration by cyanide are shown where blue diamonds represent Cu^{2+} and green ovals represent CN^-. Option 1 depicts one cyanide binding to each copper without removing it from the complex; option 2 depicts one cyanide binding to each copper and removing it from the dendrimer; option 3 depicts two cyanide ions binding to each copper and removing it from the dendrimer.

The first possible mechanism claims that each dendrimer bound copper (II) ion binds one cyanide ion, changing the electronics of the coordination complex and interrupting copper FRET quenching. Fabbrizzi and Poggi reported the behavior of metal-amine complexes as

anion receptors in their extensive review, including copper(II)bis-diamine complexes pertinent to dendrimer bound copper (II).[30] Figure 3-20 shows the structure of this compound.

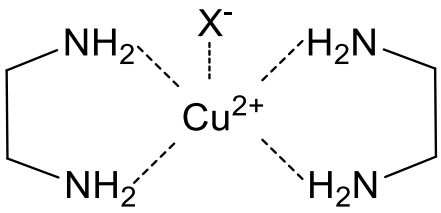

Figure 3-20. Copper(II)bis-diamine with a single bound anion, as reported by Fabbrizzi and Poggi.

The four coordinate amine structure of copper(II)bis-diamine parallels the surroundings that copper experiences in the PAMAM dendrimer, as depicted in Figure 1-10 in Chapter 1. Fabbrizzi explained that bis-diamine bound copper (II) has a tendency to bind just one anion, and that this anion addition is thermodynamically favored by the presence of alkyl substituents on the nitrogen atoms. This suggests that the copper (II) bound to the alkyl-rich dendrimer would behave similarly, binding one cyanide ion. This is supported by an experiment done on SNPG4-R to determine the applicability of the turn-on sensor in a realistic matrix, and is demonstrated in Figure 3-21.

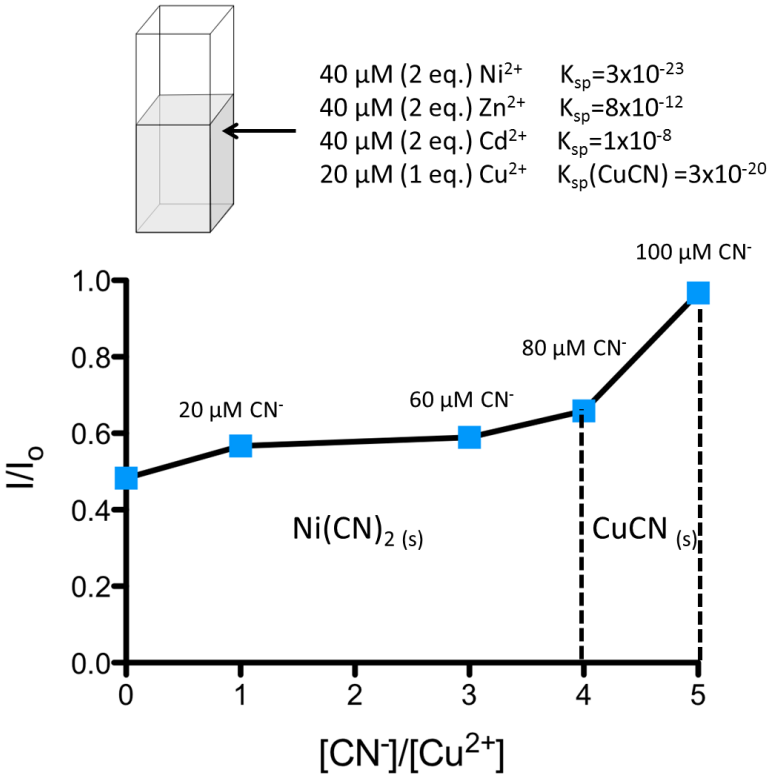

Figure 3-21. Turn-on cyanide sensing of 0.066 mg/mL SNPG4-R in 2:1 EtOH:HEPES buffer (10 mM, pH 7) with a complex matrix of 40 µM added Ni^{2+}, Zn^{2+}, Cd^{2+} each and 20 µM Cu^{2+}.[22,31]

In this experiment, 40 µM Ni^{2+}, Zn^{2+}, and Cd^{2+}, which do not bind to G4, were added to a solution containing 20 µM Cu^{2+} and SNPG4-R. Cyanide was titrated into the solution until the fluorescence was restored, and 5 equivalents (compared to Cu^{2+}) were required to fully restore the signal. The K_{sp} values for the metal ions provide insight into this result; only nickel has a smaller K_{sp} value than copper with cyanide, meaning most of the cyanide complexes the nickel before the copper.[22, 31] The first four equivalents had little effect on the fluorescence, implying that the cyanide was forming $Ni(CN)_2$; only the fifth equivalent was responsible for the signal restoration. This suggests as 1:1 ratio of copper:cyanide is needed to fully restore the fluorescence, but does not assume that the copper (II) has altered its charge. This experiment does not differentiate between 1:1 *binding* of copper and cyanide, or 1:1 *binding and removal*, the next possible mechanism.

The second possible mechanism also requires a 1:1 copper:cyanide ratio. However, this mechanism claims the removal of copper from the dendrimer as $CuCN_{(s)}$. In their paper using copper-modified quantum dots as a cyanide sensor, Shang *et al*. claim this mechanism of

fluorescence return.[13] However, this is only possible if there was a reduction from copper (II) to copper (I) upon binding to the surface of quantum dots. Diallo and coworkers proved that PAMAM dendrimer-bound copper remains copper (II), which would rule out this mechanism as an option.[2] However, Kurnia *et al*. state that cyanide has the ability to reduce copper (II) to copper (I) due to $d_{\pi}-p_{\pi^*}$ back-bonding of the d^{10} Cu(I) orbitals to the π^* orbitals of cyanide.[32] Therefore, it is possible that the cyanide is reducing the copper and removing it as $CuCN_{(s)}$. This is supported by the red shift in peak emission wavelength back to its original, pre-copper wavelength; if the copper were still bound to the dendrimer, the electronic environment would not be the same as free SNPGx-Dye. However, the fact that this reduction of copper by cyanide is highly solvent and pH dependent and that the dendrimer stabilizes copper (II) does not support the likelihood of this mechanism.

The third and final possibility for the mechanism of fluorescence return is that the copper is removed from the dendrimer as $Cu(CN)_{2(s)}$. This mechanism is supported by Diallo's proof that the copper remains copper (II) inside the dendrimer, as well as the stability of $Cu(CN)_2$ in the literature.[2, 33] A 2:1 ratio of cyanide:copper was observed with SNPG4-F when the fluorescence was fully restored; this will be further discussed in section 3.4.5. This also supports a 2:1 removal mechanism. No precipitate, turbidity, or scattering was ever observed upon the addition of cyanide to copper quenched SNP systems, but it cannot be assumed that the precipitate would be visible at these concentrations. The red-shift of the peak emission wavelength that supported mechanism 2 also supports this option, as it suggests complete removal of the copper.

It is currently impossible to determine which of these three mechanisms are occurring in this work. Experimental and literature results support and refute all three, and more research is necessary to finalize a conclusion. While the mechanism of quenching does not affect the ability of the SNP systems to function successfully as turn-on sensors, understanding it would allow the sensor to be further improved and provide new insight in the dendrimer field.

3.4.2 Effect of Dendrimer Generation on Fluorescence Return

The SNPGx-Dye series was optimized to determine which PAMAM dendrimer generation was the most effective turn-on cyanide sensor. While the shape and size of the dendrimer changes with generation, the way in which copper is bound is similar in all generations; therefore, cyanide should behave similarly for all generations. Figure 3-22 shows the results of copper quenching and subsequent cyanide sensing for SNPG1-R, SNPG3-R, SNPG4-R, and SNPG5-R.

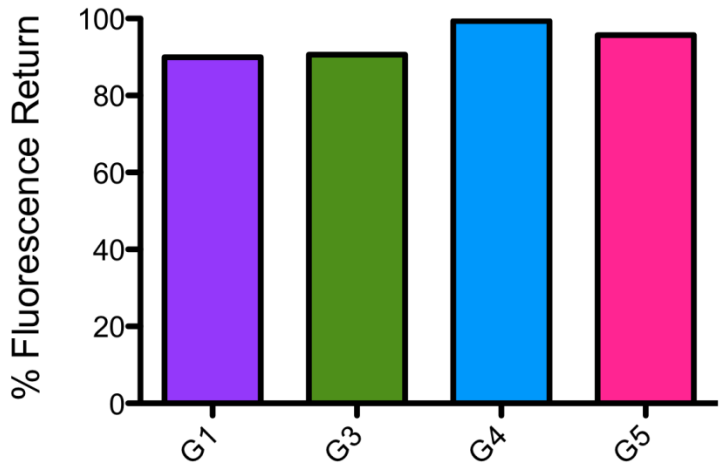

Figure 3-22. Percent fluorescence return for 0.066 mg/mL SNPGx-R in 2:1 EtOH:HEPES buffer (10 mM, pH 7) are shown to be similar for all tested dendrimer generations after quenching by 20 μM Cu^{2+} with 2 equivalents of cyanide.

The results show that cyanide has no preference for any generation of dendrimer. This supports the hypothesis that cyanide is small enough to penetrate the dendrimer and reach the copper, regardless of shape and packing around the nanoparticle. Cyanide is able to penetrate the larger, more closely packed generations just as easily as the smaller, more open generations. It is expected that larger, more bulky chelators like EDTA may show some preference for the smaller more open generations. However, this hypothesis was not tested.

3.4.3 Effect of pH on Fluorescence Return

The pH of SNPGx-R solutions was studied to determine if cyanide sensing was affected by changing the pH of the solution, which changes the protonation states of the dendrimer. Copper quenching was not affected by pH, as seen in section 3.3.3, and the same was hypothesized for cyanide sensing. However, the results in Figure 3-23 disprove this hypothesis.

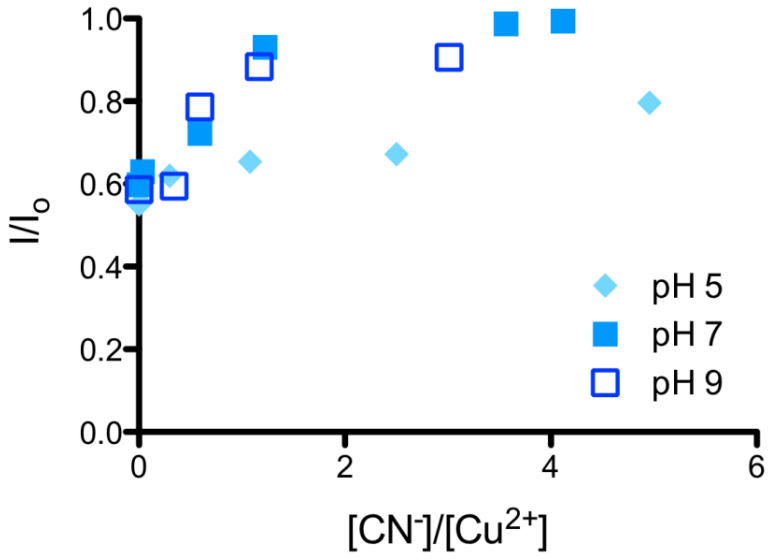

Figure 3-23. Normalized fluorescence intensity (I/I_o) turn-on sensing results for 0.066 mg/mL SNPG4-R in 2:1 EtOH:HEPES buffer (10 mM) with 20 μM added copper and subsequently added cyanide at pH 5, 7, and 9.

At pH 7 and 9, the turn-on sensing is almost identical. The only protonation difference between these pH values are the exterior terminal amine sites; at pH 7, the terminal amines are protonated and at pH 9 they are mostly deprotonated. These results suggest that cyanide has no preference for copper binding between a positive and neutral surface. This is further evidence supporting the hypothesis that the majority of the copper is located in the interior of the dendrimer, as exterior identity does not affect turn-on sensing.

Curiously, adjusting the pH to 5 drastically reduces the effectiveness of the turn-on sensor. Originally, this result was postulated to be due to the equilibrium of cyanide or the protonation of the dendrimer. Cyanide is in equilibrium with its conjugate acid hydrogen cyanide, HCN; below pH 9, this equilibrium strongly favors HCN.[34-35] Figure 3-23 shows that the HCN equilibrium does not affect cyanide and copper interactions, as fluorescence restoration is essentially identical at pH 7 and 9.

One possible explanation for the surprising result at pH 5 lies in the protonation of the dendrimer. At this acidic pH, both the interior and exterior of the dendrimer should be fully protonated and positively charged. This differs from pH 7, which has a neutral interior and a positive exterior. As discussed previously, most of the copper is thought to reside in the interior of the dendrimer; therefore, the exterior charge has little effect on turn-off or turn-on sensing. However, the charge of the interior nitrogens seems vital in turn-on sensing. It is possible that

the negatively charged cyanide ions are electrostatically attracted to the protonated interior nitrogens on the dendrimer, prohibiting cyanide-copper interactions and prohibiting fluorescence restoration. This would imply that the cyanide feels a stronger pull from the dendrimer than from the coordinated copper. Because this charge-based attraction is not covalent bonding, it may not change the electronics of the SNPGx-Dye system, leaving the fluorescence and the emission maximum unchanged. To prove this hypothesis, a large excess of cyanide should be added to the copper quenched system to overpower the electrostatic dendrimer-cyanide interactions; however, this experiment has not currently been done. This hypothesis is further corroborated in the next section.

3.4.4 Effect of Surface Charge on Fluorescence Return

Having studied the effects of positive and neutral charges within the dendrimer, it was logical to also study negative exterior surface charges. The carboxylic acid-modified SNP used in section 3.3.4 were also used to determine the effect of surface charge on turn-on cyanide sensing. The results of section 3.4.3 showed that a positive or neutral surface charge did not affect cyanide sensing, as most of the copper is located in the dendrimer's interior. Figure 3-24 displays the results of turn-on sensing experiments for cyanide using the SNPG4-R-COOH particles at pH 5 and 7.

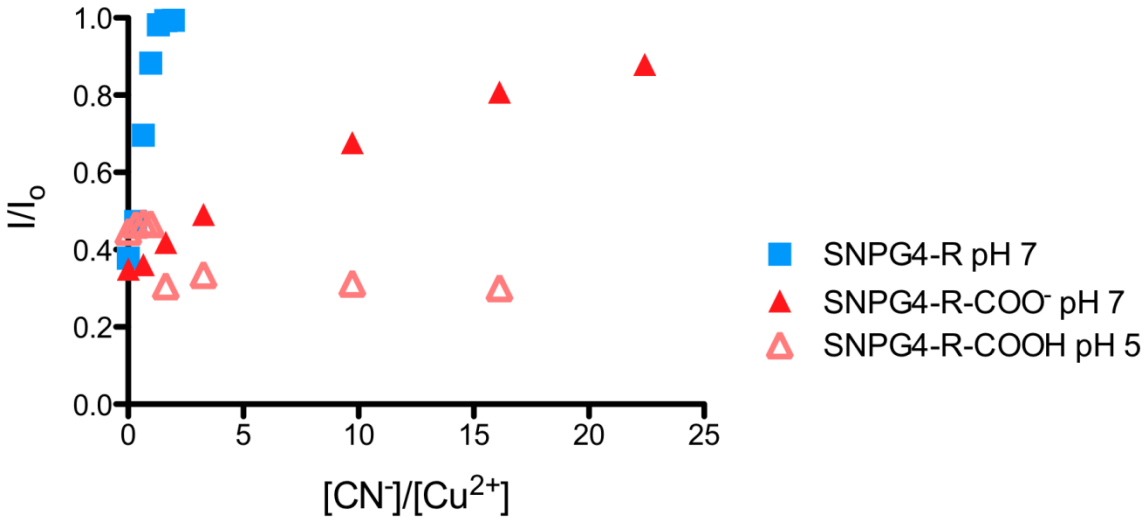

Figure 3-24. Normalized fluorescence intensity (I/I_o) turn-on sensing results for 0.066 mg/mL SNPG4-R and SNPG4-R-COOH in 2:1 EtOH:HEPES buffer (10 mM) with 20 μM added copper and subsequently added cyanide at pH 5 and 7.

The data for SNPG4-R at pH 7 represents the turn-on sensing that is discussed in previous sections of this chapter, where the fluorescence is fully restored after 1.3 equivalents of cyanide have been added. In comparison, the SNPG4-R-COOH particles both at pH 7 and pH 5 are clearly inferior. Again, the results lie in the protonation state of the dendrimer (shown in Figure 3-8 in section 3.3.4).

At pH 5, the SNPG4-R-COOH particles have a neutral surface and a positive interior. As essentially no fluorescence is restored, this supports the hypothesis in section 3.4.3; the cyanide anions must be preferentially interacting with the positively charged dendrimer over the copper or are excluded from the dendrimer. This prevents copper-cyanide interactions, and results in no turn-on sensing. At pH 7, the SNPG4-R-COOH particles have a negative surface and a neutral interior. While the neutral interior supports cyanide interactions with copper, the sensing is not as efficient as expected; it requires around ten times more cyanide than its positive or neutral surface counterparts. This result implies that the negative surface repels the cyanide anion and prevents it from penetrating the dendrimer. Eventually, enough cyanide is added to overcome this electrostatic repulsion. The drastic difference between pH 5 and 7 here reinforces the importance of understanding that the copper is mostly in the interior of the dendrimer.

The results of this section in conjunction with the previous section suggest that the optimum protonation state for cyanide sensing is a neutral interior with a neutral or positive exterior. The results also confirm that the majority of the copper is in the interior of the dendrimer, as was hypothesized by the results of both turn-off and turn-on sensing.

3.4.5 Effect of Organic Dye on Fluorescence Return

SNPG4-R and SNPG4-F were used to test the effect of organic dye on turn-on sensing for cyanide. The fluorescein-modified particles showed an advantage in turn-off copper sensing due to dye loading, and a similar result was predicted for turn-on sensing. This hypothesis was tested two ways: first, by comparing the anion selectivity of the two systems, and second, by comparing the shape of their cyanide titration curves. Figure 3-25 shows the results of the selectivity experiment.

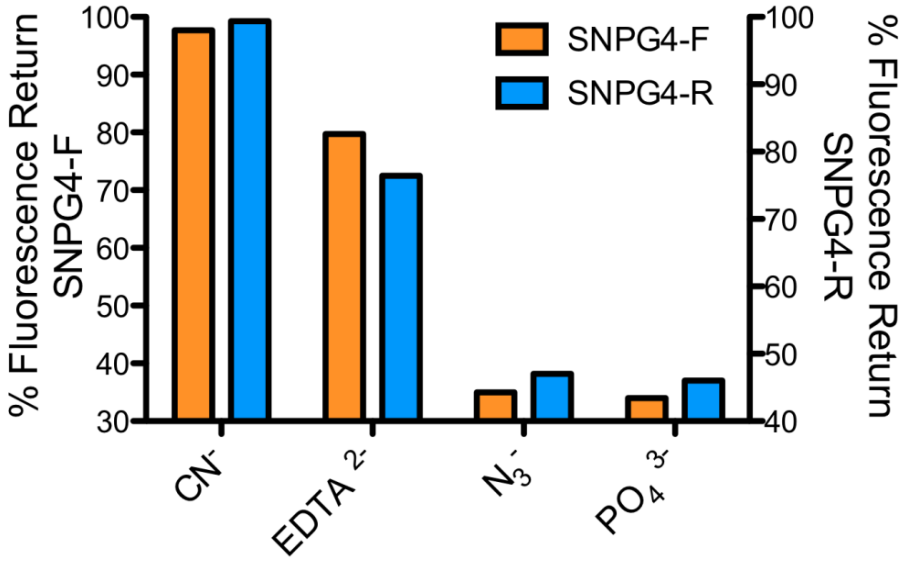

Figure 3-25. Percent fluorescence return after the addition of 2 equivalents of anions for 0.066 mg/mL SNPG4-R and SNPG4-F in 2:1 EtOH:HEPES buffer (10 mM, pH 7) after 60% quenching by 20 μM Cu^{2+}. The data is plotted on separate axes because each system was quenched to a different percent upon copper addition.

The data is plotted with a dual y-axis because the R and F systems were quenched differently by the same amount of copper. The SNPG4-F system was quenched to around 30%, and the SNPG4-R system to 40%. Therefore, the bars in the plot above should be compared to their corresponding axis. The selectivity discussed in section 3.4.1 with SNPG4-R for cyanide was also observed for SNPG4-F. Both dyes behaved similarly with respect to all anions tested.

The turn-on titration curves were also examined for both dye systems, and are seen in Figure 3-26. The results here were more surprising than the selectivity results. A subtle difference exists between the two systems in that the fluorescein-based system requires nearly two equivalents of cyanide to fully restore the fluorescence, whereas the rhodamine-based system requires only 1.3 equivalents.

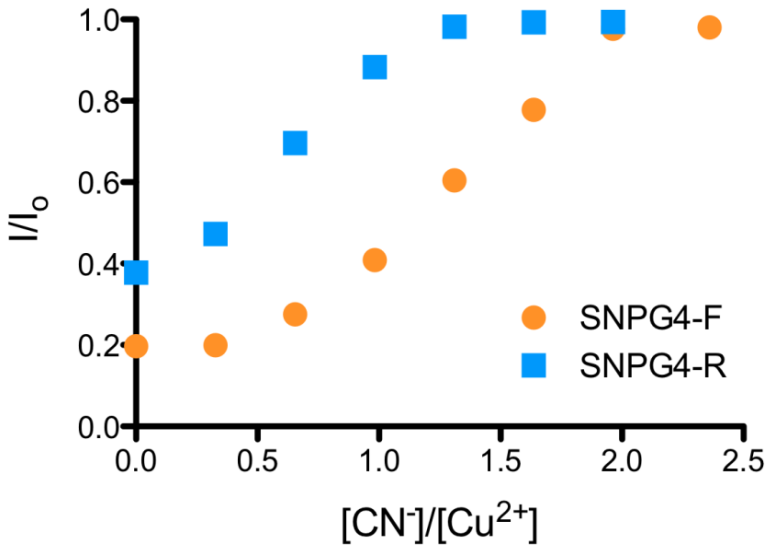

Figure 3-26. Normalized fluorescence return (I/I_o) after the addition cyanide for 0.066 mg/mL SNPG4-R and SNPG4-F in 2:1 EtOH:HEPES buffer (10 mM, pH 7) after quenching by 20 μM Cu^{2+}.

One possible explanation for this result lies in the starting points of each experiment. As discussed in section 3.3.5, SNPG4-F is quenched more effectively with copper than SNPG4-R. This was most likely due to the larger number of bound FITC dyes, originating from the size and structure of FITC. Another possible explanation for the result in Figure 3-26 is the charge of the dyes; RITC carries a positive charge on one of its arms, whereas FITC has neutral arms. Both dyes would have deprotonated carboxylic acids at neutral pH, leaving RITC as a neutral zwitterion and FITC as a negatively charged molecule. This negative charge scattered around the surface may repel the cyanide anion, similarly to the deprotonated surface of SNPG4-R-COOH at pH 7. A larger amount of cyanide would be required to overcome the small but significant repulsion from FITC, which most likely explains the surprising result in Figure 3-26.

3.5 Analytical Parameters of Copper (II) and Cyanide Sensing

To quantify the sensitivity of the SNPG4-Dye turn-off and turn-on sensors, the limit of detection (LOD), limit of quantification (LOQ), and limit of linearity (LOL) were calculated for copper (II) and cyanide ions. The limit of detection and limit of quantitation were determined following the procedure outlined in section 3.2.3 and using equations 3-3 and 3-4 respectively, where *s* is the standard deviation of seven replicate samples, and *m* is the slope of the linear curve of intensity vs. concentration.[12, 22] The limit of linearity was determined graphically.

$$LOD = \frac{3s}{m} \quad 3\text{-}3$$

$$LOQ = \frac{10s}{m} \quad 3\text{-}4$$

Table 3-3 summarizes the limit of linearity, limit of detection, and limit of linearity for SNPG4-R and SNPG4-F with copper (II) and cyanide. The results for turn-off copper sensing follow the quenching results discussed in section 3.3 and show that the FITC modified SNP are more effective than the RITC modified SNP. Both systems exhibit narrow linearity ranges. The results for turn-on cyanide sensing prove that dye has no effect on the LOL or LOD, and show that SNPG4-F has a larger concentration region of linearity.

Table 3-3. Analytical Parameters of SNPG4-R and SNPG4-F for turn-off and turn-on sensing.

		SNPG4-R	SNPG4-F
Cu^{2+}	LOD (μM)	0.38 ± 0.09	0.21 ± 0.04
	LOQ (μM)	1.3 ± 0.3	0.6 ± 0.1
	LOL(μM)	0.2-1.0	0.2-1.2
CN^-	LOD (μM)	0.97 ± 0.03	0.98 ± 0.05
	LOQ (μM)	3.2 ± 0.1	3.2 ± 0.2
	LOL(μM)	6.0-27.0	6.0-40.0

The analytical parameters in Table 3-3 prove that both the turn-off and turn-on sensors perform well below the legal limits of 20 μM copper (II) and 7 μM cyanide set by the EPA.[11, 24] The limit of detection results for copper and cyanide sensing are well below or similar to the results of other fluorescent sensing systems.[11-13, 23-24] Together, these results imply that the SNPG4-Dye sensors are successful as turn-off and turn-on sensors.

3.6 Conclusion

The SNPGx-Dye systems were synthesized to be sensitive and selective copper (II) sensors. Turn-off quenching results prove that the sensor is selective for copper (II) over other common metal ions, most likely due to FRET quenching between the tethered dye and the absorbance band that arises from Cu^{II}-Gx interactions. At low copper concentrations, Stern-Volmer analysis proved that SNPG4-F is the most effective turn-off system. This is most likely due to the size and shape of the dendrimer and the optimal dye loading of the fluorescein. While pH has little effect on the amine-terminated dendrimer copper quenching, carboxylation of the terminal amines showed that a negative surface allows for even more efficient quenching due to electrostatic interactions between the copper and the negative surface. Turn-off quenching

results with SNPG4-R-COOH also suggested that most of the copper(II) was located in the interior of the dendrimer. The optimized systems were shown to be sensitive, giving limits of detection and quantitation below EPA standards.

Following copper quenching, the subsequent turn-on sensing for cyanide was also optimized. The SNPGx-Dye systems are selective for cyanide over EDTA, azide, and phosphate at low anion:copper ratios; this unforeseen result confirms that most of the copper is coordinated in the interior of the dendrimer. The turn-on sensing is not dendrimer generation dependent, but does rely drastically on the charge of the interior amines and therefore on pH. Carboxylation of the dendrimer's terminal amines showed that a negative surface charge reduced the effectiveness of the sensor as it may repel cyanide. Therefore, an amine terminated surface was more effective than a carboxylate surface in turn-on cyanide sensing. The loading and charge of the tethered fluorescent dyes suggested a slight preference for RITC over FITC, but the two systems experience similar limits of detection. The mechanism of cyanide sensing is still undetermined. The sensitivity of the turn-on systems were similar to comparable fluorescent systems and were well below EPA standards.

Together, these results show that SNPGx-Dye systems are sensitive and selective sensors for copper (II) and cyanide in mixed ethanol-aqueous media. The known coordination relationship between copper (II) and PAMAM dendrimers was exploited to obtain a customized turn-off sensor that is controlled by dendrimer generation. The same system was then used as a turn-on sensor for cyanide, and the previously unexplored relationship between dendrimer protonation and anion-metal binding was studied. Both the turn-off and turn-on sensors were optimized for sensitivity and selectivity and were proven effective even in a complex, competitive matrix. Further research needs to be done to solidify the mechanism of fluorescence restoration. The FRET sensing mechanism for turn-off sensing inspired the experiments in Chapter 4, which focus on using the SNPGx-Dye system as a FRET sensor for small organic molecules and to determine the dye spacing on the surface of the SNP.

3.7 References

1. Zhou, L.; Russell, D. H.; Zhao, M.; Crooks, R. M., Characterization of Poly(amidoamine) Dendrimers and Their Complexes with Cu2+ by Matrix-Assisted Laser Desorption Ionization Mass Spectrometry. *Macromolecules* **2001,** *34* (11), 3567-3573.
2. Diallo, M. S.; Christie, S.; Swaminathan, P.; Balogh, L.; Shi, X.; Um, W.; Papelis, C.; Goddard, W. A., III; Johnson, J. H., Jr., Dendritic Chelating Agents. 1. Cu(II) Binding to Ethylene Diamine Core Poly(amidoamine) Dendrimers in Aqueous Solutions. *Langmuir* **2004,** *20* (7), 2640-2651.
3. Chen, J.; Zeng, F.; Wu, S.; Su, J.; Zhao, J.; Tong, Z., A facile approach for cupric ion detection in aqueous media using polyethyleneimine/PMMA core-shell fluorescent nanoparticles. *Nanotechnology* **2009,** *20* (36), 365502/1-365502/7.
4. Bergonzi, R.; Fabbrizzi, L.; Licchelli, M.; Mangano, C., Molecular switches of fluorescence operating through metal centered redox couples. *Coord. Chem. Rev.* **1998,** *170*, 31-46.
5. Crooks, R. M.; Zhao, M.; Sun, L.; Chechik, V.; Yeung, L. K., Dendrimer-Encapsulated Metal Nanoparticles: Synthesis, Characterization, and Applications to Catalysis. *Acc. Chem. Res.* **2001,** *34* (3), 181-190.
6. Zhao, M.; Crooks, R. M., Homogeneous hydrogenation catalysis with monodisperse, dendrimer-encapsulated Pd and Pt nanoparticles. *Angew. Chem., Int. Ed.* **1999,** *38* (3), 364-366.
7. Boaz, H.; Rollefson, G. K., The Quenching of Fluorescence. Deviations from the Stern-Volmer Law. *Journal of the American Chemical Society* **1950,** *72* (8), 3435-3443.
8. Buboltz, J. T.; Bwalya, C.; Reyes, S.; Kamburov, D., Stern-Volmer modeling of steady-state Förster energy transfer between dilute, freely diffusing membrane-bound fluorophores. *Journal of Chemical Physics* **2007,** *127* (21), 215101.
9. Chen, Y.; Rosenzweig, Z., Luminescent CdS Quantum Dots as Selective Ion Probes. *Analytical Chemistry* **2002,** *74* (19), 5132-5138.
10. Buboltz, J. T., Steady-state probe-partitioning fluorescence resonance energy transfer: a simple and robust tool for the study of membrane phase behavior. *Phys. Rev. E: Stat., Nonlinear, Soft Matter Phys.* **2007,** *76* (2-1), 021903/1-021903/7.
11. Zong, C.; Ai, K.; Zhang, G.; Li, H.; Lu, L., Dual-Emission Fluorescent Silica Nanoparticle-Based Probe for Ultrasensitive Detection of Cu2+. *Anal. Chem. (Washington, DC, U. S.)* **2011,** *83* (8), 3126-3132.
12. Cui, J.; Wang, S.; Huang, K.; Li, Y.; Zhao, W.; Shi, J.; Gu, J., Conjugation-induced fluorescence labelling of mesoporous silica nanoparticles for the sensitive and selective detection of copper ions in aqueous solution. *New J. Chem.* **2014,** *38* (12), 6017-6024.
13. Shang, L.; Zhang, L.; Dong, S., Turn-on fluorescent cyanide sensor based on copper ion-modified CdTe quantum dots. *Analyst (Cambridge, U. K.)* **2009,** *134* (1), 107-113.
14. Montealegre, C.; Rasines, B.; Gómez, R.; de la Mata, F. J.; García-Ruiz, C.; Marina, M. L., Characterization of carboxylate-terminated carbosilane dendrimers and their evaluation as nanoadditives in capillary electrophoresis for vegetable protein profiling. *Journal of Chromatography A* **2012,** *1234* (0), 16-21.
15. Cakara, D.; Kleimann, J.; Borkovec, M., Microscopic Protonation Equilibria of Poly(amidoamine) Dendrimers from Macroscopic Titrations. *Macromolecules* **2003,** *36* (11), 4201-4207.
16. Lakowicz, J. R., *Principles of Fluorescence Spectroscopy, 2nd Ed.* Kluwer Academic/Plenum Publishers, 1999.
17. Magde, D.; Rojas, G. E.; Seybold, P., Solvent Dependence of the Fluorescence Lifetimes of Xanthene Dyes. *Photochem. Photobiol.* **1999,** *70* (737).

18. Rhodamine B Isothiocyanate http://www.sigmaaldrich.com/catalog/product/aldrich/283924?lang=en&region=US.
19. Fluorescein Isothiocyanate. http://www.sigmaaldrich.com/catalog/substance/fluoresceinisothiocyanateisomeri38938332632711?lang=en&region=US.
20. McHedlov-Petrossyan, N. O.; Vodolazkaya, N. A.; Doroshenko, A. O., Ionic equilibria of fluorophores in organized solutions: the influence of micellar microenvironment on protolytic and photophysical properties of rhodamine B. *J. Fluoresc.* **2003,** *13* (3), 235-248.
21. Smith, S.; Pretorius, W., Spectrophotometric determination of pKa values for fluorescein using activity coefficient corrections. *Water SA* **2002,** *28* (4), 395-402.
22. Harris, D. C., *Exploring Chemical Analysis*. 4 ed.; 2009.
23. Zeng, Q.; Cai, P.; Li, Z.; Qin, J.; Tang, B. Z., An imidazole-functionalized polyacetylene: convenient synthesis and selective chemosensor for metal ions and cyanide. *Chem. Commun. (Cambridge, U. K.)* **2008,** (9), 1094-1096.
24. Rhaman, M. M.; Alamgir, A.; Wong, B. M.; Powell, D. R.; Hossain, M. A., A highly efficient dinuclear Cu(II) chemosensor for colorimetric and fluorescent detection of cyanide in water. *RSC Adv.* **2014,** *4* (97), 54263-54267.
25. Chen, J.; Russo, R.; Chao, W.; Margerum, L. D.; Malachowski, M. R.; White, R.; Thawley, Z.; Thayer, A.; Rheingold, A. L.; Zakharov, L. N., Synthesis, structure, redox properties and azide binding for a series of biphenyl-based Cu(ii) complexes. *Dalton Transactions* **2007,** (24), 2571-2579.
26. Dhara, K.; Saha, U. C.; Dan, A.; Sarkar, S.; Manassero, M.; Chattopadhyay, P., A new water-soluble copper(II) complex as a selective fluorescent sensor for azide ion. [Erratum to document cited in CA153:439676]. *Chem. Commun. (Cambridge, U. K.)* **2010,** *46* (48), 9262.
27. Casella, L.; Gullotti, M.; Pallanza, G.; Buga, M., Spectroscopic and binding studies of azide-copper(II) model complexes. *Inorg. Chem.* **1991,** *30* (2), 221-7.
28. Wadas, T. J.; Wong, E. H.; Weisman, G. R.; Anderson, C. J., Copper Chelation Chemistry and its Role in Copper Radiopharmaceuticals. *Current Pharmaceutical Design* **2007,** *13* (1), 3-16.
29. Lin, Y.-M.; Yen, S.-C., Effects of additives and chelating agents on electroless copper plating. *Applied Surface Science* **2001,** *178* (1–4), 116-126.
30. Fabbrizzi, L.; Poggi, A., Anion recognition by coordinative interactions: metal-amine complexes as receptors. *Chem. Soc. Rev.* **2013,** *42* (4), 1681-1699.
31. Table of Solubility Product Constants. http://owl.cengage.com/departments/NYInstitTechBrownHolme2e/appendix/ksp.html
32. Kurnia, K.; Giles, D. E.; May, P. M.; Singh, P.; Hefter, G. T., Cyanide thermodynamics 2. Stability constants of copper(I) cyanide complexes in aqueous acetonitrile mixtures. *Talanta* **1996,** *43* (12), 2045-2051.
33. Chung, S.-Y.; Nam, S.-W.; Lim, J.; Park, S.; Yoon, J., A highly selective cyanide sensing in watervia fluorescence change and its application to in vivo imaging. *Chemical Communications* **2009,** (20), 2866-2868.
34. Cotton, F.; Wilkinson, G.; Murillo, C.; Bochmann, M., *Advanced Inorganic Chemistry, 6th Ed.* Wiley: New York, 1999.
35. D 6696-05 Standard Guide for Understanding Cyanide Species. International, A., Ed. 2005.

Chapter 4
Forster Resonance Energy Transfer (FRET) Using SNPGx-Dye

This chapter focuses on using SNPGx-Dye particles as Forster Resonance Energy Transfer (FRET) sensors to sense for 8-Anilino-1-naphthalenesulfonic acid (ANS) and to determine the distance between dendrimer-bound species and tethered fluorescent dyes. Additionally, FRET is used with a new, dual dye SNPG4-RF system to determine the dye spacing between the dendrimer-tethered dyes.

4.1 Introduction

The concept of FRET is discussed extensively in Chapter 1, due to its importance in the copper turn-off sensing mechanism. FRET is a distance dependent, photophysical energy transfer process that relies on spectral overlap between the emission spectrum of an energy donor and the absorbance spectrum of the energy acceptor.[1] FRET is responsible for the quenching of SNPGx-Dye systems by copper, due to the spectral overlap between the 605 nm absorbance band of Cu^{II}-Gx and the emission of the tethered fluorescent dye.[2] Figures 1-11 and 1-14 in Chapter 1 summarize the FRET process spectrally. When the donor is excited, some of its energy is transferred to the acceptor, causing an increase in the absorbance and emission of the acceptor and a decrease in the emission of the donor. This energy transfer is only possible if the two species are fixed between 1 and 10 nm apart.[1]

Each pair of fluorescent species, also called a FRET pair, has its own Forster distance (R_0), also called the critical distance.[1, 3] The critical distance is defined as the distance when transfer efficiency (E) is 50%.[3] Equation 4-1, also shown in Chapter 1, shows the relationship between the critical distance and the actual distance between the two dyes (r) in terms of efficiency.[1, 4]

$$E = \frac{{R_0}^6}{{R_0}^6 + r^6} \qquad 4\text{-}1$$

Equation 4-2 shows that the efficiency can also be expressed in terms of the fluorescence intensity of the FRET donor in the presence (I_{DA}, where I is the fluorescent intensity and DA stands for “donor and acceptor”) and absence (I_D, where D stands for “donor” only) of the FRET acceptor.[1]

$$E = 1 - \frac{I_{DA}}{I_D} \qquad 4\text{-}2$$

Combining Equations 4-1 and 4-2 to form Equation 4-3 shows that the actual distance between the energy donor and acceptor (r) can be determined from the fluorescent intensity of the donor if the critical distance is known.

$$E = 1 - \frac{I_{DA}}{I_D} = \frac{R_O^6}{R_O^6 + r^6} \qquad 4\text{-}3$$

FRET is widely used to determine the distance between the energy acceptor and the donor using equation 4-3. Recently, many biological systems have used FRET to determine distances involved in protein folding, nucleic acid structures, and in interactions between DNA, RNA, and proteins.[1, 5-7] With Equation 4-3 in mind, a new SNPG4-RF system was designed following the same synthesis of SNPG4-R, but replacing the RITC with and equal amounts of RITC and FITC. This gave a G4-modified SNP with both the acceptor and donor of a known FRET pair, RITC and FITC, tethered to the dendrimer. If FRET was observed spectrally, the average distance between the tethered dyes could be calculated to give a better idea of the dye spacing on the SNPGx-Dye systems.

Besides being used for distance determination, FRET also provides an increasingly popular simple and sensitive detection method for small analytes. Recently, FRET has been used to sense for a number of analytes including sugars, enzymes, metal ions in live cells, cysteine-like thiols, methylated DNA, and many other small molecules.[3, 8-11] Inspired by these sensors and previous work done in this research group, the ability of the SNPG4-R system to detect small conjugated analytes was evaluated.

The FRET-mediated copper (II) quenching in Chapter 3 relied on the RITC dye as an energy donor, and the red shifted Cu^{II}-Gx as the energy acceptor. However, it is also possible that the RITC dye could be a FRET acceptor if another species was bound in the dendrimer with an overlapping blue shifted emission. As the diameter of a G4 dendrimer falls within the FRET distance requirements of 1-10 nm, any small conjugated organic molecule that binds within the dendrimer could also be a likely FRET donor. This would allow the same system that sensed for copper and cyanide to also sense for small organic molecules.

This hypothesis was tested using 8-Anilino-1-naphthalenesulfonic acid (ANS). This research group has studied the relationship between ANS and PAMAM dendrimers extensively in the past, and proved that ANS binds inside the dendrimer due to electrostatic and hydrophobic interactions. Figure 4-1 shows the chemical structure of ANS, which is negatively charged due to the sulfonic acid pKa of 0.37.[12]

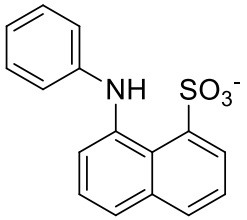

Figure 4-1. The structure of 8-Anilino-1-naphthalenesulfonic acid (ANS) is shown at pH > 0.37.

The ANS-dendrimer binding induces an increase in ANS fluorescence and a shift in emission wavelength for the bound ANS, which is around 480 nm.[13] Therefore, ANS is an ideal substrate to test the hypothesis that small organic molecules that bind in the dendrimer can be sensed through FRET. Figure 4-2 summarizes the difference between this FRET sensing and the turn-off FRET sensing for copper (II).

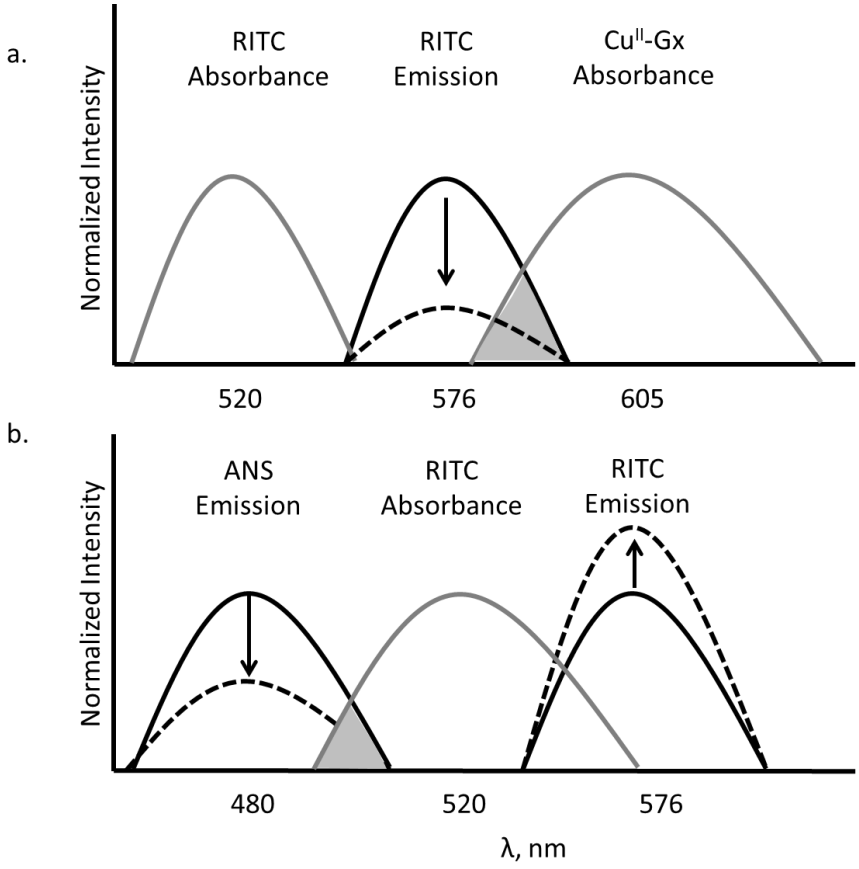

Figure 4-2. The normalized emission (black) and absorption (grey) spectra for a) RITC and dendrimer-bound copper (II) and b) RITC and dendrimer-bound ANS. The dotted lines represent the spectra when both the energy donor and acceptor are present, and the solid lines represent free donor or acceptor in solution. The RITC changes from an energy donor in a) to an energy acceptor in b).

The spectral overlap between ANS emission and SNPG4-R absorbance (or SNPG4-F) allows the tethered dye to behave as a FRET acceptor, whose fluorescent emission increases when ANS is bound to the dendrimer. Unlike the FRET sensing of copper (II) in Chapter 3, FRET sensing of ANS is confirmed by *two* changes in emission: a decrease for the donor, and an increase for the acceptor. The turn-off copper (II) sensing is only observed using the donor (RITC), as the Cu^{II}-Gx is not fluorescent. FRET sensing of ANS also allows the distance (*r*) between the dendrimer bound ANS and the tethered fluorescent RITC to be calculated, giving insight to the location of bound molecules within the dendrimer.

Of course, sensing for ANS in aqueous solution is not a priority facing analytical chemists as it is not a highly common or dangerous molecule. However, it represents a proof of concept that small, conjugated organic molecules that interact with the dendrimer could be sensed for using FRET and the same SNPGx-Dye systems that were previously used to sense for copper (II) and cyanide.

4.2 Experimental

The following sections summarize the synthesis of SNPG4-RF, as well as the procedures used to determine dye spacing of dendrimer-tethered dyes and to sense for ANS. All chemicals and instrumentation used are listed in Chapters 2 and 3.

4.2.1 Preparation of SNPG4-RF

Two systems were synthesized to determine the dye spacing of dendrimer-tethered dyes: a concentrated (SNPG4-RF-C) and dilute (SNPG4-RF-D) dye loading of RITC and FITC. The concentrated system was designed to have similar dye loadings as the previously synthesized SNPG4-R systems, and the dilute system had 10 times less dye as a reagent. Once the dyes on the surface were quantified, the effect of dye loading on FRET efficiency was then studied. The preparation of both SNPG4-RF-C and D systems followed the scheme in Figure 4-3, but with different amounts of dye.

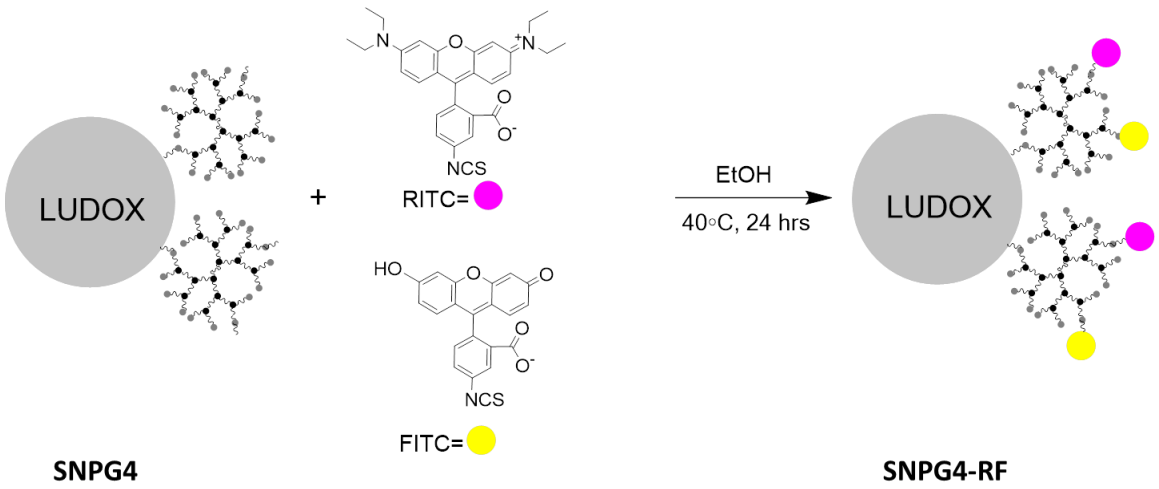

Figure 4-3. SNPG4 modification with both RITC and FITC to obtain a dendrimer coated SNP surrounded by two fluorescent FRET partners.

SNPG4-RF-C:

SNPG4 (295 mg) was taken up in 70 mL dry ethanol, and an excess of equal amounts of RITC and FITC (2.5 mg of each) was added. The reaction was stirred at 40°C under a nitrogen atmosphere for 24 h away from light. The resulting mixture was centrifuged at 15,000 RPM for 60 min. The fluorescent supernatant was decanted, and the resulting solid was washed with ethanol and centrifuged at 15,000 RPM for 30 min. The supernatant was decanted, and the washing was repeated until no fluorescence remained in the wash. The remaining material was vacuum dried and stored in a desiccator overnight, yielding 200 mg of a red-orange solid (**SNP-Gx-RF-C**).

SNPG4-RF-D:

A 0.036 mg dye/mL stock solution of both RITC and FITC was made in EtOH by adding 2.5 mg of each dye to 70 mL of EtOH (representing the dye concentration of the SNPG4-RF-C reaction). SNPG4 (295 mg) was taken up in 63 mL dry ethanol, and 7 mL of the stock dye solution was added to dilute the stock by 10 in the reaction flask. The reaction was stirred at 40°C under a nitrogen atmosphere for 24 h away from light. The resulting mixture was centrifuged at 15,000 RPM for 60 min. The fluorescent supernatant was decanted, and the resulting solid was washed with ethanol and centrifuged at 15,000 RPM for 30 min. The supernatant was decanted, and the washing was repeated until no fluorescence remained in the wash. The remaining material was vacuum dried and stored in a desiccator overnight, yielding 180 mg of a pale pink-orange solid (**SNP-Gx-RF-D**).

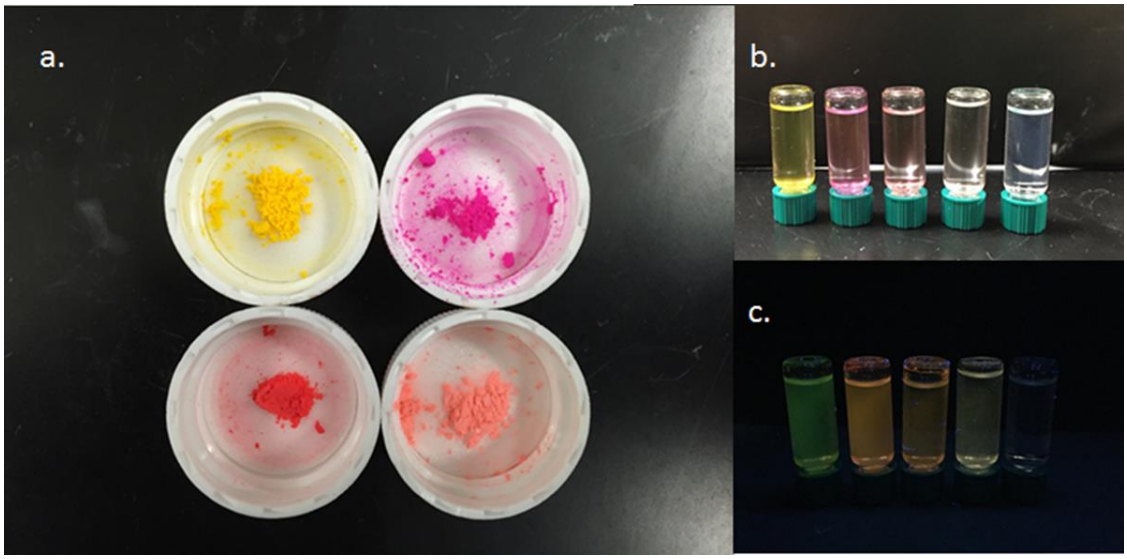

Figure 4-4. The SNPGx-Dye systems synthesized in this thesis are shown: a) from left to right, top to bottom: SNPG4-F, SNPG4-R, SNPG4-RF-C, SNPG4-RF-D; b) in 2:1 EtOH: H2O from left to right: SNPG4-F, SNPG4-R, SNPG4-RF-C, SNPG4-RF-D; c) excited with a long wavelength 365 nm UV lamp in the same order as b).

Dye Loading for SNPG4-RF systems:

The dye loadings for both SNPG4-RF-C and SNPG4-RF-D were required to set up FRET control experiments. The dilute system was too dilute to test by UV-Visible spectrophotometry, so fluorescence spectroscopy was necessary. However, dye loading for both RITC and FITC within the same SNP system was problematic as the excited donor transfers its energy to the acceptor and increases its emission. Therefore, the dye loading of the acceptor only (RITC) was quantified by exciting at 520 nm, which is red-shifted past the excitation wavelength of the donor (FITC). The dyes were assumed to have equal concentrations on the surface; this assumption may not be accurate, but was the only reasonable option to determine control measurements.

A series of standard solutions of RITC were created in ethanol, and fluorescence emission measurements were taken with λ_{ex}=520 nm and λ_{em}=576 nm to create a calibration curve. A sample of SNP-Gx-RF (~1-2 mg) was sonicated in 25 mL of ethanol for 30 minutes. The measurements at the corresponding wavelength and the calibration curve were used to quantify the acceptor dye loading of the dual-dye SNP. The dye loading for RITC was assumed equal to the FITC concentration.

Table 4-1 shows the results of the dye loading for the concentrated and dilute dye loadings on the SNP. The 10 times more concentrated synthesis gave 1.5 times higher dye

loading. This result suggests that the excess dye used in the typical SNPG4-Dye synthesis is large, and only a small fraction of those dyes are bound to the dendrimer.

Table 4-1. RITC and FITC dye loading for SNPG4-RF systems assuming an equal ratio of dyes.

	RITC Loading (μmol/g)	Assumed FITC Loading (μmol/g)
SNPG4-RF-C	18	18
SNPG4-RF-D	12	12

The total dye loading of the SNPG4-RF-C is 36 μmol/g, which is similar to the SNPG4-R dye loading in Chapter 2. However, it is important to understand that this is still an assumption based on the forced 1:1 ratio of RITC and FITC. Previously, FITC had higher dye loadings than RITC at the same concentration; this was hypothesized to be due to small functional groups and electrostatic interactions between the negative dye and the positive dendrimer surface. However, literature FRET studies with multiple dyes in solution including RITC and FITC have assumed that the initial synthetic dye ratio is also present after synthesis.[14] While the differences between FITC and RITC dye loadings are effectively ignored in this work to obtain preliminary FRET results and a proof of concept, more experimentation is necessary if this work is continued in the future.

4.2.2 Procedures

Fluorescence spectroscopy was performed on a Horiba Jobin Yvon FluoroMax-4 spectrofluorometer using Jobin Yvon FluorEssence Software. Emission spectra were collected with excitation and emission slit widths of 5 nm, and the emission spectra collection started $\geq$10 nm to the red of the excitation wavelength.

4.2.2.1 Dye Spacing on SNPG4-RF

The following procedure was repeated for SNPG4-RF-C and SNPG4-RF-D:

A 0.066 mg/mL solution of SNPG4-RF in 2:1 EtOH:HEPES buffer (10 mM, pH 7) was sonicated at room temperature for 30 minutes. The fluorescence intensity of 3.00 mL of the solution was measured with λ_{ex}=495 nm and λ_{em}=510-650 nm. As the FRET efficiency is calculated from the fluorescence intensity of the donor, a control of SNPG4-F in the absence of RITC was required to determine the efficiency and therefore the dye spacing. A solution of SNPG4-F in 2:1 EtOH:HEPES buffer (10 mM, pH 7) was made to have the same concentration

of FITC as the SNPG4-RF solution, and its fluorescence was measured with λ_{ex}=495 nm and λ_{em}=510-650 nm.

4.2.2.2 ANS Sensing with SNPG4-R

A 0.066 mg/mL solution of SNPG4-R in 2:1 EtOH:HEPES buffer (10 mM, pH 7) was sonicated at room temperature for 30 minutes. The fluorescence intensity of 3.00 mL of the solution was measured with λ_{ex}=380 nm and λ_{em}=400-650 nm (this is the RITC acceptor control excited at FRET wavelength). A solution of ANS in 2:1 EtOH:H_2O was added to make the concentration of ANS less than the concentration of RITC and the fluorescence was measured with λ_{ex}=380 nm and λ_{em}=400-650 nm (this is the FRET measurement). A second control was made of 3.00 mL of a 0.066 mg/mL sonicated solution of SNPG4 with no tethered dye in 2:1 EtOH:HEPES buffer (10 mM, pH 7). The same amount of ANS was added to this solution, and the fluorescence was measured with λ_{ex}=380 nm and λ_{em}=400-650 nm (this is the ANS donor control). These measurements give an acceptor control, a donor control, and a FRET system measurement to give a complete FRET picture.

The extinction coefficient of the acceptor (SNPG4-R) was required to calculate the critical distance of ANS sensing. The absorbance at 576 nm of the same 0.066 mg/mL solution of SNPG4-R from above (no ANS) was used to calculate the extinction coefficient using Beer's Law. The concentration of the dye was known, as dye loading had been previously performed on the SNPG4-R particles, allowing the extinction coefficient to be calculated.

4.3 Distance Determination of Dye Spacing on SNPG4-RF

The newly synthesized SNPG4-RF-C and SNPG4-RF-D systems were tested to determine if FRET between the dendrimer-tethered RITC and FITC dyes was possible, and if the distance between the two dyes could be obtained. The hypothesis was that the more concentrated synthesis would allow the dyes to be closer together, and fall within the 1-10 nm FRET distance.[1] The dilute synthesis would yield a poorer FRET efficiency, as some of the dyes may be outside the required FRET distance. Figure 4-5 shows the results of the procedure described in section 4.2.2.1 for SNPG4-RF-C and SNPG4-RF-D.

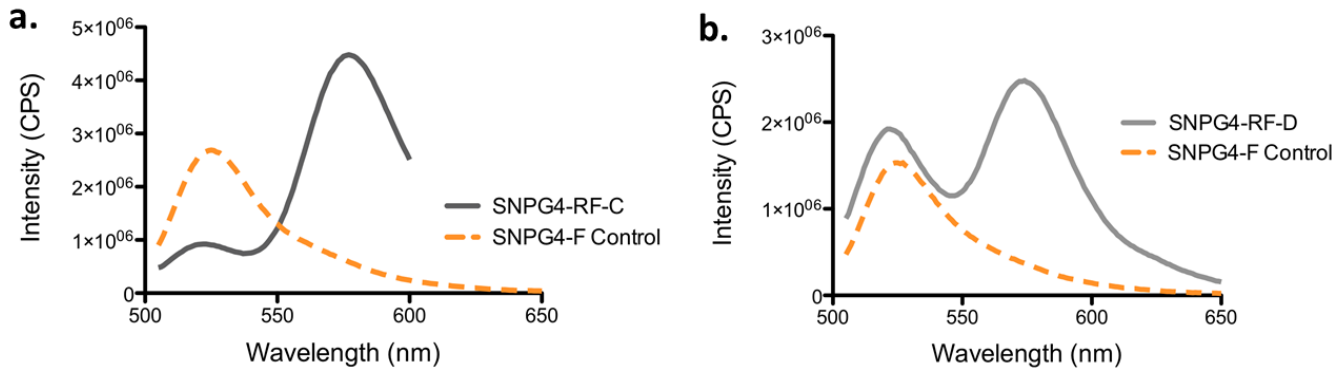

Figure 4-5. Emission spectra 0.066 mg/mL in 2:1 EtOH:HEPES buffer (10 mM, pH 7) for a) SNPG4-RF-C and b) SNPG4-RF-D (solid lines). The donor controls (dotted lines) are solutions of SNPG4-F made to the same concentration of FITC as the SNPG4-RF system (λ_{ex}=380 nm).

The results in Figure 4-5 suggest that FRET is occurring in the concentrated system, and not in the dilute system as the fluorescence intensity of the donor, FITC, decreases in the concentrated system. This is because the excited donor is able to transfer some of its energy to the acceptor, which results in less donor fluorescence. This is *not* observed in the dilute system; instead, no significant change in donor emission is observed. These preliminary results suggest that the dyes in the dilute system are too far apart (>10 nm) to participate in FRET.

The efficiency of the FRET system (SNPG4-RF-C) was calculated to be 0.66, or 66%, using Equation 4-2. One advantage of using RITC and FITC in this experiment is they are a common FRET pair. Therefore, the critical distance value, R_0, is known to be 4.0 nm.[15] The average FRET spacing between the two dyes in this system, r, was calculated to be 3.6 nm using Equation 4-3.

As the SNPG4-RF-C system was modeled after the SNPG4-R system in terms of dye concentration, the FRET spacing between two dyes was used to estimate the amount of dye molecules on each dendrimer under ideal conditions and realistic conditions. Spherical packing of smaller spheres (S_1) onto a larger sphere (S_2) can be estimated by projecting a square with sides equal to the radius of S_1 onto the surface of S_2. The LUDOX SNP is a 20 nm sphere, and a G4 PAMAM dendrimer has a diameter of 4.4 nm as discussed in Chapter 1. If G4 dendrimers packed ideally onto the surface of the spherical SNP, roughly 64 G4 dendrimers could fit around one SNP. According to the FRET experiment above, the average distance between two dyes on the surface is 3.6 nm. If the entire surface area of the G4 dendrimer were available for dye loading, then 4.7 dyes could fit on each dendrimer. Figure 4-6 depicts this spherical packing. However, the dye will probably not penetrate the dendrimer, so most likely only about half of

each dendrimer is available for incoming dye. Additionally, the G4 dendrimers will not pack perfectly around the SNP. If the dendrimers only pack half as efficiently as possible, and only half of the dendrimer is available for dye loading, 1.2 dyes will be bound to each dendrimer.

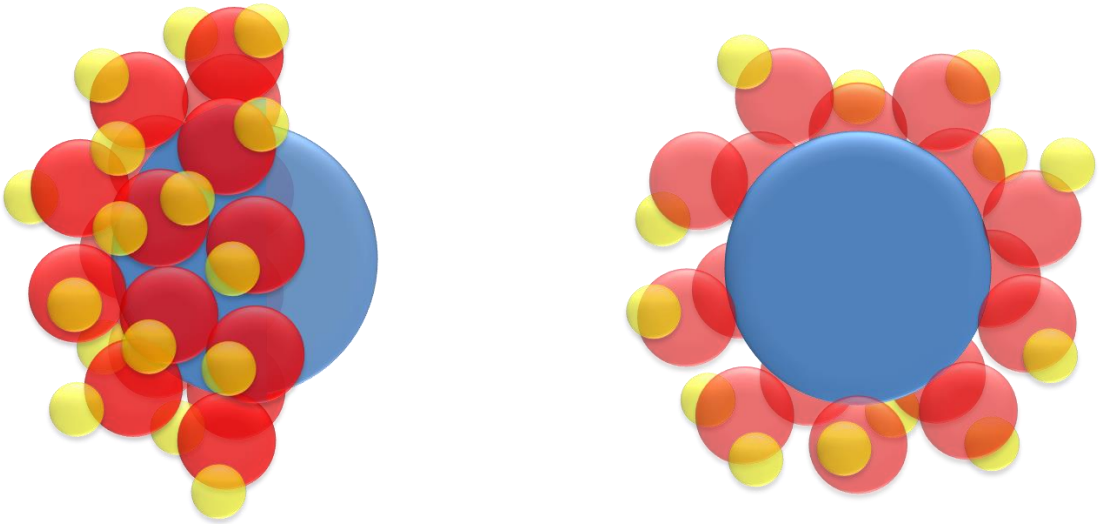

Figure 4-6. Theoretical PAMAM dendrimer (S_1, red) and dye (yellow) packing on the surface of LUDOX (S_2, blue) is visualized with a half-coated SNP (left) and a cross section (right).

These results suggest that each G4 dendrimer may have 1-5 dyes tethered to it, depending on the packing efficiency of dendrimers and dyes. While this is an estimate, it is helpful in verifying the hypothesis that multiple dyes can be tethered to each dendrimer. Of course, the dendrimers are not perfectly spherical and the FRET distance obtained is an average dye spacing. However, this FRET-based model proves that it is *possible* for more than one dye to bind on the surface of each dendrimer.

4.4 FRET Sensing of ANS Dye Using SNPG4-R

As discussed in Chapter 1, the emission spectrum of an energy donor and the absorbance spectrum of an energy acceptor must overlap to induce FRET. Both the SNPG4-R and SNPG4-F systems were evaluated as potential FRET acceptors for ANS sensing, as the emission spectra of ANS is blue-shifted compared to both systems and is centered at 480 nm. SNPG4-R was the optimal partner for ANS sensing. The spectral overlap between the *excitation* spectra of SNPG4-F and ANS is too large, causing FITC to be excited by the ANS excitation. This is called cross talk, and is sometimes unavoidable but should be minimized if possible.[4] The better spacing between the excitation spectra of SNPG4-R and ANS allows for more

reliable and consistent measurements, with only a fraction of the cross talk seen by SNPG4-F. Figure 4-7 shows the required spectral overlap between SNPG4-R and ANS.

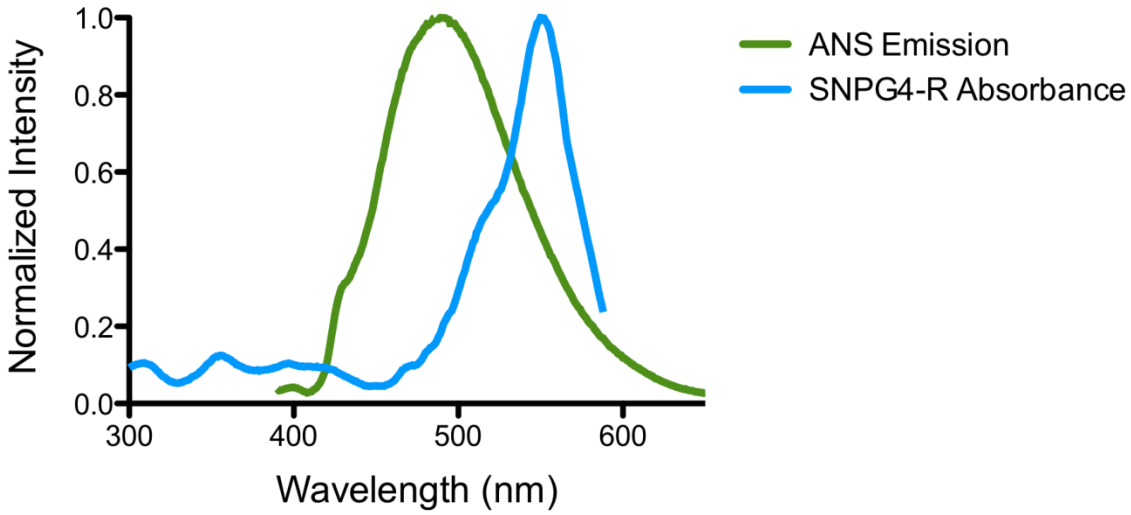

Figure 4-7. The spectral overlap between the emission spectrum of dendrimer-bound ANS (λex=380 nm) and the absorption spectrum of SNPG4-R is shown in 2:1 EtOH: HEPES buffer (10 mM, pH 7).

When the energy donor, G4-bound ANS, is excited at 380 nm, it transfers some of its energy to the acceptor, RITC. The fluorescence of the ANS is quenched, and the fluorescence of the RITC increases as it absorbs energy from the dendrimer bound ANS. Figure 4-8 summarizes the FRET results for SNPG4-R and ANS following the procedure outlined in section 4.2.2.2.

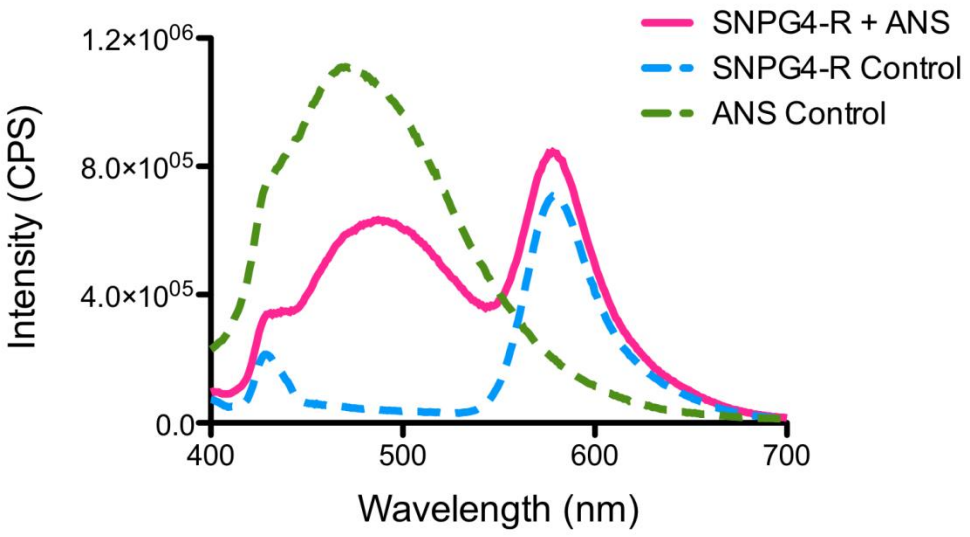

Figure 4-8. Emission spectra of 0.066 mg/mL SNPG4-R in 2:1 EtOH:HEPES buffer (10 mM, pH 7) with 0.4 μM ANS show the Forster resonance energy transfer from the donor (ANS) to the acceptor (RITC). The donor control is 0.4 μM ANS bound to SNPG4 in the absence of RITC, and the acceptor control is 0.066 mg/mL SNPG4-R with no added ANS. The controls are represented by dotted lines, and the FRET measurement is a solid line. All spectra were collected with λ_{ex}=380 nm.

The results in Figure 4-8 confirm the hypothesis that FRET is occurring between ANS and RITC. The ANS emission is quenched, and the RITC emission increases as it absorbs energy from the bound ANS. The "ANS Control" in Figure 4-8 is a solution of SNPG4 and ANS, with no dye. This allows the ANS to bind in the dendrimer as it does with SNPG4-R. The change is emission is much larger for the donor, ANS, than the acceptor, RITC. This disparity is common in FRET work, as most FRET sensors are designed having a larger number of FRET donors than acceptors to increase efficiency.[16] The larger number of acceptors increases the likelihood that FRET will occur, but also increases the number of acceptor molecules that do not experience FRET. Therefore, a larger percentage of the donor molecules than acceptor molecules are involved in the FRET process, resulting in a more significant spectral change for the donor. This is one of the reasons why FRET efficiency is calculated from the intensity difference of the donor.

The efficiency of the FRET system shown in Figure 4-8 is 46% by Equation 4-2.The low efficiency may be due to the spacing of the two species, or to the use of G4 dendrimers as a linker between the acceptor and donor. Sindbert *et al.* state in their FRET research with nucleic acids that longer, more flexible linkers can lower the efficiency of energy transfer from the donor

to the acceptor, by absorbing energy or altering the dyes environment through microscale motion.[6] However, similar efficiencies are used successfully and commonly in FRET sensing.[1, 4, 14, 17]

A control experiment using ANS and SNP-R without dendrimer was done to confirm the dendrimer's role in FRET. No FRET efficiency was seen between SNP-R and ANS. This result confirms that the ANS must be bound within the dendrimer to participate in FRET with the SNP bound RITC dye. Without the dendrimer to bind to, the ANS is free in solution. As FRET relies on two dyes at fixed distances, ANS does not transfer any of its excited energy to the RITC.

The 46% FRET efficiency can also be used to determine the spacing between ANS and the RITC dye using Equation 4-1. However, this equation relies on the critical distance, R_0, described in section 4.1. While well-known FRET pairs have critical distance values in the literature, ANS and RITC have never been used together in FRET and no R_0 value has ever been reported. In their paper on the practical use of corrected fluorescent spectra in proteins, Hink *et al.* discussed the computational work involved in determining a critical distance value.[18] In support of the work done by Hink et al., Visser, Vysotski, and Lee produced an excel spreadsheet that calculates the R_0 value based on the variables in the succeeding equations.[19] This spreadsheet was used to determine the critical distance for ANS and SNPG4-R. The critical distance for two fluorophores is determined from Equation 4-4, where K^2 is the dipole orientation factor, ϕ_o is the quantum yield of the donor in the absence of the acceptor, n is the refractive index of the solvent, and J is the degree of spectral overlap between the donor emission and the acceptor excitation.[3, 18-19]

$$R_o = 0.2108[K^2 \phi_o n^{-4} J]^{1/6} \qquad 4\text{-}4$$

A value of 2/3 was used for the dipole orientation factor K^2, which is commonly used for organic fluorophores.[3, 19] The quantum yield of the donor, ANS, in 2:1 EtOH:H_2O is 0.05.[20] The refractive index of 2:1 EtOH:H_2O is 1.36.[21] The spectral overlap, J, is determined by Equation 4-5. The spreadsheet produced by Visser *et al.* was especially useful in determining this spectral overlap, as the donor emission spectrum is normalized (F_D) and the acceptor excitation spectrum is scaled to its molar extinction coefficient (ε_A).[3, 18-19] The extinction coefficient for the SNPG4-R acceptor was determined to be 28,000 $M^{-1}cm^{-1}$ through Beer's law (details in section 4.2.2.2). This value, along with the emission spectra for ANS and the excitation spectra for SNPG4-R, were entered into the spreadsheet to determine the spectral overlap and the subsequent critical distance value.

$$J = \int_0^\infty F_D(\lambda)\varepsilon_A(\lambda)(\lambda^4)d\lambda \qquad 4\text{-}5$$

The calculations shown above gave a critical distance, R_0, of 29.0 Å, or 2.9 nm. This represents the distance at which the energy transfer between ANS and G4-bound RITC is 50%. The actual distance between ANS and RITC, *r*, was determined to be 3.0 nm using the 46% efficiency and Equation 4-1. This falls within the accepted FRET distance of 1-10 nm, and helps to visualize the FRET spacing on SNP. The diameter of a G4 dendrimer is 4.4 nm, as discussed in Chapter 1. Therefore, this FRET spacing supports the hypothesis that the ANS is bound to the interior of the dendrimer. Figure 4-9 shows a scaled representation of what the FRET interaction between ANS and RITC looks like. The FRET experiments discussed in this section also give clues to the spacing between copper (II) bound in the dendrimer and RITC. Although their binding interactions differ, ANS and copper (II) both bind to the interior of G4 PAMAM dendrimers and interact with RITC dyes tethered to the exterior of the dendrimer. While the FRET distance of 4.4 nm is specific to ANS, it is hypothesized that copper (II) would have a similar FRET distance.

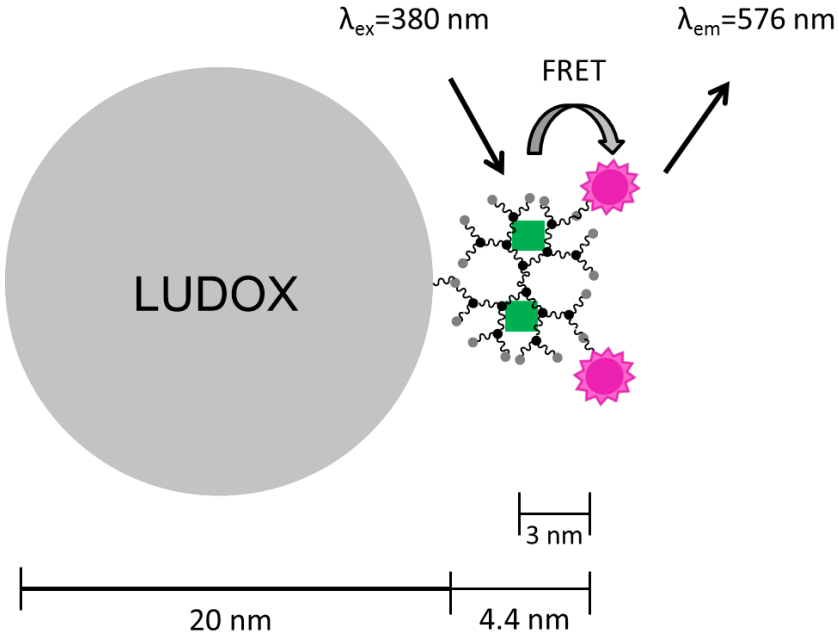

Figure 4-9. The FRET spacing at pH 7 between dendrimer-bound ANS (green) and tethered RITC dyes (pink) is shown to scale, where the FRET spacing *r* is calculated to be 3.0 nm.

The successful FRET between ANS and SNPG4-R effectively determined the distance between dendrimer bound species and tethered dyes. These results also prove that the same

system that senses copper (II) and cyanide can sense conjugated organic molecules. The effect of concentration and pH on ANS sensing are discussed in the next sections. While ANS is not a highly toxic or abundant molecule, the work done in this section is a proof of concept. The future implications of these results are further discussed in section 4.5.

4.4.1 Effect of pH on FRET Efficiency

The FRET observed for ANS and SNPG4-R hinges on the negatively charged ANS binding electrostatically inside the positive dendrimer. As the protonation of the dendrimer relies on pH, the FRET efficiency should also be pH dependent. The protonation of a PAMAM dendrimer is shown in Figure 1-9 in Chapter 1. The pKa values of the interior tertiary amines and terminal primary amines for a G4 dendrimer are 6.3-6.9 and 9.0-10.3, respectively.[22] At pH<6, the interior and exterior of the dendrimer are positive; at pH values between 7 and 9, the interior is neutral and the exterior is positive; at pH>10, the interior and exterior are both neutral. Therefore, ANS should have difficulty binding at pH 10 and FRET should be less efficient. Figure 4-10 shows the results of FRET experiments at pH 4, 7, and 10.

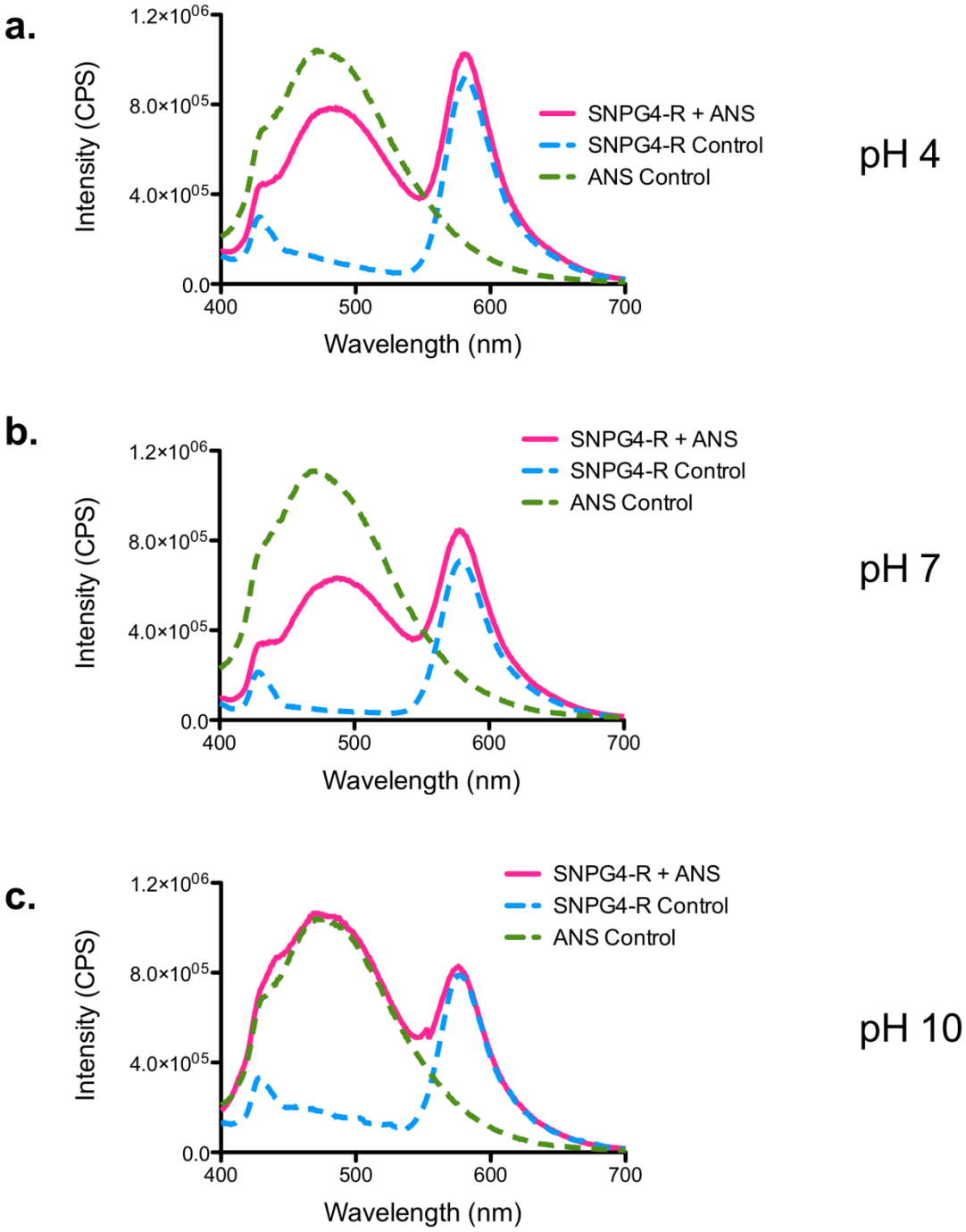

Figure 4-10. Emission spectra of 0.066 mg/mL SNPG4-R in 2:1 EtOH:H2O at: a) pH 4; b) pH 7; and c) pH 10 with 0.4 μM ANS show the Forster resonance energy transfer from the donor (ANS) to the acceptor (RITC). The donor control is 0.4 μM ANS bound to SNPG4 in the absence of RITC, and the acceptor control is 0.066 mg/mL SNPG4-R with no added ANS. All spectra were collected with λ_{ex}=380 nm.

The results in Figure 4-10 show that no FRET occurs at pH 10 based on donor emission, as the ANS does not transfer any of its energy to the dendrimer bound RITC. This suggests the negatively charged ANS cannot electrostatically bind with the neutral dendrimer, leaving it free in solution. As FRET relies on the donor and acceptor being at a *fixed* distance apart, free ANS cannot participate in FRET. FRET does occur at pH 4 and pH 7 with respective efficiencies of 24% and 46% calculated using Equation 4-2. The difference between the FRET efficiencies at these pH values was not as predicted. The dendrimer is fully protonated at pH 4, while at pH 7 only the exterior amines have a positive charge. Therefore, assuming the calculated R_0 does not change significantly with pH, the efficiency at pH 4 should be higher. However, the ANS is not in excess; the amount of ANS added is five times less than RITC. Therefore, the ANS is not necessarily bound throughout the whole dendrimer at pH 4. It may bind preferentially to the interior, as the positive charges are more abundant. This is confirmed by the calculation of *r*, the average FRET distance using Equation 4-1, which is 3.5 nm at pH 4 compared to 3.0 nm at pH 7. At pH 7, most of the ANS should bind to the exterior protonated amines and not the neutral interior nitrogens. The distance between ANS and RITC is shorter for the exterior-bound ANS at pH 7, making the energy transfer more efficient.

If this experiment were repeated with an excess concentration of ANS, it is hypothesized that the FRET efficiency at pH 4 would be greater than pH 7. The entirely positive pH 4 dendrimer would be able to bind more ANS than the partially positive pH 7 dendrimer. While this experiment was not tested in these fundamental FRET experiments, it may be a useful experiment for future FRET work. At the donor and acceptor concentrations used in this work, pH 7 was determined to be the most efficient. The effect of concentration on FRET at pH 7 is studied in the next section.

4.4.2 Effect of Donor and Acceptor Concentration on FRET Efficiency

Having determined an optimum pH for FRET studies, the effect of energy donor and acceptor concentration was optimized to determine the most efficient FRET system. FRET is most likely to occur when a single donor molecule is surrounded by a number of acceptor molecules.[16] In this work, this can be pictured as a single ANS molecule with many RITC dyes surrounding it. In previous experiments, the ratio of the donor, ANS, to the acceptor, RITC, was around 1:10 to maximize energy transfer. This ratio was modified to investigate the effect of the ratio of donor:acceptor concentrations on FRET efficiency. Figure 4-11 shows the results of these experiments.

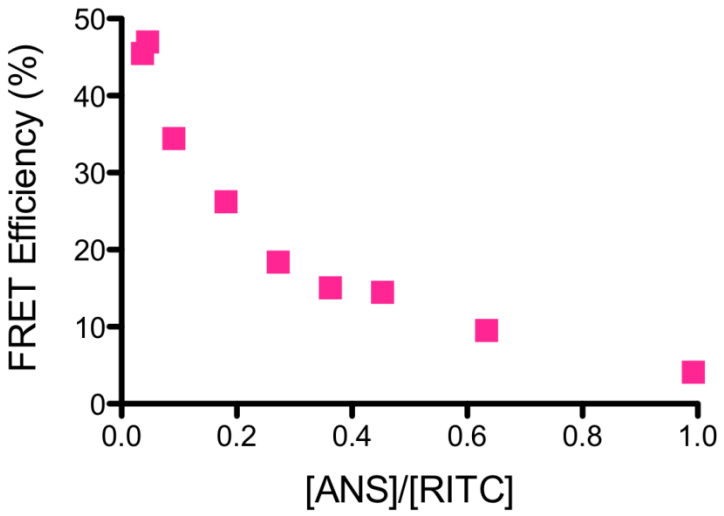

Figure 4-11. The effect of FRET donor and acceptor concentration is shown for 0.066 mg/mL SNPG4-R at pH 7 with increasing amounts of ANS. FRET efficiencies were calculated using Equation 4-2 and control measurements of SNPG4-bound ANS and SNPG4-R without ANS (λex=380 nm, λem, ANS=480 nm, λem, RITC=576 nm).

The results in Figure 4-11 shows that lowering the ratio of donor:acceptor leads to more efficient FRET. This confirms the hypothesis that increasing the number of acceptors surrounding the donor molecule also increases the FRET efficiency. The ratio of 0.1 that was used in previous experiments is proven to be near the optimum ratio. In future FRET experiments with ANS or other organic molecules, a similar ratio should be used to achieve optimal efficiency.

4.5 Future FRET Applications

The experiments discussed in section 4.4 show that SNPG4-R can sense for ANS via FRET. As mentioned previously, detecting ANS in aqueous solutions is not a priority for analytical chemists; however, the methods used in ANS sensing can also be applied to other, more important small organic molecules. Any conjugated organic molecule that is small enough to bind in the dendrimer can be sensed with the SNPG4-Dye system by customizing the tethered dye to have optimal spectral overlap between the emission of the analyte and the excitation of the tethered dye. Figure 4-12 shows the proposed analytes and sensing mechanisms.

Phenanthrene (Phe) is a polycyclic aromatic hydrocarbon (PAH), a class of molecules that are highly regulated environmental pollutants, and their sensitive detection is growing in

importance.[23] Lard *et al.* sensed for phenanthrene using FRET in their work using dye modified free PAMAM dendrimers.[24] Specifically, they modified G5 PAMAM dendrimers with Alexa Fluor 350, whose absorbance at 350 nm has a strong spectral overlap with the 380 nm emission of dendrimer-bound phenanthrene. The phenanthrene bound hydrophobically to the dendrimer, and transfered some of its energy to the Alexa Fluor dye upon excitation at 350 nm. An increase in emission was detected for the dye, while a corresponding decrease in emission occurred for phenanthrene. The maximum FRET efficiency was less than 30%. The authors suggested that the interior of the large G5 dendrimers (5.7 nm diameter) was not accessible to the sizeable Phe due to preferential binding at the exterior amines, reducing the amount of binding sites. They also cited dendrimer aggregation as a major source of their poor efficiencies, as the dendrimers were not tethered to a sensing platform. By adhering slightly smaller G4 dendrimers (4.4 nm diameter) to silica nanoparticles, both of these issues may be alleviated, thus increasing the efficiency. Additionally, Lard *et al.* attempted to optimize their sensor by changing the ratio of Phe:dendrimer. However, it would be better to optimize the Phe:dye ratio, as the ratio of the donor:acceptor ratio leads directly to FRET (Equation 4-2). Work has begun in this research group to modify the SNPG4 system with Alexa Fluor 350 to improve upon the work done by Lard *et al.* and further explore the FRET efficiency.

Recent work by Gao *et al.* used FRET to sense 2,4,6-trinitrotoluene (TNT) in solution and vapor.[25] TNT is a highly explosive nitroaromatic compound that is usually detected by expensive and time consuming gas chromatography.[26] Gao *et al.* modified 200 nm silica nanoparticles with (3-Aminopropyl)triethoxysilane (APTES), the same amine used in the first step of the SNPGx-Dye synthesis in this thesis work. They reacted FITC or Rhodamine X (ROX, similar to RITC) dyes with APTES, resulting in an SNP-NH_2-Dye system that strongly resembled the SNPGx-Dye work done in this work, yet without the polyamine dendrimer. The electron deficient TNT binds to the electron rich primary amines of APTES causing absorption bands at 525 nm and 630 nm. This complex acts as the energy acceptor, just as the Cu^{II}-Gx complex is the energy acceptor for SNPGx-Dye. The fluorescent dye was the energy donor, whose fluorescence was quenched when TNT was bound to the amines. Therefore, the SNP-NH_2-Dye system synthesized by Gao *et al.* functions as a TNT sensor by the same FRET mechanism as the copper sensing of SNPGx-Dye system. In the future, the research results in this thesis could be applied to a TNT sensor mirroring the APTES based sensor described above. Incorporating PAMAM dendrimers as ligands for TNT binding would exponentially increase the number of amine binding sites, and therefore increase the sensitivity of the sensor. Theoretically, the SNPG4-F system would have ideal spectral overlap with the TNT-Gx complex.

The FRET mechanism discussed in this chapter leads to one final application using the SNPGx-Dye systems. Recent physical chemistry and biological work has investigated the interaction between PAMAM dendrimers and amino acids to study protein interactions.[27-28] Specifically, tryptophan (Trp) and tyrosine (Tyr) are fluorescent aromatic amino acids that are known to bind hydrophobically to dendrimers. Therefore, the SNPGx-Dye system could be customized with a fluorescent dye whose excitation spectrum overlaps with the emission spectrum of dendrimer-bound Trp or Tyr. When the amino acid-dendrimer complex is excited, it should transfer energy to the tethered fluorescent dye, behaving as a FRET sensor similar to the ANS sensor described in section 4.4 and the Phe sensor proposed previously. This use of FRET-based amino acid sensing could provide insight into the distance dependence of protein or DNA interactions, which is relevant to both biological and drug industries.

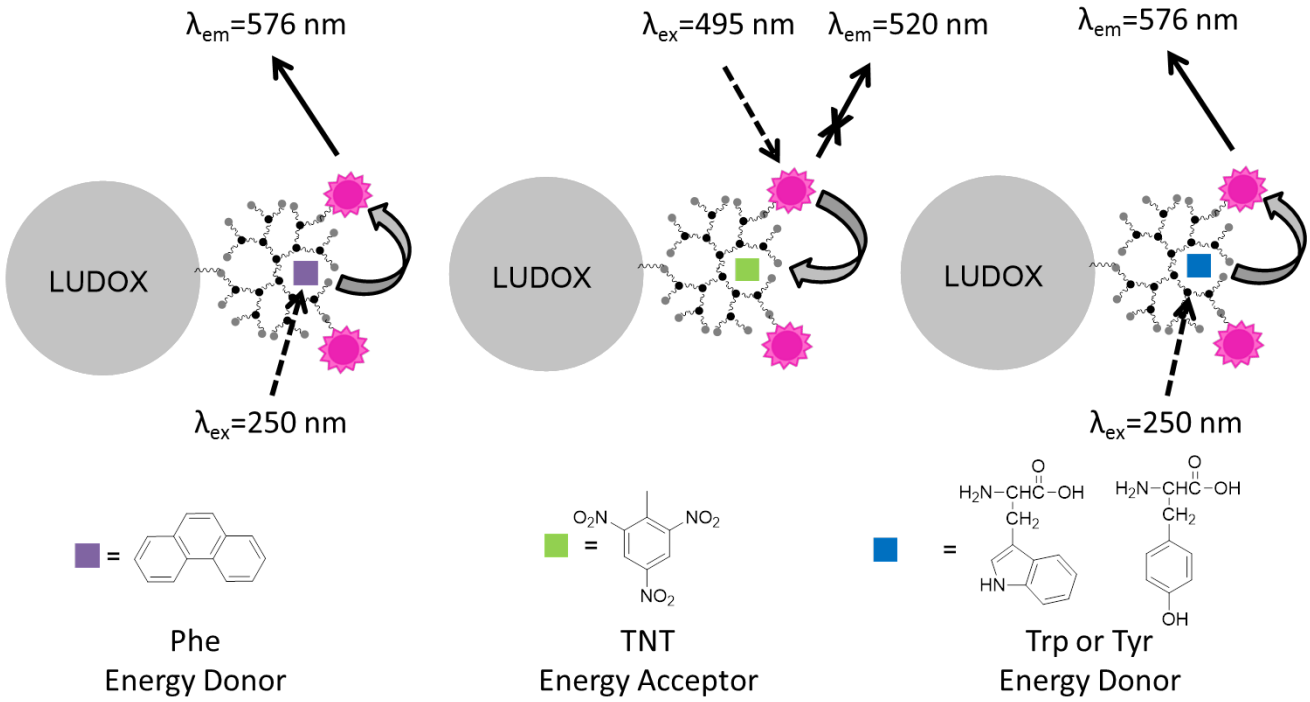

Figure 4-12. Three future FRET sensing experiments are proposed for phenanthrene, TNT, and tryptophan or tyrosine using SNPG4-Dye.

In conclusion, the SNPGx-Dye systems used in this thesis as copper (II), cyanide, and ANS sensors are proposed as FRET sensors for phenanthrene, TNT, and aromatic amino acids tryptophan and tyrosine. These small, organic molecules interact with the dendrimer and induce energy transfer upon excitation of the analyte or the dendrimer-tethered dye. Each sensor can be customized by altering the final step of the synthetic procedure with a dye that has the ideal

spectral characteristics for FRET. The unique excitation and emission spectra of all sensing systems keep the sensors selective, and the dendrimer increases the available binding sites and enhances the sensitivity.

4.6 Conclusion

The research in this thesis focused on creating and using a series of dendrimer modified silica nanoparticles functionalized with fluorescent dyes to sense for small analytes in aqueous solution. The sensors were successfully synthesized and characterized in Chapter 2, yielding a series of SNP-Gx-Dye systems that were modified with different generations of PAMAM dendrimers and fluorescent dyes. The results in Chapter 3 demonstrated that the SNPGx-Dye systems were sensitive and selective for copper (II) ions, as the Cu^{II}-Gx complex quenched the tethered fluorescent dye by FRET. The copper (II) sensor was optimized by changing the dendrimer generation, fluorescent dye, and other parameters, and let to the conclusion that SNPG4-F was the ideal sensor. The same copper (II) sensor was subsequently used to sense for small anions that disrupted the copper quenching. The SNPGx-Dye sensors were sensitive and selective for cyanide at low concentrations, even over the strong chelator EDTA. The smaller cyanide was able to penetrate the interior of the dendrimer, where most of the copper was located, and restore the fluorescent emission by disrupting copper quenching.

This same SNPGx-Dye system was also used to sense for the small organic molecule ANS (Chapter 4) which is known to bind in PAMAM dendrimers. The bound ANS transferred some of its excited state energy to the tethered dye and allowed the FRET distance to be calculated. This sensing of small aromatic organic molecules inspired future thought experiments to sense polycyclic aromatic hydrocarbons such as phenanthrene, electron deficient molecules such as TNT, and aromatic amino acids tryptophan and tyrosine. Additionally, a new system with FRET pair dyes on the same nanoparticle (SNPG4-RF) was synthesized to determine the effect of tethered dye spacing on FRET.

The work described in this thesis provides a new SNP based sensor that utilizes the unique characteristics of PAMAM dendrimers to sense for a wide variety of analytes involved in Forster resonance energy transfer with tethered fluorescent dyes. These new sensing systems provide customizable fluorescent chemosensors that can be tailored to the analyte of interest by modifying the tethered fluorescent dye to change the spectral overlap. The branching structure of the dendrimer improves both the sensitivity and selectivity of the sensors, while the SNP platform and tethered dyes allow the system to be easily used with simple instrumentation in

aqueous solution. In the future, the same sensing system can be modified to sense additional analytes like polycyclic aromatic hydrocarbons, explosives, and amino acids.

4.7 References

1. Hillisch, A.; Lorenz, M.; Diekmann, S., Recent advances in FRET: distance determination in protein-DNA complexes. *Curr. Opin. Struct. Biol.* **2001,** *11* (2), 201-207.
2. Zhou, L.; Russell, D. H.; Zhao, M.; Crooks, R. M., Characterization of Poly(amidoamine) Dendrimers and Their Complexes with Cu2+ by Matrix-Assisted Laser Desorption Ionization Mass Spectrometry. *Macromolecules* **2001,** *34* (11), 3567-3573.
3. Yuan, L.; Lin, W.; Zheng, K.; Zhu, S., FRET-Based Small-Molecule Fluorescent Probes: Rational Design and Bioimaging Applications. *Accounts of Chemical Research* **2013,** *46* (7), 1462-1473.
4. Berney, C.; Danuser, G., FRET or No FRET: A Quantitative Comparison. *Biophysical Journal* **2003,** *84* (6), 3992-4010.
5. Haas, E., The Study of Protein Folding and Dynamics by Determination of Intramolecular Distance Distributions and Their Fluctuations Using Ensemble and Single-Molecule FRET Measurements. *ChemPhysChem* **2005,** *6* (5), 858-870.
6. Sindbert, S.; Kalinin, S.; Nguyen, H.; Kienzler, A.; Clima, L.; Bannwarth, W.; Appel, B.; Müller, S.; Seidel, C. A. M., Accurate Distance Determination of Nucleic Acids via Förster Resonance Energy Transfer: Implications of Dye Linker Length and Rigidity. *Journal of the American Chemical Society* **2011,** *133* (8), 2463-2480.
7. Lorenz, M.; Diekmann, S., Distance Determination in Protein-DNA Complexes Using Fluorescence Resonance Energy Transfer. In *Fluorescent Energy Transfer Nucleic Acid Probes: Designs and Protocols*, Didenko, V. V., Ed. Humana Press: Totowa, NJ, 2006; pp 243-255.
8. Medintz, I. L.; Clapp, A. R.; Mattoussi, H.; Goldman, E. R.; Fisher, B.; Mauro, J. M., Self-assembled nanoscale biosensors based on quantum dot FRET donors. *Nat Mater* **2003,** *2* (9), 630-638.
9. Hu, B.; Hu, L.-L.; Chen, M.-L.; Wang, J.-H., A FRET ratiometric fluorescence sensing system for mercury detection and intracellular colorimetric imaging in live Hela cells. *Biosensors and Bioelectronics* **2013,** *49*, 499-505.
10. Kar, C.; Adhikari, M. D.; Ramesh, A.; Das, G., NIR- and FRET-Based Sensing of Cu2+ and S2- in Physiological Conditions and in Live Cells. *Inorganic Chemistry* **2013,** *52* (2), 743-752.
11. Bailey, V. J.; Keeley, B. P.; Zhang, Y.; Ho, Y.-P.; Easwaran, H.; Brock, M. V.; Pelosky, K. L.; Carraway, H. E.; Baylin, S. B.; Herman, J. G.; Wang , T.-H., Enzymatic Incorporation of Multiple Dyes for Increased Sensitivity in QD-FRET Sensing for DNA Methylation Detection. *ChemBioChem* **2010,** *11* (1), 71-74.
12. 8-Anilino-1-naphthalenesulfonic acid. http://www.chemicalbook.com/ProductMSDSDetailCB8289935_EN.htm.
13. Frost, T.; Margerum, L. D., Effect of PAMAM Dendrimers on *Ru(bpy)32+ Emission Quenching by Ferrocyanide and on ANS Fluorescence: Quantitative Binding Parameters as a Function of Dendrimer Size, pH, and Buffer Composition. *Macromolecules* **2010,** *43* (3), 1218-1226.
14. Wang, L.; Tan, W., Multicolor FRET Silica Nanoparticles by Single Wavelength Excitation. *Nano Lett.* **2006,** *6* (1), 84-88.
15. Medintz, I.; Hildebrandt, N., *FRET-Forster Resonance Energy Transfer: From Theory to Applications*. Wiley: 2014.
16. Davidson, M. W.; Fellers, T. J.; Herman, B.; Frohlich, V. E. C.; Lakowicz, J. R. Fluorescence Resonance Energy Transfer (FRET) Microscopy. http://www.olympusmicro.com/primer/techniques/fluorescence/fret/fretintro.html.

17. Ernst, O. P.; Gramse, V.; Kolbe, M.; Hofmann, K. P.; Heck, M., Monomeric G protein-coupled receptor rhodopsin in solution activates its G protein transducin at the diffusion limit. *Proceedings of the National Academy of Sciences* **2007,** *104* (26), 10859-10864.
18. Hink, M. A.; Visser, N. V.; Borst, J. W.; Van Hoek, A.; Visser, A. J. W. G., Practical Use of Corrected Fluorescence Excitation and Emission Spectra of Fluorescent Proteins in Förster Resonance Energy Transfer (FRET) Studies. *Journal of Fluorescence* **2003,** *13* (2), 185-188.
19. Visser, A. J. W. G.; Vysotski, E. S.; Lee, J. Critical Transfer Distance Determination Between FRET Pairs. http://photobiology.info/Experiments/Biolum-Expt.html.
20. Turner, D. C.; Brand, L., Quantitative estimation of protein binding site polarity. Fluorescence of N-arylaminonaphthalenesulfonates. *Biochemistry* **1968,** *7* (10), 3381-3390.
21. Scott, T. A., Refractive Index of Ethanol–Water Mixtures and Density and Refractive Index of Ethanol–Water–Ethyl Ether Mixtures. *The Journal of Physical Chemistry* **1946,** *50* (5), 406-412.
22. Diallo, M. S.; Christie, S.; Swaminathan, P.; Balogh, L.; Shi, X.; Um, W.; Papelis, C.; Goddard, W. A., III; Johnson, J. H., Jr., Dendritic Chelating Agents. 1. Cu(II) Binding to Ethylene Diamine Core Poly(amidoamine) Dendrimers in Aqueous Solutions. *Langmuir* **2004,** *20* (7), 2640-2651.
23. Yang, K.; Xing, B., Sorption of Phenanthrene by Humic Acid-Coated Nanosized TiO2 and ZnO. *Environmental Science & Technology* **2009,** *43* (6), 1845-1851.
24. Lard, M.; Kim, S. H.; Lin, S.; Bhattacharya, P.; Ke, P. C.; Lamm, M. H., Fluorescence resonance energy transfer between phenanthrene and PAMAM dendrimers. *Phys Chem Chem Phys* **2010,** *12* (32), 9285-91.
25. Gao, D.; Wang, Z.; Liu, B.; Ni, L.; Wu, M.; Zhang, Z., Resonance Energy Transfer-Amplifying Fluorescence Quenching at the Surface of Silica Nanoparticles toward Ultrasensitive Detection of TNT. *Anal. Chem. (Washington, DC, U. S.)* **2008,** *80* (22), 8545-8553.
26. Toal, S. J.; Trogler, W. C., Polymer sensors for nitroaromatic explosives detection. *Journal of Materials Chemistry* **2006,** *16* (28), 2871-2883.
27. Buczkowski, A.; Urbaniak, P.; Belica, S.; Sekowski, S.; Bryszewska, M.; Palecz, B., Formation of complexes between PAMAM-NH2 G4 dendrimer and L-α-tryptophan and L-α-tyrosine in water. *Spectrochim. Acta, Part A* **2014,** *128*, 647-652.
28. Wang, M.; Gong, X.; Hu, J.; Yu, Y.; Chen, Q.; Cheng, Y., Understanding the Binding Interactions between Dendrimer and 18 Common Amino Acids by NMR Techniques. *The Journal of Physical Chemistry B* **2011,** *115* (44), 12728-12735.